Structure-function study of heterodimeric amino acid transporter, LAT1-CD98hc

GEORGE NYASHA CHIDUZA

Thesis submitted in accordance with the requirements
of the University of Liverpool for the degree of
Doctor in Philosophy

February 2019

Institute of Integrative Biology
University of Liverpool
United Kingdom

Acknowledgements

Firstly, I am grateful to my supervisory team Professor S. Samar Hasnain, Dr Svetlana Antonyuk and Dr Gareth S. A. Wright, in many ways they have gone above and beyond their responsibilities toward me as required by the university, in order to help me to this position. Professor Hasnain believes in my potential and has provided me the environment, mentorship and professional network to realise it as far as I have over the course of my PhD. Dr Antonyuk has given me essential support and guidance on theoretical as well as practical aspects throughout my research. Dr Wright has also mentored and taught me much about how to think about scientific questions, and being, not just a good but efficient experimentalist. He has been a good friend to me, supporting me in important aspects of life, without which I could not be where I am today.

I am grateful to Dr David Dickens who I worked with in the first two years of my PhD. He taught me the importance of keeping abreast with the scientific literature, and how to leverage that knowledge to drive my own research. He demonstrated to me a level of diligence I aspire to.

I would like to acknowledge the support Professor Sir Munir Pirmohamed in the early part of my PhD, where I worked under his supervision in the Wolfson Centre for Personalised Medicine, here in Liverpool.

I also want to acknowledge Dr Richard Henderson, for inducting me into the field of cryo-electron microscopy. Some of the electron micrographs from my visit to see him at Laboratory of Molecular Biology are shown in Chapter 5. I am grateful for his humility in working with my samples, preparing the first cryo-EM grids of LAT1 himself, in spite my obvious inexperience. Many thanks to Dr Stephen Muench and

Rachel Johnson for organising and setting up cryo-EM grid preparation and data collection, all of which has contributed to my thesis. Aside from the literature most of what I know about cryo-EM is from my conversation and interactions with these three.

I am also grateful to the Institute of Integrative Biology here at the University for financing my tuition through a bursary for international students, of which I was the first beneficiary and to members of the institute I have had the pleasure of knowing, that have greatly enriched my experience at the university.

Finally, I'd like to acknowledge my family and friends, most importantly, my mother Gay Chiduza. I am grateful to her for the self-sacrifice and determination she has demonstrated in raising and supporting me as a single parent. Sending me to one of the best schools in Zimbabwe, financing my tuition as international undergraduate student here and supporting me throughout my PhD. Every good thing I am and have in life I owe to her.

Abstract

The L-type neutral amino acid transporter 1 (LAT1/SLC7A5) is one of 7 light chains that can form a heteromeric amino acid transporter (HAT) with the type II single pass glycoprotein CD98hc (SLC3A2). LAT1-CD98hc transports essential amino acids and some of their catabolites, such as tryptophan, methionine and kynurenine, across the plasma membranes of normal and cancer cells. It is also a drug transporter, carrying drugs such as gabapentin and L-DOPA across the blood brain barrier. The atypical heterodimeric nature of LAT1-CD98hc and its role in disease and drug delivery, motivate the structural characterisation of the HAT. Sequence analysis revealed two putative cholesterol binding motifs conserved between dDAT and LAT1 as well as 32 putative CRAC/CARC motifs. The crystal structures of various bacterial homologues of LAT1 were used for structure prediction, in order to visualise these putative cholesterol binding motifs and assess their plausibility. Here is presented the first binding mode analysis of ligands to the inward facing occluded conformation of LAT1. Substrates had lower predicted free energies of binding to the inward facing conformation compared to the outward open. The putative gating residue F252 may play a role in binding to aromatic substrates via π-π stacking in the outward open conformation and with all substrates via π-cation bonding with their amino termini in the inward facing occluded conformation. Based on the docking analysis, inhibitors of LAT1, JPH203 and SKN203 are predicted to transportable substrates of the transporter and KMH233 a non-transportable competitive inhibitor with a unique binding mode. LAT1 was overexpressed in HEK293 cells and co-purified with CD98hc to a sufficient biochemical homogeneity for structural characterisation. The role of

cholesterol hemisuccinate in stabilizing detergent solubilized LAT1-CD98hc was established. Detergent solubilized and purified LAT1-CD98hc was subject to structural analysis by single particle electron cryo-microscopy to a resolution of 12 Å. Multibody 3D auto-refinement and principal component analysis revealed flexibility and limited interaction between CD98hc ectodomain and LAT1, contrary to predictions based on homology to LAT2-CD98hc. Docking of CD98hc allowed for visualisation and generation of molecular movies of the structural dynamics of LAT1-CD98hc ectodomain, based on these the ectodomain of CD98hc seems tethered to LAT1 via the inter-subunit disulphide bond and interaction between their transmembrane domains.

Table of Contents

List of Figures

List of Tables

List of movies

Movie 1 ……https://youtu.be/FhEPXdU9Bu4
Movie 2……https://youtu.be/bH5CgIpwhsU
Movie 3……https://youtu.be/YvZ0p1dt-Hw

List of Abbreviations

^{18}F-FBPA – 4-borono-2-^{18}F-fluoro-phenylalanine

AhR – aryl hydrocarbon receptor

A_r – atom mass in Daltons

BBB – blood brain barrier

BCH – 2-aminobicyclo-[2,2,1]-heptane-2-carboxylic acid

BNCT – boron neutron capture

BPA – 4-borono-L- phenylalanine

CARC – CRAC-like motifs

CHAPS – 3-((3-cholamidopropyl) dimethylammonio)-1-propanesulfonate

CHS – cholesterol hemisuccinate

CRAC – cholesterol recognition/interaction amino acid consensus

cryo-EM – cryo-electron microscopy

CTF – contrast transfer function

dDAT – *Drosophila Melanogaster* dopamine transporter

DED – direct electron detectors

DDM – n-dodecyl beta maltoside

DOF – depth of field

EM – electron microscopy

FDG – fluorodeoxyglucose

HAT – heteromeric amino acid transporter

HBBS – Hank's Balanced Salt Solution

HEK293 – human embryonic kidney cell-line

HEK293SG – human embryonic kidney cell-line, suspension adapted and N-acetylglucosaminyltransferase I deficient

IDO – indoleamine 2,3-dioxygenase (IDO)

LAT1 – L-type neutral amino acid transporter 1

LAT2 – L-type neutral amino acid transporter 2

LMNG – lauryl maltose neopentyl glycol

mTORC1 – mechanistic target of rapamycin

PCA – principal component analysis

PET – positron emission tomography

SE-HPLC – size exclusion high pressure liquid chromatography

SLC – solute carrier

SNR – signal to noise ratio

TBS – Tris buffered saline

TBST - Tris buffered saline with Tween

TDO – tryptophan 2,3 dioxygenase

TEM – transmission electron microscopy

T_3 – triiodothyronine

TM – transmembrane helix

VPP – Volta phase plate

Chapter 1 – Introduction

This chapter introduces the transporter that is the subject of this thesis, its physiological roles and clinical significance. Background on its biochemistry is also given. The main technique, around which many of the experiments are geared, cryo-electron microscopy is introduced in this the chapter. The objectives of the study are given at the end of chapter.

INTRODUCTION TO LAT1-CD98hc

Heterodimeric amino acid transporters (HATs) are rare among the estimated 400 solute carrier (SLC) transporter genes annotated in the human genome (Schlessinger et al., 2010). There are 7 HATs with subunits belonging to the SLC3 and SLC7 gene families. SLC3A1 and SLC3A2, the heavy chains, are type II single pass transmembrane glycoproteins that act as chaperones for the transport active light chains of some members of the SLC7 family. SLC3A2, also known as CD98hc or 4F2hc, forms heterodimers with SLC7A5 – 8 and SLC7A10 – 11, while SLC3A1 only complexes with SLC7A9. Within the HATs, the two subunits are linked together by a disulphide bridge between a conserved cysteine in the loop between transmembrane helices 3 and 4 of the light chain and a cysteine in the heavy chain. All HATs function as obligatory exchangers/antiporters exchanging one substrate for another (Devés and Boyd, 2000; Reviewed by Fotiadis, Kanai and Palacín, 2013).

The L-type amino acid transporter 1/SLC7A5 (LAT1) is a 55 kDa polytopic integral membrane protein that has been shown to function as a Na^+-independent secondary active antiporter of neutral L-amino acids and in some cases their catabolites. Substrates of LAT1 include leucine, isoleucine, valine, phenylalanine, tyrosine, tryptophan, methionine and histidine (Kanai et al., 1998; Mastroberardino

et al., 1998). CD98hc is 68 kDa and functions as a chaperone for LAT1, stabilizing and facilitating its translocation to the plasma membrane (Nakamura et al., 1999).

LAT1-CD98hc - its role in normal and disease physiology

LAT1 is expressed in a number of tissues throughout the body, namely the foetal liver, placenta, brain, testis, bone marrow, and leucocytes, in descending magnitude of expression, whereas CD98hc seems to be expressed more ubiquitously (Yanagida et al., 2001). The expression of LAT1-CD98hc at the placenta has been suggested to be essential for the development of the foetus because of the transporter's role in the uptake of essential amino acids and thyroid hormones (Ritchie and Taylor, 2001). The catabolism of tryptophan, a substrate of LAT1-CD98hc, by indoleamine 2,3-dioxygenase (IDO) to kynurenine, which is also a LAT1-CD98hc substrate, in the placenta has been shown to play a role in the suppression of the maternal immune system, preventing the rejection of the foetus because it is allogenic (Tafuri et al., 1995; Sinclair et al., 2018). An increasing number of tumours have been shown to ectopically express the LAT1-CD98hc complex (Cantor and Ginsberg, 2012; Zhao et al., 2015). It is hypothesised that CD98hc plays a similar role in cancer cells as in lymphocyte activation, which is the amplification of β1 and β3 integrin signalling, reducing anchorage dependence and promoting cell proliferation by modulating cyclin dependant kinase regulation through extracellular signal-regulated kinase signalling (Cantor and Ginsberg, 2012). LAT1-CD98hc interacts directly with β1 integrins in a CD98hc dependant manner, this occurs particularly in ordered lipid microdomains (Kolesnikova et al., 2001). The mechanism by which this

complex plays its role in lymphocyte activation remains to be elucidated (Cantor and Ginsberg, 2012). LAT1 is responsible for the transporter activity of the HAT, an activity that has also been shown to be pro-tumorigenesis (Napolitano et al., 2015). The substrates that LAT1 supplies, are essential amino acids, necessary for protein synthesis and the replenishment of tricarboxylic acid cycle intermediates used in the synthesis of other macromolecules, necessary for the survival and dysregulated proliferation of tumour cells (DeBerardinis et al., 2007). Leucine, a substrate of LAT1, is sensed by sestrin2 leading to the activation of mechanistic target of rapamycin complex 1 (mTORC1), which in turn promotes growth while inhibiting autophagy (Saxton et al. 2016; Nicklin et al. 2009). The mechanistic target of rapamycin pathway has been identified as a key regulator of both aerobic glycolysis and protein synthesis, which have been highlighted in the “hallmarks of cancer” (DeBerardinis et al., 2008; Hanahan and Weinberg, 2011). LAT1-CD98hc is expressed and essential for the differentiation of activated T-lymphocytes during an adaptive immune response, providing another potential mechanism by which the transport function of LAT1-CD98hc is beneficial to the progress of cancer (Cantor and Ginsberg, 2012; Sinclair et al., 2013). mTORC1 plays a role in T cell antigen response, by reprogramming the metabolism of the cell for increased protein synthesis and proliferation, both of which are mediated by the upregulation of LAT1 in response to the engagement of T cell antigen receptor. Another downstream effector of the T cell antigen receptor is the MYC family of transcription factors which regulate transcription of mRNA for proteins necessary in the metabolic reprograming of characteristic of T cell differentiation such as the glucose transporter GLUT1 (Jones and Thompson, 2007) (Figure 1). Glioma cell-lines have been shown to produce the tryptophan catabolite,

kynurenine, which suppresses T cell proliferation (Frumento et al., 2002). Kynurenine is transported by LAT1-CD98hc and an agonist of the aryl hydrocarbon receptor (AhR), which binds to a DNA binding element in intron 2 of the LAT1 gene, recruiting p300, a histone acetyltransferase, that promotes LAT1 gene transcription (Lo and Matthews, 2012). Taken together with the fact that the enzyme that catalyses the rate-limiting step in the synthesis of kynurenine in glioma cells, tryptophan-2,3-dioxygenase, is itself regulated by AhR, LAT1-CD98hc is at the centre of an autocrine/paracrine signalling network that allows cancers cells to modulate immune responses to their advantage (Opitz et al. 2011; Kaper et al. 2007; Tomblin et al. 2016). This complex signalling network and its role in cancer remains to be further and definitively elucidated (Figure 1).

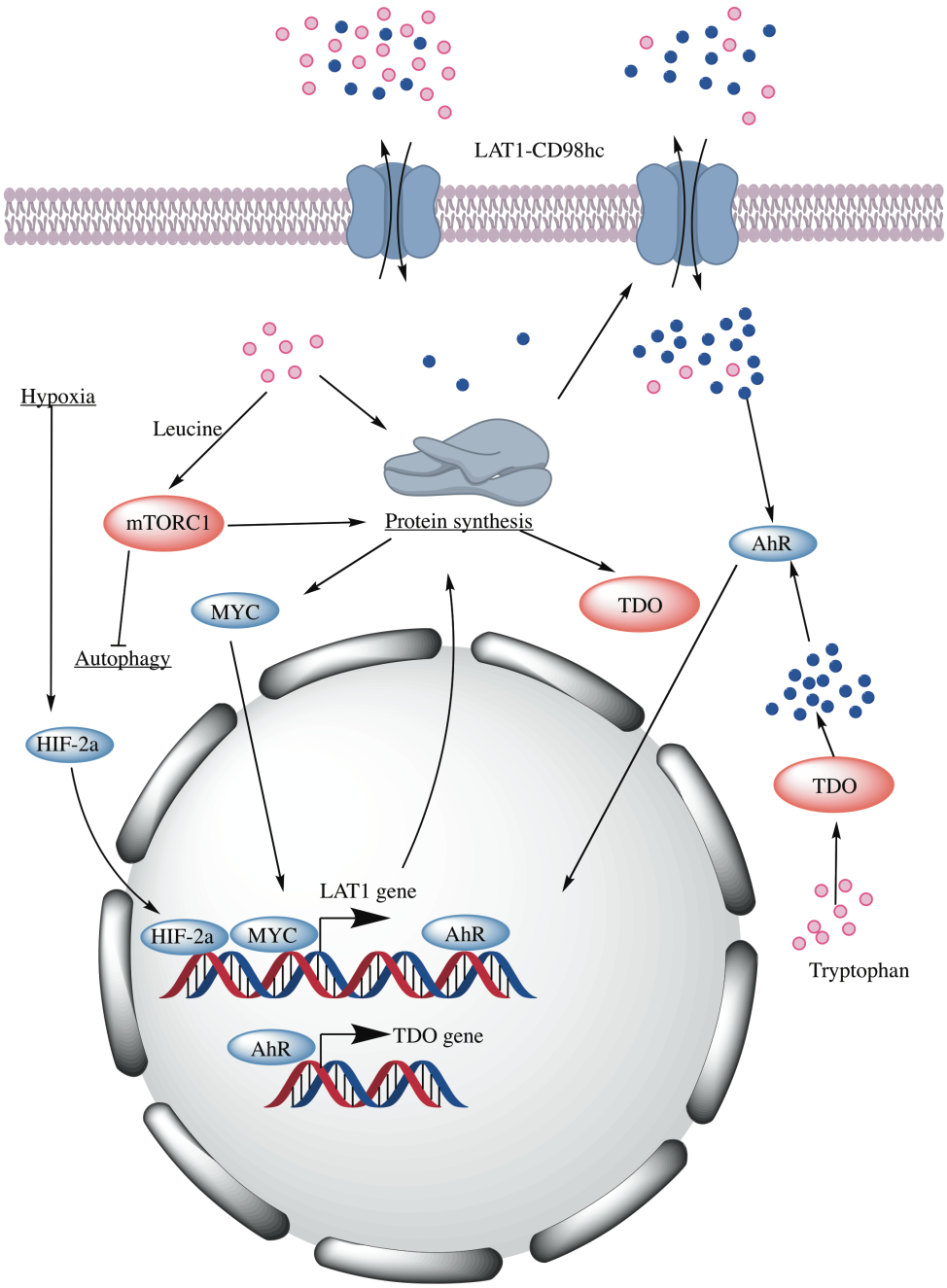

Figure 1 - Summary LAT1-CD98hc gene regulatory network. LAT1-CD98hc is a secondary active antiporter ectopically expressed in several cancers. The antiporter translocates essential amino acids (EEA) (pink circles), such as leucine and tryptophan and some of their catabolites such as kynurenine (dark blue circles), across the cell membrane. The MYC family of proto-oncoproteins upregulates LAT1 expression which in turn upregulates MYC protein synthesis in a feed-forward loop that drives tumour proliferation in cancer. EEA are substrates for protein synthesis and the synthesis of precursors for other macromolecules so therefore sustain tumour growth. Leucine has been shown to facilitate the activation of mTORC1 which promotes growth via increased mRNA translation while inhibiting autophagy. Kynurenine is an agonist of the AhR which upregulates the expression of TDO and LAT1, thereby increasing kynurenine synthesis, transport of tryptophan into and kynurenine out of the cell. Kynurenine is taken up by T-cells via LAT1 resulting in their suppression, allowing cancer cells to escape destruction by them.

LAT1-CD98hc is regulated by several proto-oncogenes, suggesting alternative pathways for its ectopic expression in tumours. An example of this is the regulation of LAT1 by AhR, whose ligands can be either be pro- or anti-tumorigenic as has been mentioned above (Safe et al., 2017). Recruitment of the AhR-ARNT complex to the LAT1 gene was demonstrated to increase proliferation in breast cancer cell-lines (Tomblin et al., 2016). HIF2α has also been implicated in cancer as part of the mechanism through which the oxygen sensing pathways can promote oncogenesis. HIF2α upregulates the expression of LAT1, by binding to hypoxia response elements in the promoter and intron 1 of the LAT1 gene, which in turn leads to the activation of mTORC1 as described above (Elorza et al., 2012). MYC proteins are another example of proto-oncogenes that have been demonstrated to regulate the expression of LAT1 by, after dimerization with MAX, binding directly to the MYC consensus motif (E-box) in promoter of the LAT1 gene (Adhikary and Eilers, 2005; Hayashi et al., 2012; Yue et al., 2017). The expression of C-MYC in tumours has been shown to correlate with the expression of both LAT1 and CD98hc (El Ansari et al., 2018b; a). Knock-down or inhibition of LAT1 results in lower N- and C-MYC expression suggesting a feed forward loop between the transporter and oncogenes that drives tumorigenesis (Figure 1). In addition to the downregulation of MYC proteins in response to LAT1 inhibition, cell cycle regulator, cyclin D1 and cell death regular, BCL2 were also downregulated, further elaborating the mechanism by which LAT1 promotes tumour growth and survival. (Yue et al., 2017). There remains work to be done in further characterising the regulation of LAT1-CD98hc and how the HAT in turn influences the expression and activity of other oncogenes in cancer. The focus above has been on the regulation of LAT1 expression since it has been shown that

CD98hc is upregulated in response to LAT1 upregulation (Khunweeraphong et al., 2012; Cormerais et al., 2016).

LAT1 and CD98hc both have activities that promote tumour growth, with the transport activity of their HAT suggested to be the main mechanism by which the complex promotes cancer and this is summarised in Figure 1 (Cormerais et al., 2016). At present there is limited information about this mechanism at the atomic level, something that is hindering progress in the exploitation of LAT1-CD98hc for the diagnosis, management and treatment of cancer.

LAT1-CD98hc as a tumour biomarker in various cancers.

Molecular and genetic biomarkers offer a robust and reproducible means of diagnosing cancer, choosing the best treatment and or management options as well as predicting the outcomes of these clinical strategies for patients. Tumour biomarkers can also play an important role during drug development by allowing for stratification of clinical trial participant cohorts and in measuring the efficacy of the potential therapeutic under development. Ideally a good tumour biomarker allows for distinction between benign and malignant neoplasia, can be quantitively correlated with the degree of malignancy and lastly, can be assayed with relative ease and robustness. LAT1-CD98hc, being expressed in a small number of tissues in normal physiological conditions while also being ectopically expressed in tumours, makes a good candidate for a tumour biomarker (Figure 2). Evidence to support this hypothesis is building. For example, LAT1 has been shown to be upregulated in breast cancer, with high LAT1 expression levels being correlated with tumour size, tumour

grade and patient survival outcome. Furthermore, LAT1 is differential expressed between the various breast cancer types and the subtypes within them. For example in estrogen receptor positive breast cancer, LAT1 expression levels correlate with the proliferation phenotype of the tumour, with LAT1 expression being higher in luminal B compared to A malignancies (El Ansari et al., 2018b). Similar observations have been made with respect to CD98hc in breast cancer (El Ansari et al., 2018a).

Three more examples of where LAT1-CD98hc is a potentially effective tumour marker, are in stratification of glioblastomas, the diagnosis of prostate cancer and as a predictor of resistance to chemotherapy in pancreatic ductal adenocarcinoma. High grade gliomas have been shown to express high levels of LAT1 whereas expression is barely detectable in low grade gliomas (Nawashiro et al., 2005; Kobayashi et al., 2008). In addition to being a potentially good biomarker for high grade gliomas, LAT1 is highly expressed in infiltrating gliomas, which are often difficult to remove entirely by surgery, making LAT1 a good target for the development of adjuvant chemotherapeutics (Nawashiro et al., 2005; Kobayashi et al., 2008). In prostate cancer LAT1 immunohistochemical staining has been shown to be a potentially useful supplement to prostate specific antigen blood tests, for routine screening, and to the Gleason score for malignancy grading. In cases of inoperable prostate cancer, patients with high LAT1 expression have a poor prognosis, with most of them living less than 5 years after the first biopsy examination (Sakata et al., 2009). Finally, high expression of LAT1 was found to correlate negatively with responsiveness to adjuvant and systemic chemotherapy in pancreatic ductal adenocarcinoma (Altan et al., 2018).

Despite various strands of evidence supporting the development of LAT1-CD98hc as a tumour biomarker, clinical trials are required before it can be integrated as a biomarker in clinical practice and drug development.

LAT1 as a target for tumour imaging markers and radiotherapy development

Positron emission tomography (PET) is useful for non-invasive biological imaging that can be used in conjunction with other imaging modalities such as computed tomography, facilitating the diagnosis, staging and treatment of cancer (Griffeth, 2005). PET is often used to exploit metabolic changes that occur during the development and progression of cancer, as is the case with the popular tracer ^{18}F-fluorodeoxyglucose (FDG), which targets changes in energy metabolism (d'Amico, 2015). Given the variety of physiological and pathophysiological states that affect glucose metabolism, such as activity in the brain or inflammation, PET using FDG is prone to high imaging background and false positives thus amino acid PET tracers have been developed and used, giving lower background signal while showing preferential accumulation in malignant tumors (Jager et al., 2001). The expression of LAT1 in a small number of normal tissues and upregulation in a large number of tumors, make it an ideal transporter to target for the development of PET tracers (Figure 2) (Wei et al., 2016; Nodwell et al., 2017). L-3-^{18}F-α-methyl tyrosine is one such example of a LAT1 specific PET tracer that has shown effectiveness in clinical trials, preferentially accumulating in malignant tumors rather than in benign neoplasia or normal tissue, as a result functions as an effective prognostic marker in non-small cell lung carcinoma (Wiriyasermkul et al., 2012).

Boron neutron capture therapy (BNCT) is a radiotherapy that has been used against high grade gliomas (Barth et al., 2012). It is dependent on the presence of ^{10}B, which can be delivered to and enriched in the tumour tissue relative to normal tissue, using 4-borono-L- phenylalanine (BPA). 4-borono-2-^{18}F-fluoro-phenylalanine (^{18}F-FBPA) was developed to allow the estimation of BPA accumulation in tumour tissues using non-invasive PET scanning. The accumulation of ^{18}F-FBPA was shown to correlate with LAT1 expression, which was not surprising given that both ^{18}F-FBPA and BPA are LAT1 substrate analogues (Yoshimoto et al., 2013). The use of ^{18}F-FBPA accumulation in tumour cells as a predictor of BPA accumulation in cells, can be useful in predicting outcomes BNCT in patients.

The targeting of LAT1 for the development of radio-imaging tracers and for the delivery of targeted radiotherapy, is an area that has not been fully explored. The examples of where this has been done are all based on mimicking known natural substrates of LAT1. Structural characterisation of LAT1 may enable different approaches to exploit the ectopic expression of the transporter for imaging and radiotherapy in various cancers.

LAT1-CD98hc as a target for antitumor chemotherapeutic development

LAT1 was determined, through transport inhibition assays, to be the serendipitous target of the chemotherapeutic melphalan (Uchino et al., 2002). This is consistent with a later finding that LAT1 expression is a significant prognostic indicator for the success of melphalan treatment of multiple myeloma (Isoda et al., 2014). When overexpressed, LAT1-CD98hc promotes growth of low level tumour

cells and inhibiting it using 2-aminobicyclo-[2,2,1]-heptane-2-carboxylic acid (BCH) has cytostatic and chemotherapeutic effects on tumour cells, providing further evidence of the HAT's potential as a drug target (Kobayashi et al., 2008). Using a canine model of melanoma, it was demonstrated that the cytostatic effect of chemotherapeutics such as carboplatin and doxorubicin for example, can be enhanced by inhibiting LAT1 using BCH or melphalan (Fukumoto et al., 2013). Another inhibitor of LAT1, JPH203, was designed using the thyroid hormone T_3 as a scaffold (Figure 2). JPH203 has been shown to inhibit leucine uptake, growth and induce apoptosis in cancer cells. It is potentially a high affinity inhibitor of LAT1-CD98hc, with IC_{50} as low as 0.14 and 0.06 μM (Oda et al., 2010; Yun et al., 2014; Choi et al., 2017). The inhibitor is currently in phase I clinical trials for solid tumours. Two other LAT1 inhibitors have been developed and validated *in vitro*, these are SKN103 and KMH233. They are still to be tested for safety and efficacy in animal models and in human (Huttunen et al., 2016; Kongpracha et al., 2017).

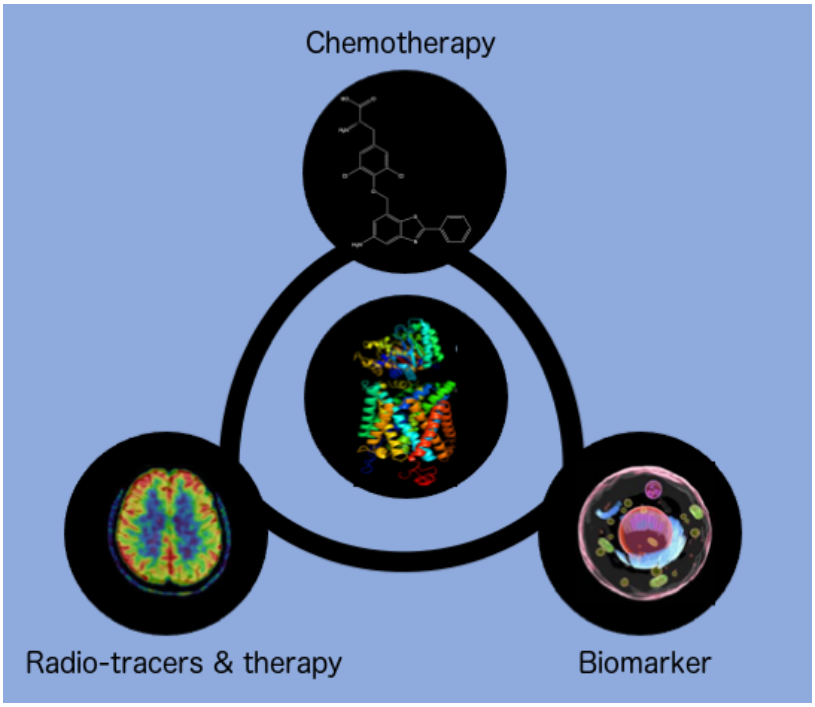

Figure 2 – LAT1-CD98hc at the centre of cancer diagnosis and treatment. LAT1 (predicted structure) and CD98hc (ectodomain crystal structure) shown at the centre of the image function as heterodimeric transporter. This transporter has been found upregulated in numerous cancers making it a potential biomarker. Through its transport activity, LAT1-CD98hc can facilitate the uptake of radiotracers for PET imaging and radio- compounds into cancer cells for the purpose diagnosis, prognosis and treatment of tumours. Finally, due to the role of the transporter in cancer metabolism it can be targeted for the development of chemotherapeutics. A detailed knowledge of the structure and thence mechanism of the transporter would lead to significant strides in these three areas of oncology.

LAT1-CD98hc as a drug transporter.

LAT1-CD98hc's importance as a target for small molecule drug development extends beyond chemotherapeutics. The HAT has been shown to transport drugs like L-DOPA and gabapentin across the blood brain barrier (BBB) (Kageyama et al., 2000; Dickens et al., 2013). This is worth noting since it is estimated that only 2 % of small molecule drugs can cross the BBB, therefore the BBB poses a significant hurdle in the development of small molecule therapeutics for neurological diseases (Pardridge,

2005). The idea of making pro-drugs by conjugating them to LAT1 substrates has been put forward and significant efforts made towards achieving this (Rautio et al., 2013). In one study the drug valproic acid was conjugated to the benzene ring of phenylalanine, a LAT1 substrate, in order to make prodrugs with improved BBB penetration. All the variants of the valproic prodrugs crossed the BBB with one of the meta- substituted versions demonstrating a 10 fold higher affinity and a 2 fold increase in transport compared to the other variants (Peura et al., 2011). Another approach has been to understand the structure-function relationship of LAT1 by determining a pharmacophore for the transporter using *in silico* structure prediction, *in vitro* transport assays and rat brain perfusion experiments, which in turn informs chemical synthesis of potential LAT1 ligands (Killian et al., 2007; Ylikangas et al., 2013, 2014; Augustyn et al., 2016; Nagamori et al., 2016; Zur et al., 2016; Chien et al., 2018). The experimental solution of an atomic structure of LAT1-CD98hc would greatly facilitate these efforts as it would give a detailed understanding of how the transporter recognises and transports its substrates.

Biochemical and structural properties of LAT1-CD98hc.

It was suggested based on hydropathy plot analysis of LAT1's amino acid sequence, the HAT light chain was composed of 12 transmembrane helices (TM). Association via a conserved disulphide bond between its C164 and C109 of CD98hc was also established by sequence analysis and co-immunoprecipitation. Both the N and C termini are predicted to be located in the cytoplasm (Figure 4) (Kanai et al., 1998; Mastroberardino et al., 1998). Homology modelling of LAT1 based on AdiC and

ApcT predicts that comprise a LeuT-fold where the first 10 helices adopt a 5 + 5 inverted repeat with the repeats related by a 2 fold pseudo-symmetry axis and TMs 11 and 12 wrapping around the edge of the repeats (Dickens et al., 2013; Geier et al., 2013). LeuT-fold transporters are predicted to carry out transport via the alternative access mechanism (Reviewed by Kazmier, Claxton and Mchaourab, 2017) (Figure 3). In this mechanism the transporter alternates between being open on one side of the membrane, allowing for substrate to bind and being released on the opposite side of the membrane as the transporter changes conformation, opening on the opposite side (Jardetzky, 1966) (Figure 3). It has been shown that LAT1 operates downstream of Na^+ dependant transporter such as SLC1A5, which exploit Na^+ gradients generated Na^+/K^+ pumps to concentrate LAT1 substrates such as glutamine which are exchanged for substrates such as essential amino acids, that the cell cannot synthesise (Nicklin et al., 2009). LAT1 has been demonstrated to have asymmetric substrate affinities on the extra- and intracellular binding sites with the K_m values on the intracellular side being 2 – 3 orders of magnitude lower than on the extracellular side, this means that LAT1 acts as an influx transporter for substrates that are at lower concentration in the cell than outside (Meier et al., 2002).

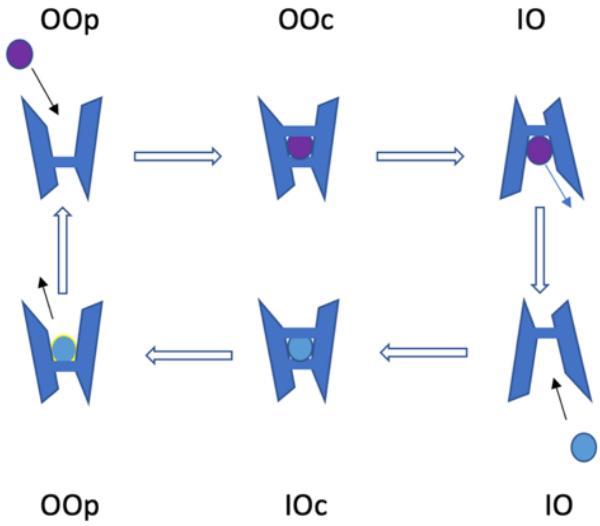

Figure 3 - Schematic of alternative access mechanisms of secondary active LeuT transporters. *It is hypothesised and supported by crystal structures that LeuT transporters have a single substrate binding site that is either open for substrate (blue/green circles) binding in the outward facing conformation the extracellular side (OOp) or inward facing conformation the cytosolic side (IO) of the plasma membrane. There are intermediate states, between these two conformations in which the substrate binding site is occluded in the outward facing or inward facing direction (OOc and IOc respectively).*

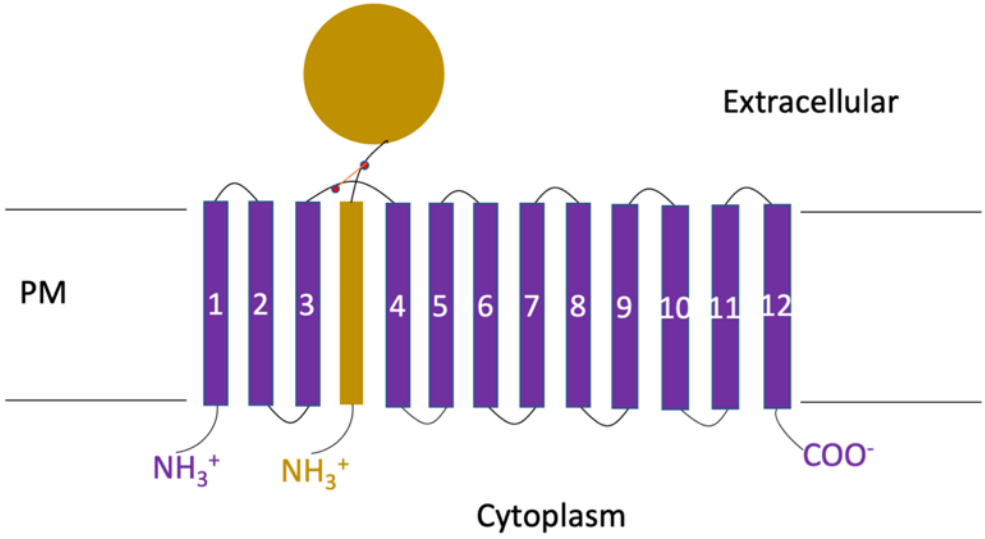

Figure 4 - Topology of LAT1-CD98hc heterodimer. Transmembrane domains are shown as rectangles in the plasma membrane (PM). CD98hc shown in gold and LAT1 in purple. Both termini of LAT1 are intracellular and the subunit has no large soluble domains whereas CD98hc has a large extracellular N-terminal domain, the ectodomain, a single TM and intracellular C terminus. The inter-subunit disulphide bond (red) is located between the loop linking CD98hc's ectodomain to its TM, and the loop between TM3 and 4 of LAT1.

Based on radioligand binding assays and comparison of known substrates, it was proposed that the negative and positive charges of the carboxyl and amino groups were recognised by residues in the substrate binding site while hydrophobic interactions were important for recognition of the side chain of a substrate (Uchino et al., 2002). The substrate binding site was predicted to be located in the centre of the protein, between TM1,TM3, TM6, TM8, TM10, with residues 62 – 66 and 253 – 255 predicted to recognise the carboxyl and amino groups via hydrogen bonding with their Cα backbone, while the hydrophobic side chains of residues like I139, V148, F252, F402, W405, interacted with the side chain of the substrate (Geier et al., 2013). Evidence that an amino acid group is not a requirement for transport by LAT1 has recently come from radioligand transport assay experiments with carboxylic acid bioisosteres of the LAT1 substrates (Nagamori et al., 2016; Zur et al., 2016). LAT1 has also been shown to transport not only L-α amino acids but also D-α, β and γ amino acids, although physiological relevance for this is still to be established (Nagamori et al., 2016; Chien et al., 2018). The widening of the LAT1 structure-activity relationship, made LAT1 an even more valuable target for delivery of small molecule therapeutics to tissues expressing it, but also highlights the limits of cellular assays and structure prediction in the absence of an experimentally determined atomic models of the transporter which allow for a detailed and accurate characterisation at this level of the transporter's structure activity relationship.

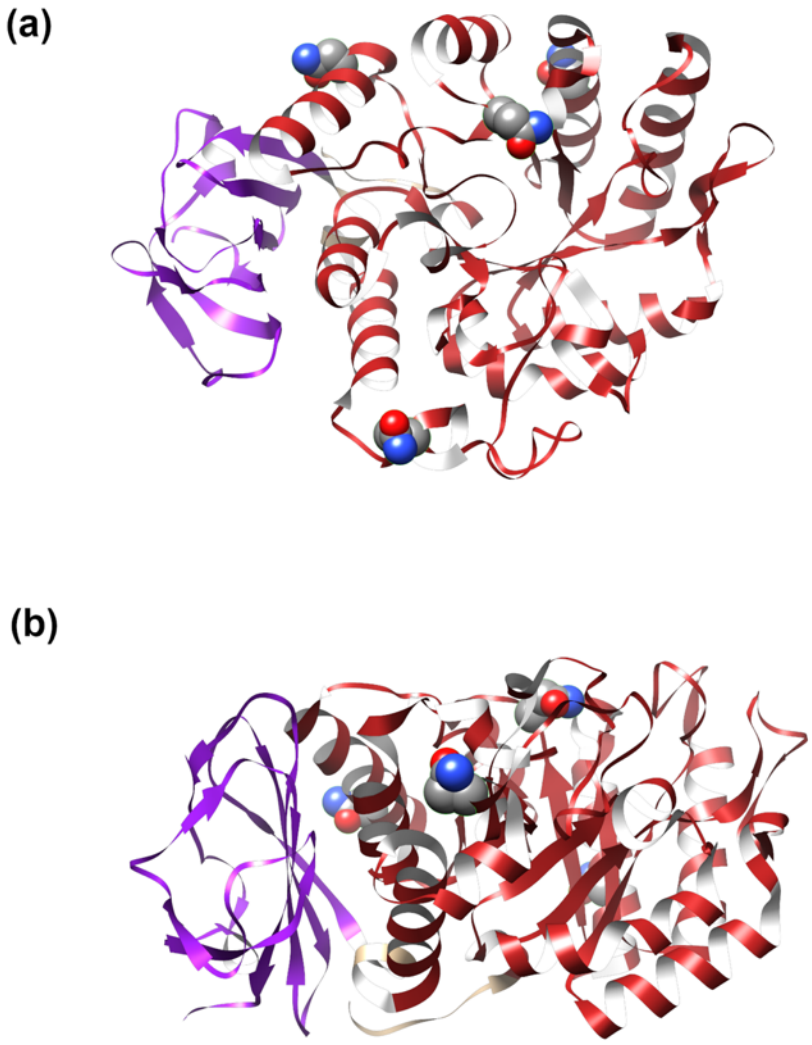

Figure 5 - Top (a) and side (b) views of the X-ray crystal structure of monomeric CD98hc ectodomain (PDB ID:2DH2). CD98hc's ectodomain bears resemblance to α amylases, with the characteristic A-domain comprised of a $(\beta/\alpha)_8$ TIM barrel (red) and a C domain comprised of 8 anti-parallel strands folded into a β sandwich. Glycosylated asparagine residues are shown as spheres with N and O atoms coloured blue and red respectively.

CD98hc comprises a 184 amino acid long intracellular C terminal domain, a transmembrane helix and a large 424 amino acids long ectodomain (Figure 5), (Uniprot ID P08195). The heavy chain is N-link glycosylated at N365, N381, N424 and N506, all of which are located in the ectodomain and are solvent accessible (Fort et al., 2007; Powlesland et al., 2009). The functional relevance of these glycans remains to elucidated. C109, located in a linker between the transmembrane helix and

ectodomain of CD98hc, covalently binds to a conserved cysteine, C164 in the case of LAT1, in the loop between TM3 and 4 of the light chains (Kanai et al., 1998; Mastroberardino et al., 1998). The ectodomain has an α amylase like fold with A and C domains typical for these enzymes but no B domain (Figure 5). Despite the similarity, comparative structural analyses, which revealed a lack of key catalytic residues and extensive screening of α-glycosidase activity, did not reveal any such activity. The ectodomain did not show any signs of glycosylation binding either (Fort et al., 2007).

HETEROLOGOUS EXPRESSION OF HATS FOR STRUCTURAL STUDY

Several attempts at the heterologous expression and purification for structural characterisation of CD98hc and several of its light chains have been reported in the literature. The structure of the soluble ectodomain of CD98hc, amino acids 115-530 (Uniprot ID P08195-2), was determined to 2.1 Å using crystals grown from protein expressed in *E. coli* strain, Rosetta (DE3) pLysS (Figure 5) (Fort et al., 2007). Galluccio *et al.,* 2013 published a protocol for the expression of LAT1 and CD98hc hexa-his and glutathione-S-transferase tagged fusion proteins respectively using the same *E. coli* strain. No obvious attempt at targeting the fusion protein to the plasma membrane was made, necessitating recovery from the insoluble fraction of the cell lysate, the expressed LAT1. The detergent sarkosyl, chaotrope, urea and reducing agent dithioerythritol were used to do this, before Ni^{2+} affinity purification, during which the sarkosyl was exchanged for triton X100. After purification, using glutathione sepharose 4B resin, the GST tag on CD98hc was cleaved off by incubation with thrombin and separated by size exclusion chromatography (Galluccio et al.,

2013). LAT1-CD98hc expressed and purified as described by Galluccio *et al.,* 2013 has been reconstituted in proteoliposomes and used in functional transport assays (Napolitano et al., 2015, 2017b). Despite the successful structure determination of the ectodomain of CD98hc expressed in *E. coli,* there has been no progress on the structural characterisation of the rest of CD98hc with or without any of its associated light chains, using this prokaryotic expression system. Palacin and co-workers, who had successfully solved the ectodomain structure of CD98hc, proceeded to adopt the *P. Pastoris* system for expression of a complete HAT complex for the purpose of structural study. Using DDM for membrane solubilisation and a tandem affinity coupled with size-exclusion chromatography purification strategy, enough LAT2-CD98hc was produced for structural characterisation by negative stain cryo-EM to 21 Å. A combination of this low-resolution map of the protein complex in detergent, *in silico* modelling and docking, as well mutagenesis and cross-linking experiments, revealed insights into the interaction of the ectodomain of CD98hc and LAT2, as discussed in detail below (Rosell et al., 2014). Improvements to the sample preparation of LAT2-CD98hc were made using a mixture of DDM, LMNG (lauryl maltose neopentyl glycol), CHS (cholesterol hemisuccinate) and glycerol for solubilising the HAT complex, yielding a more monodisperse and kinetically stable sample for structural studies (Meury et al., 2014).

LAT1 has previously been expressed in human cells for the purposes of characterizing its function and for developing and screening prodrugs and inhibitors (Dickens et al., 2013; Zur et al., 2016; Puris et al., 2017; Chien et al., 2018). In addition to being able to address functional questions in a human cell-line expression system, there is no need to co-express both the light and heavy chains since the ubiquitously

expressed heavy chain is upregulated, in response to LAT1 overexpression (Khunweeraphong et al., 2012). HEK293 cell-lines are currently the mammalian expression system of choice for membrane protein structural biology (Chaudhary et al., 2012; Goehring et al., 2014). The first HEK293 cell line was derived in 1973 by the transformation of kidney cells from an aborted human embryo, using adenovirus 5 DNA and other variant cell-lines have since been developed from it including the HEK293T and HEK293SG cell-lines (Lin et al., 2014). The HEK293SG cell is useful for the production of membrane and glycoproteins for structural biology as it is suspension adapted making it easier to grow at the scale necessary and also has a loss of function mutation in N-acetylglucosaminyltransferase I, rendering it incapable of complex glycan synthesis (Reeves et al., 2002; Lin et al., 2014). The simpler glycans produced by HEK293SG cells are sensitive endoglycosylases like EndoH, and are easy to remove if not required after purification. Chaudhary *et al.,* have developed a detailed protocol for stable transfection and large-scale suspension culture that is easy and cheap to implement (Chaudhary et al., 2012). For the work reported here, LAT1-CD98hc was expressed and purified from HEK293SG cells and the initial solubilisation and purification conditions were adapted from Meury *et al.*, 2014.

INTRODUCTION TO SINGLE-PARTICLE RECONSTRUCTION USING CRYO-ELECTRON MICROSCOPY

Transmission electron microscopy (TEM) has been used for the study of molecular organization, dating back to the first 3D reconstruction of a biomolecular structure by De Rosier and Klug in 1968. This first reconstruction was from a TEM

micrograph of phage particles, to a resolution of 35 Å (De Rosier and Klug, 1968). Resolutions higher than those estimated to be possible by single particle analysis of heavy metal stained samples (>15 Å), (Klug and Berger, 1964; De Rosier and Klug, 1968) were demonstrated using unstained 2D crystalline samples, by Henderson and Unwin, when they solved the structures of bacteriorhodopsin and catalase to 7 and 9 Å respectively (Henderson and Unwin, 1975; Unwin and Henderson, 1975). More recently, from about 2008 and onward, the field has undergone what has been described as a "resolution revolution", with structure determination of biomolecules by single particle TEM is at resolutions where atomic details are well resolved (<4Å) (Reviewed by Cheng and Walz, 2009; Kühlbrandt, 2014). The impact of this revolution was recognised by the award of the 2017 Nobel prize in Chemistry to Richard Henderson, Jacques Doubchet and Joachim Frank "for developing cryo-electron microscopy for the high-resolution structure determination of biomolecules in solution". 3D single particle reconstruction from 2D projections from TEM micrographs of particles in vitreous ice, usually referred to just as cryo-EM in the literature, is the particular mode of TEM that has undergone this resolution revolution.

In order to achieve resolutions comparable to X-ray crystallography by cryo-EM several obstacles have been overcome, namely the interaction of electrons with air, the deleterious effects of radiation and the vacuum on biological specimens, and the weak phase scattering of atoms typical of biological samples. In order to prevent the scattering of the imaging electron beam by air particles, the column of the electron microscope is operated under a high vacuum, which can desiccate biological specimens destroying the structure of interest. For cryo-EM imaging of biological

specimens in high vacuum, the vitrification of the specimen and operation of the electron microscope column at cryogenic temperatures, hence the prefix cryo-, was developed and is used, preventing desiccation of the specimen (Figure 6) (Dubochet et al., 1985). Vitrification also reduces the impact of radiation damage by limiting the spread of free radicals from their origin in the sample and also allows for use of higher electron doses, than otherwise useful, for data collection (Reviewed by Chiu, 1986). The third obstacle mentioned above is the weak phase scattering of electrons by biological specimens, which, together with the low electron doses necessary to limit radiation damage, result in low contrast images with low signal to noise ratio (SNR) (Unwin and Henderson, 1975; Henderson, 1995). In addition to this, inelastic and secondary scattering events, which are more common than the signal producing elastic scattering events, contribute to the background, lowering the SNR (Figure 7) (Henderson, 1995; Angert et al., 1996). The problem of low SNR in cryo-EM data has been addressed on the hardware/practical level mainly by the development of direct electron detectors, which because of their higher dynamic quantum efficiency, contribute less to the noise in the image and higher frame rate, provide more data enabling reduction of noise and blurring from other sources such as beam induced motion of the specimen. On the processing level, SNR is improved by imaging aberration correction, image alignment and averaging techniques, which are discussed in more detail below (Frank, 2006; McMullan et al., 2016; Sigworth, 2016). With respect to small molecular weight proteins (<400 kDa), which have a lower SNR than larger proteins, the Volta phase plate (VPP) has been useful for increasing contrast in the micrographs of such samples, facilitating the solution of their

structures to high resolution (Danev and Baumeister, 2016; Khoshouei et al., 2016, 2017).

The remainder of this section will discuss various stages of structure determination by single particle cryo-EM, from sample preparation, data collection to data processing summarized in Figure 6.

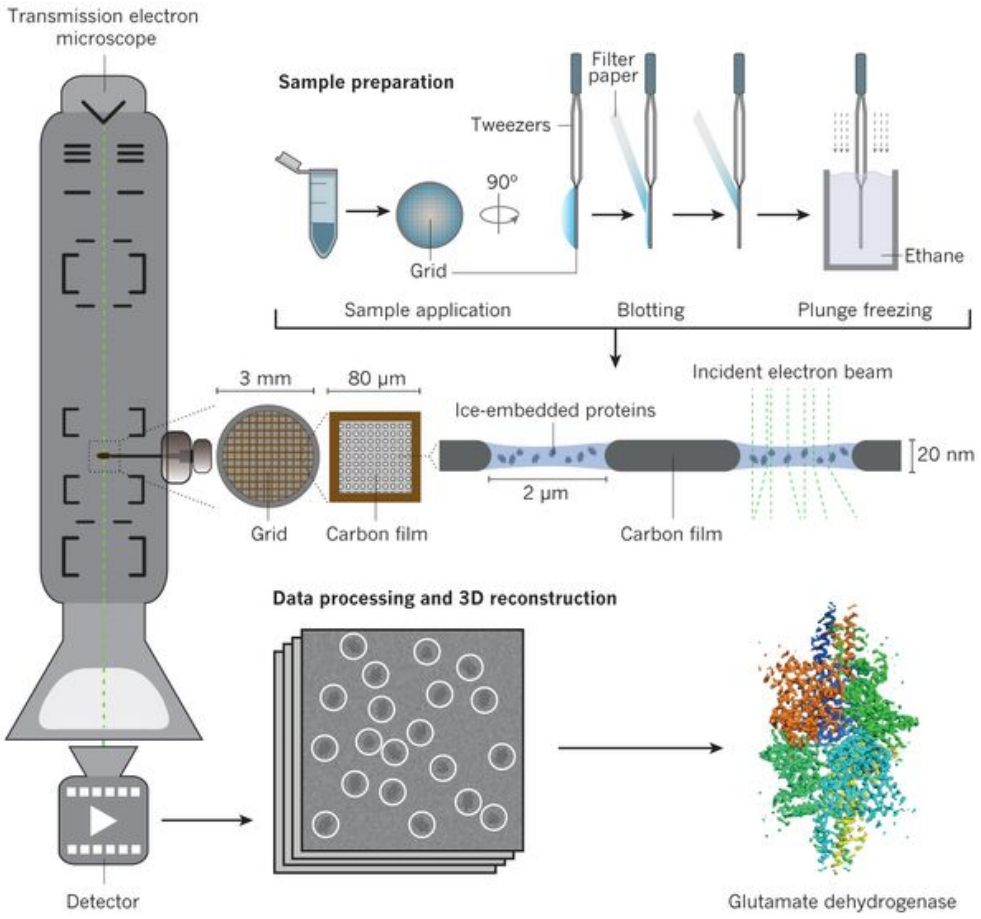

Figure 6 - Single particle cryo-EM sample preparation, data collection and processing. A solution of the particle of interest, in this example glutamate dehydrogenase, is applied to a grid, blotted and plunge frozen, ideally producing a monolayer of the particle in various orientations, embedded in vitreous ice. The specimen is imaged in a TEM microscope producing 2D images of the particle which can be analysed to reveal the 3D structure of the particle. Taken from Fernandez-Leiro and Scheres, 2016.

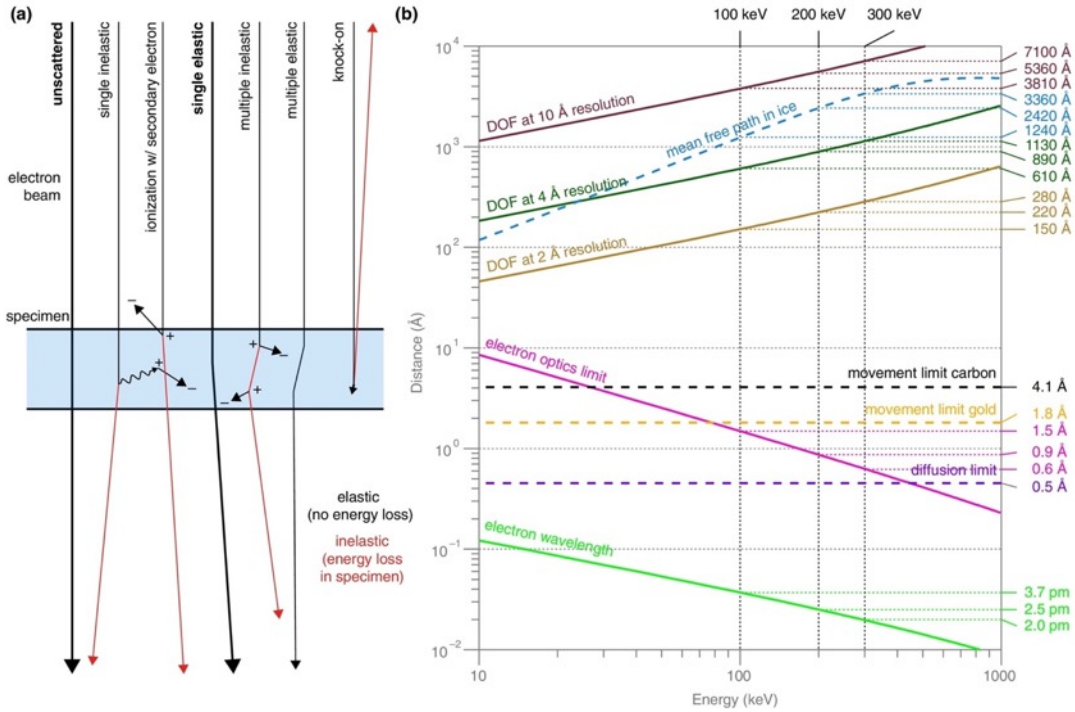

Figure 7 - Physical limitations on cryo-EM specimen preparation. a) Possible interaction electron may have specimen during imaging. Events are arranged in order of probability from left to right. Phase contrast is produced by the interference of the unscattered beam and the elastically scattered while inelastic scattering damages the structure of the specimen and all other events don't contribute to the signal but rather to the background. Factors considered in specimen design are shown in b) plotted against energy of the imaging electron beam. DOF is depth of field. Taken from Christopher J. Russo and Passmore, 2016.

Sample preparation and data collection.

Approaches to single particle reconstruction are predicated on the assumption that the 2D projections obtained from cryo-EM micrographs are of the same particle, differing only in their relative orientations (Reviewed by Sigworth, 2016). This necessitates that a particle of interest be purified to biochemical and conformational homogeneity and be kinetically and thermodynamically stable enough for analysis by cryo-EM. In this respect single particle cryo-EM is similar to crystallography in its sample requirements and therefore approaches used for the purification and stabilization of biomolecular complexes, such as heterologous

expression and affinity chromatography are applicable (e.g. Newby *et al.*, 2009). Cryo-EM unlike crystallography requires smaller amounts of sample, 0.25 pmol vs 500 pmol, and does not require crystals, facilitating the study of difficult to produce and crystallise samples such as membrane proteins (Frank, 2006; Vinothkumar, 2015). Once purified, negative-stain cryo-EM is often used to assess the quality of the sample preparation, allowing for assessment of homogeneity, particle size and integrity before moving on to cryo-EM. Buffer components that may increase noise (background signal) in cryo-EM micrographs of vitrified samples such as glycerol, sucrose or detergent are used sparingly or completely avoided if possible (Passmore and Russo, 2016; Thompson et al., 2016). For imaging in the electron microscope, the purified sample is applied to a substrate, often a metal grid supporting a perforated substrate such as amorphous carbon, and blotted to create thin layer of liquid which is plunge frozen in liquid ethane (Figure 6) (Cho et al., 2013; Passmore and Russo, 2016). Ideally, micrographs for 3D reconstruction should be collected from specimen grids with an ice thickness sufficient to accommodate a monolayer of the single particle of interest, in a wide distribution of orientations and, concentrated enough to maximise the number of particles per image without overlap. Vitreous ice thickness is an important variable to control, as thick ice lowers SNR. Obviously, it must not exceed the mean free path of electrons at the energies used for cryo-EM (Figure 7) (Angert et al., 1996; Russo and Passmore, 2016). Factors affecting the quality of a grid are: (i) the grid type, a variety of hole sizes and substrates are available; (ii) the duration and plasma used for glow discharging grids in order to render them more hydrophilic and (iii) blotting duration and force, all three of which determine ice thickness and particle distribution. All these factors must be optimised

empirically and devices for glow discharging and plunge freezing have been developed to facilitate and make the optimisation of these parameters more reproducible (Passmore and Russo, 2016; Thompson et al., 2016; Drulyte et al., 2018).

Once the sample and grid preparation have been optimised, collection of a data set large enough for single particle reconstruction to a resolution where atomic details are visible, can be done. Data collection for such purposes is typically done with 300 keV microscopes equipped with direct electron detectors, although 200 keV microscopes have also been shown to be effective for collecting data that can lead to near atomic resolution structures (Herzik et al., 2018a; Thompson et al., 2019). The optimal dose rate used for the data collection depends on the detector being used, as each detector has a dose rate at which detective quantum efficiency is maximal (McMullan et al., 2016). Current direct electron detectors (DDE) can be operated in two modes, a faster (1.5 – 5x faster) integrating mode, where signal is summed over the pixels of the detector and a slower counting mode, where each incident electron is detected with pixel or sub-pixel accuracy, giving an enhanced contrast. The choice of detector mode is dictated by the size of the particle, specimens >400 kDa can be collected in integrating mode, while smaller particles benefit from the enhanced contrast of the counting mode (Thompson et al., 2019). It is also now typical to record micrograph “movies” which are useful for correcting beam induced motion in the specimen improving the SNR of the final micrographs (Campbell et al., 2012; Li et al., 2013). Another consideration is whether to use a VPP if available, generally useful for small particles <100 kDa although sub-nanometre structures have been reported for data collected without VPP for particles of proteins

as small as 50 kDa (Herzik et al., 2018b). Typically micrograph movies in a data set are collected with a range of defocus values, to enhance phase contrast and adequately sample the reciprocal space (Zhu et al., 1997). VPP allows for collection of micrographs at values closer to focus by shifting the phase of the transmitted beam relative to the scattered beam, enhancing phase contrast (Danev and Baumeister, 2016; Danev et al., 2017). Once set up data collection proceeds automatically usually for at least 24 hrs or several days, depending on the requirements of the specimen. Some of the processing can be done as the data is collected, informing the data collection process (Thompson et al., 2019).

Data processing and single particle reconstruction in cryo-EM.

Cryo-EM data sets can range from hundreds to thousands of DED micrograph movies, depending on the sample in question and the time available for data collection. The individual frames of these movies often have a low SNR owing to the low doses typically used for data collection and imaging aberrations of the microscope itself. The first steps in the processing of a data set, also referred to as pre-processing, increases the SNR by averaging the frames of the movies and by correcting for the effects of imaging aberrations on the micrographs as described by the contrast transfer function (CTF). Other sources of signal degradation are addressed in the pre-processing are, the effect of movement of the specimen induced by the electron beam and, radiation damage. Programs like MotionCor, can align movie frames and produce average micrographs where the contribution of each frame to the average is weighted by the amount of radiation damage in it (Ripstein

and Rubinstein, 2016; Zheng et al., 2017). Given the voltage and spherical aberration of the microscope, the defocus can be estimated and CTF correction for the micrograph movie frames or aligned movies can be performed using programs like Gctf and CTFFIND (Rohou and Grigorieff, 2015; Zhang, 2016).

After pre-processing, particle co-ordinates can be defined by input from the user (manual picking), automatically (auto-picking) or by a compromise between the two (Zhu et al., 2004; Vargas et al., 2013). There are various cryo-EM processing packages such as RELION, XMIPP and EMAN2, which have particle picking modules that differ in their implementation and often the choice of program is for subjective reasons (Scheres, 2012b; de la Rosa-Trevín *et al.*, 2013; Ludtke, 2016; Zivanov *et al.*, 2018). User input provides an opportunity for introducing bias into the processing by, for example by favoring some orientations over others in manual picking, providing biased references for some methods of auto-picking or by using parameters that lead to picking of high resolution noise matching the references (Henderson, 2013). Low pass filtering micrographs and particle references or using reference free auto-picking followed by visual inspection of picked particles are some strategies to reduce bias. Once defined, particle co-ordinates are then used to extract, as individual images, the particles allowing for further processing by 2D classification. 2D classification involves the alignment of particles in order to determine which particles are projections of the specimen in the same orientation, forming an ideal 2D class, then averaging the images in the same class to boost the signal while reducing signal independent noise. Alignment algorithms maximize cross-correlation between particles in a class or use a Bayesian approach where each particle makes a weighted contribution to each class average. In both cases this done

iteratively to exploit the increase in SNR with each iteration, as the outputs from the last iteration are used as inputs for the next iteration. The Bayesian approach is the same as a the cross-correlation approach in the ideal noise free case but better accounts for the typical cryo-EM case of low SNR (Scheres, 2012a, 2012c). Classification can be reference free or done by matching projections in the particle set to projections computed from a model (Frank, 2006). Reference based 2D classification has the risk of introducing model bias and requires a suitable reference be provided. 2D class averages are useful for distinguishing particles of the macromolecule of interest from contaminants such as crystalline ice or carbon support, and incomplete or damaged molecules from intact ones, allowing for the selection of a homogenous particle set for further image processing (Scheres, 2016). Heterogeneity in the particle set can also be addressed using classification in 3D. For the 3D reconstruction using iterative methods such as those implemented in the popular RELION program, an initial 3D model is required for 3D classification and for 3D auto-refinement. This initial model can be a crystal structure or better, to avoid model bias, one generated from the data itself as can be done using programs such PRIME, cryoSPARC and RELION (Elmlund et al., 2013; Punjani et al., 2017; Zivanov et al., 2018).

Several rounds of 2D classification, 3D classification and 3D auto-refinement may be necessary before achieving the highest possible resolution from the data, particularly when dealing with large and or heterogenous data sets (Scheres, 2016). Despite the premise of single particle reconstruction as described so far, conformational heterogeneity is frequently encountered sometimes at scales that are not obvious in 2D and 3D classification but limit the final resolution and quality

of the final 3D reconstruction. As a result, other tools have been developed for addressing heterogeneity for the purpose of not only improving the quality of the reconstruction but also informing the structure function relationship of the biomolecule under study. Particle subtraction, were a binary mask is used to generate 2D projections from the data that have density within that mask subtracted, is useful for 3D reconstructions where flexible regions limit the accuracy of image alignment and the final reconstruction (Bai et al., 2015). Another approach useful for addressing molecular flexibility is multibody 3D auto-refinement, where parts of the particle that are presumed to move as rigid bodies with respect each other, are separately and iterative refined (Nakane et al., 2018). Principle component analysis of the variation in the particle set allows for the visualization of molecular motions that may be key to understating the function of the biomolecule and through quantitative analysis of this variation, the energy landscape of these motions can be inferred (Haselbach et al., 2018).

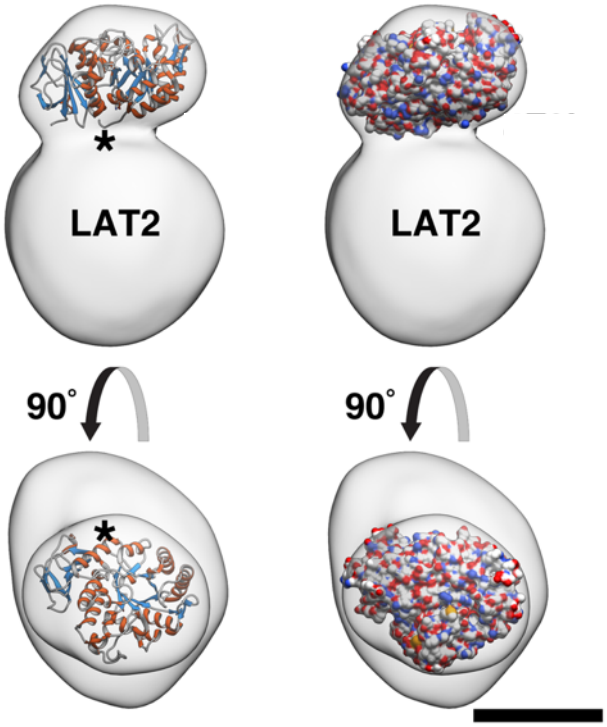

Figure 8 - Negative stain cryo-EM structure of LAT2-CD98hc. Detergent solubilized and LAT2-CD98hc was visualized by negative stain cryo-EM and the resultant 2D projection used for single particle reconstruction of the protein detergent complex structure to 21 Å. The crystal structure of CD98hc, blue and red ribbon on the left and spheres on the right, was docked into the smaller lobe of the EM map with the C terminus close to the larger lobe. The scale bar shown is 50 Å. Image was adapted from Meury *et al.*, 2014.

Negative stain single particle reconstruction of LAT2-CD98hc and insights into quaternary structure of heterodimer.

L-type neutral amino acid transporter 2/SLC7A8 (LAT2) is paralogue of LAT1 sharing 52% sequence identity with it. As stated previously LAT2 forms a covalently linked heterodimer with CD98hc of 124 kDa. LAT2 and LAT1 have overlapping substrate affinities, transporting large hydrophobic L amino acids such as tryptophan and phenylalanine. LAT2, in addition, has a higher affinity for more hydrophilic substrates such as glutamine, cysteine and serine (Meier et al., 2002). Transport by LAT2 is also sodium and pH independent and it is predicted to function as an antiporter by the alternative access mechanism (Figure 3). LAT2-CD98hc is

expressed, in order of descending magnitude in the kidney, placenta, brain, liver and spleen (Pineda et al., 1999).

The 21 Å structure of LAT2-CD98hc is at present the only reported structure of a heteromeric amino acid transporter (Figure 8). It was determined using single particle reconstruction from negative stain TEM micrographs of the detergent solubilised complex (Rosell et al., 2014). The reconstruction revealed a bilobate structure, with the smaller lobe tilted relative to the large lobe. Due to the low resolution, features of the complex, such as which part of the reconstruction corresponded to LAT2 and which to CD98hc, were not obvious so nanogold labelling of LAT2 via a his_6 tag on the protein allowed for localisation of the LAT2 in the larger lobe of the reconstruction (Meury et al., 2014). It was suggested that the complex was not only bound to detergent but lipids as well because of the size of the large lobe in EM map and molecular weight of the complex by size exclusion being 406 kDa (Meury et al., 2014; Rosell et al., 2014). The crystal structure of the ectodomain of CD98hc docked well into the smaller lobe. The lack of internal structure in the EM map did not allow for docking of a LAT2 model (Figure 8). This is consistent with negative stain cryo-EM, since the heavy metal stain used and visualized in the 2D projections is on the exposed surfaces of the biomolecule (Brenner and Horne, 1959; Ohi et al., 2004; Thompson et al., 2016). In order to explore the interaction of LAT2 and CD98hc, Rosell *et al.* combined *in silico* docking of the CD98hc crystal structure and a homology model of LAT2 with mutagenesis and crosslinking experiments. An extensive dimer interface was proposed, where CD98hc ectodomain almost completely covers the extracellular face of LAT2, interacting predominantly with

hydrophobic residues. This extensive interaction was suggested to be the mechanism by which CD98hc stabilises LAT2 (Rosell et al., 2014).

OBJECTIVES

The objectives of this study were to:

- Exploit published sequence, structural and biochemical knowledge on LeuT-fold transporter and homologues of LAT1 to understand its structure and function. (Chapter 3)
- To develop an expression system and purification protocol suitable for the production of LAT1-CD98hc for biochemical and structural characterisation. (Chapter 4)
- Solve structure of LAT1-CD98hc by cryo-electron microscopy and relate this information to its function. (Chapter 5)

Chapter 2 – Materials and Methods

This chapter describes the methods used to address the objectives of this study and to test hypotheses reported in the literature and arising from the work reported here. The results of the experiments in this chapter are reported in chapters 3 – 5 and discussed in chapter 6.

Prediction of cholesterol binding/interaction sites by sequence analysis

The amino acid sequences for human LAT1 and the *Drosophila melanogaster* dopamine transporter (dDAT) (NCBI accession numbers NP_003477.4 and NP_523763.2 respectively) were aligned using PROMALS3D (Pei et al., 2008) with default settings. The alignment was used to identify residues in cholesterol binding sites I & II of the dDAT that were conserved in LAT1, thus defining putative cholesterol binding sites in LAT1. An alignment of LAT1 orthologous was performed using Clustal O to determine whether the putative cholesterol binding sites are conserved. Orthologues were chosen from *Canis lupus familiaris*, *Bos Taurus*, *Rattus norvegicus*, *Mus musculus*, *Gallus gallus*, *Danio rerio, Drosophila melanogaster*, and *Xenopus tropicalis* (NCBI accession numbers XP_850176.2, NP_777038.1, NP_059049.1, NP_035534.2, NP_001025750.1, NP_001121830.1, NP_001245996.1, and NP_001135465.1 respectively). Annotation and scoring of similarity at each position was done in Jalview. The LAT1 sequence was also submitted to Consurf for conservation analysis, using default settings (Ashkenazy et al., 2016).

The Fuzzpro package of the EMBOSS suite (Rice et al., 2000) was used to search the primary sequence of LAT1 for CRAC/CRAC-like motifs in manner similar to Listowski *et al.*, 2015. The search patterns were defined as [LV]-X(1,5)-Y-X(1,5)-[RK],

[RK]-X(1,5)-Y-X(1,5)-[LV], [LV]-X(1,5)-F-X(1,5)-[RK], and [RK]-X(1,5)-F-X(1,5)-[LV], where (1,5) is one to five amino acids and X is any amino acid. The identified motifs were visualized on the outward facing open model of LAT1, generated and validated as described below, with sites that were within the predicted membrane spanning/facing regions put forward as putative cholesterol interaction/binding sites. The membrane embedded regions of the model were predicted using the PPM webserver (Lomize et al., 2012).

Table 1 - Top 5 hits for LAT1 templates from the HHpred server.

Nr	Hit	Name	Probability	E-value	SS	Cols	Target Length
1	5OQT_A	Amino acid transporter, L-Alanine, Uncharacterized; SLC7, APC, LeuT fold, TRANSPORT; HET: CLR, OLC; 2.86A {Geobacillus kaustophilus (strain HTA426)}	100	2.2e-32	49.9	453	471
2	5J4I_A	Arginine/agmatine antiporter; AdiC, Transporter, Membrane Protein, Transport; 2.207A {Escherichia coli O157:H7}	100	3.1e-31	49.2	445	453
3	3GIA_A	Uncharacterized protein MJ0609; membrane protein, transporter, Cell membrane; HET: D10, BCN; 2.32A {Methanocaldococcus jannaschii}	100	7.5e-31	51.2	438	444
4	4DJK_A	Probable glutamate/gamma-aminobutyrate antiporter; LeuT, glutamate-GABA antiporter, TRANSPORT PROTEIN; 3.097A {Escherichia coli}	100	1.7e-30	49.6	462	511
5	2JLN_A	MHP1; HYDANTOIN, TRANSPORTER, MEMBRANE PROTEIN, NUCLEOBASE-CATION-SYMPORT-1; 2.85A {MICROBACTERIUM LIQUEFACIENS}	99.51	2e-12	40.2	453	501

Comparative modelling and validation of LAT1 in outward facing open and inward facing occluded conformations

The sequence for LAT1 (NCBI accession number NP_003477.4) was submitted to the HHpred server (Soding et al., 2005), to search using default parameters, for homology modelling templates in the PDB. The top five outputs are shown in Table 1, and further information from the PDB and literature is summarized in Table 2, with

templates chosen highlighted in red. The apo outward facing structure of AdiC from *Escherichia coli* and the alanine bound inward facing and occluded structure of the APC transporter from *Geobacillus Kaustophillus*, PDB IDs 5J4I and 5OQT (Figure 9 & Figure 10) respectively, were chosen as templates for modelling LAT1 using MODELLER v9.19 (Webb and Sali, 2016). 10 decoys per template were generated and the decoy with the lowest DOPE (Discrete Optimised Protein Energy) score was carried forward for optimization via the ModRefiner server with a template (Xu and Zhang, 2011). DOPE per residue scores were calculated in MODELLER and Ramachandran plot analysis (Lovell et al., 2003) done for both the best MODELLER decoy from each template before and after submitting to the ModRefiner server (Xu and Zhang, 2011). Structure alignments and annotation of models was performed in Chimera (Pettersen et al., 2004).

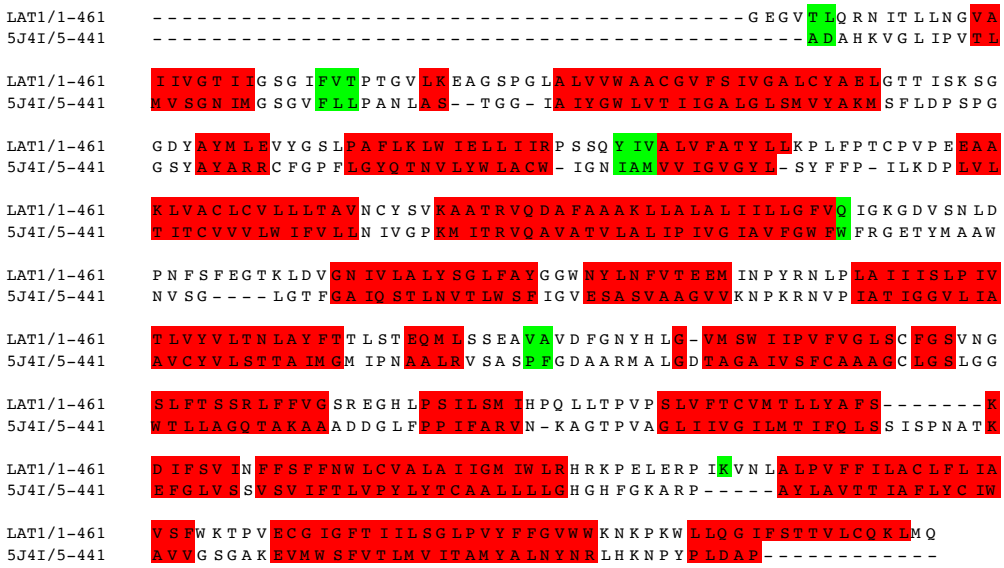

Figure 9 - Sequence alignment of LAT1 and AdiC used for homology modelling. LAT1 sequence is residues 41 – 456 of the canonical sequence. Alpha helices and beta strands are highlighted in red and green respectively as predicted by the JPred server via Jalview (Waterhouse et al., 2009).

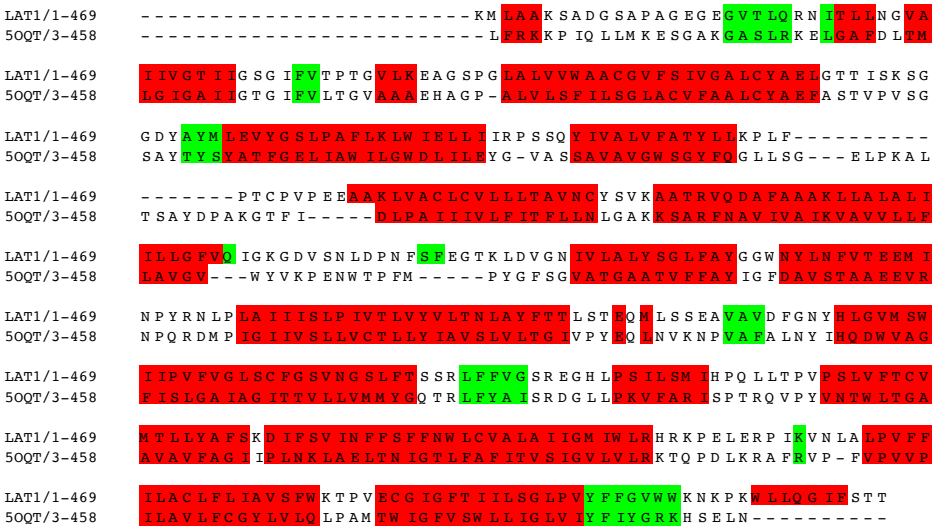

Figure 10 - Sequence alignment of LAT1 and GkApcT used for homology modelling. Alpha helices and beta strands are highlighted in red and green respectively as predicted by the JPred server via Jalview.

Table 2 - Summary of suitable homology templates for modelling LAT1.

Protein	Sequence identity with LAT1(%)	Sequence similarity with LAT1(%)	PDB ID	Resolution (Å)	Conformation
GkApcT	23	33.4	5OQT	2.86	Inward facing occluded/L-Ala
			6F34 (M321S)	3.13	Inward facing occluded/L-Arg
EcAdiC (dimer)	19	25.9	5J4I	2.2	Outward facing open
			5J4N	2.6	Outward facing open/agmatine
			3L1L	3	Outward facing occluded/L-Arg
			3LRB	3.61	Outward facing open
			3NCY	3.2	Outward facing open
			3OB6 (N101A)	3	Outward facing open/L-Arg
MjApcT	20	24.6	3GIA	2.32	Inward facing occluded apo
			3GI8 (K158A)	2.59	Inward facing occluded apo
EcGadC	15	16.2	4DJK	3.09	Inward open
			4DJI	3.18	Inward open

Docking of LAT1 ligands in LAT1 models

The homology models of LAT1 in the apo-outward-open and inward occluded conformations were used for docking after refinement as described above. 3D structures of L-tryptophan, L-phenylalanine, L-isoleucine, L-leucine, L-valine, L-methionine, L-histidine, L-kynurenine and triiodothyronine (T_3) were downloaded from the human metabolome database and those of (S)-2-aminobicyclo-[2,2,1]-heptane-2-carboxylic acid (BCH), (S)-2-amino-3-(4-((7-(3-aminophenyl)naphthalen-1-yl)methoxy)-3,5-dichlorophenyl)propanoic acid (SKN103), (S)-2-Amino-3-(3-((2,4-dicyano-3-(4-(2-(methylamino)-2-oxoethoxy)phenyl)benzo[4,5]imidazo[1,2-a]pyridin-1-yl)-carbamoyl)phenyl)propanoic acid (KMH233) and (S)-2-amino-3-(4-((5-amino-2-phenylbenzo[d]oxa-zol-7-yl)methoxy)-3,5-dichlorophenyl) propanoic acid (JPH203) were generated from SMILES strings in Chem3D 15.1 (Cambridge Soft, Perkin Elmer) (Figure 11). The structures of all ligands were energy minimised in their zwitterion form before docking. Docking for each ligand was performed using AutoDock Vina's web service through the UCSF chimera interface using default parameters. The search volume was defined to exclude the putatively membrane embedded surfaces of the models (Pettersen et al., 2004; Trott and Olson, 2010). The interaction of the best scoring docking pose were visualized and annotated using the Dassault Systèmes BIOVIA's Discovery Studio Visualizer.

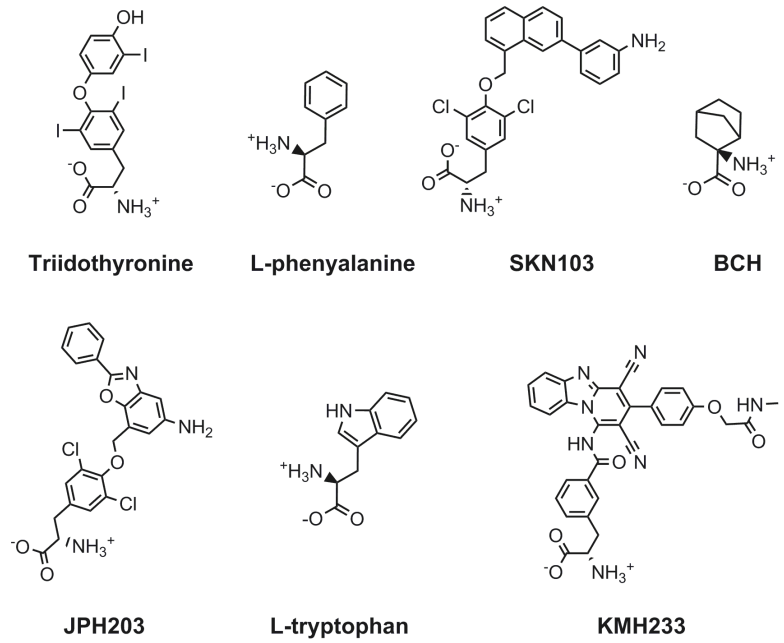

Figure 11 - 2D structures of some of the ligands docked into LAT1 models of the outward open and inward facing occluded conformations.

Cell culture

HEK293 and HEK293SG cells (suspension adapted; N-acetylglucosaminyltransferase I negative cells), were cultured adherently in high glucose Dulbecco's Minimal Essential Medium supplemented with 10 % v/v fetal Bovine Serum and incubated at 37 °C and 5 % CO_2. Suspension cultures were seeded from adherent cultures and maintained at a density of 5 x 10^5 cells mL^{-1} in 1 and 1.5 L spinner flasks at 180 rpm. The suspension culture medium was composed of minimum essential medium, Joklik modification plus 13.4 mM glucose, 24 mM sodium bicarbonate, 10% w/v primatone, 1% w/v pluronic and 5% v/v FBS. Harvesting of the suspension cultures was done every 6 days for HEK293 cells and every four days for the HEK293SG cells. Cell pellets were flash frozen and kept in cryo-storage.

Stable cell-line development

To determine the optimal concentration of G418 for stable cell line generation, nine flasks of HEK293SG cells were seeded at density of 3.33 x 10^5 cells mL^{-1}, each flask containing a medium with a specific concentration of the selection agent G418, ranging from 0 – 800 μg mL^{-1} in increments of 100 μg mL^{-1}. The flasks were observed under the microscope daily for seven days and the growth, morphology and whether or not the cells were still attached, was recorded. The optimal concentration for selecting against G418 susceptible cells was thus determined. For transfection, the cells were seeded at a density of 1 x 10^6 per well and allowed to attach before transfection. For transfection, 7 μL Lipofectamine 2000 in 250 μL optiMEM was mixed with 5 μg pcDNA3.1-LAT1-V5-His6 (Figure 12) in 250 μL optiMEM, at room temperature before adding to the cells 24 hrs after seeding. Cells were transferred to a T25 culture vessel with fresh medium and 600 μg mL^{-1} G418, to select for cells with stable genomic integration of the neomycin resistance selection marker of the plasmid. After expansion of cells to a confluent T175 flask, isolation of single cell derived colonies was performed by a plating a serial dilution from 2000 – 1.25 cells mL^{-1}, such that there was 200 – 0.125 cells per well in a 96 well plate format. 48 single cell clones were expanded up to 6 well plates, at which point frozen stocks and lysates of each clone were prepared for screening by immunoblotting. A LAT1 stably overexpressing cell-line was used as positive control, the signal from which was used to normalize during densitometry, allowing comparison from blot to blot. The highest expressing clone (HEK293SG-LAT1) was identified and expanded up to 1 L suspension culture. Plasmid and control cell-line were provided by Dr David Dickens (Dickens et al., 2013).

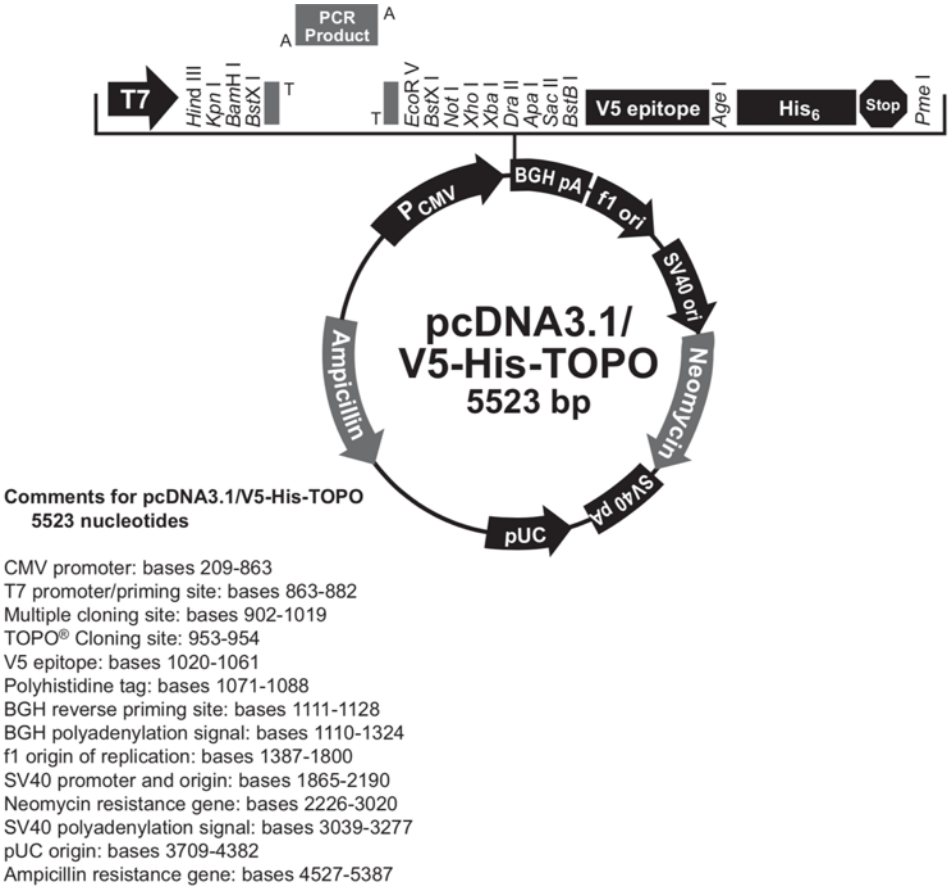

Figure 12 - pcDNA3.1/V5-His TOPO expression vector used for stable cell-line development. The sequence for LAT1 cDNA (SLC7A5, IMAGE clone 5551612) was sub-cloned into this expression vector so that LAT1 protein was produced with a V5 epitope and hexa-histidine tag by Dr David Dickens (Dickens *et al.*, 2013).

Immunoblotting

Cell lysates were prepared in RIPA lysis buffer (25 mM Tris-HCl, pH 7.6; 150 mM NaCl, 1 % sodium deoxycholate; 1 % NP-40; 0.1 % SDS; protease inhibitor cocktail, Sigma) and the sample protein concentrations determined by the detergent compatible protein assay (Bio-Rad). Protein samples were then incubated at room temperature in SDS loading buffer (0.5 M Tris-Cl; 30 % v/v glycerol; 10 % v/v SDS; 0.012 % w/v bromophenol blue) before loading on to 10 % or 12.5 % Tris-glycine SDS polyacrylamide gels. Dithiothreitol or β-mercaptoethanol was included in the loading buffer when reducing conditions were required. 20 – 40 µg total protein was loaded

per well for cell-lysates, 5 µL from each step, for analysis of LAT1-CD98hc purifications, and ColorBurst Electrophoresis marker (220 – 8 kDa, Sigma) for molecular weight estimation. Samples were incubated at room temperature for 30 minutes after mixing with SDS loading buffer. Gels were run at 200 V for 1 hr and proteins transferred from gel to PVDF membranes by wet blotting at 100 V for 1.5 hrs or by semi-dry blotting using Invitrogen's iBlot. The PVDF membranes were blocked in 0.5 % w/v semi-skimmed milk in Tris Buffered Saline with 1 % v/v tween (TBST) (25 mM TrisCl, 150 mM NaCl, 20 mM KCl, pH 7.4). Incubation with anti-His_6 mouse monoclonal (1:1000; Abcam), anti-LAT1 rabbit polyclonal (1:1000) antibodies in TBST, was performed to probe for LAT1 or anti-CD98hc rabbit polyclonal antibody (1:1000) to probe for CD98hc (1:1000; H300 Santa Cruz). Visualisation was done using anti-mouse or anti-rabbit HRP conjugated secondary antibodies by chemiluminescence and film or CCD camera (GE Image Quant or Bio-Rad ChemiDoc).

Radio ligand transport assays

Functional assays were performed using tritium labelled levodopa (^{3}[H]-L-DOPA) as a tracer at 0.15 µCi/mL in transport medium (1 µM unlabelled L-DOPA; 25 mM HEPES, pH 7.4; Hank's Buffered Salt Solution (HBSS); 0.1 % w/v BSA). The various HEK293 cell-lines were seeded at a density of 1 x 10^6 cells/mL, 24 hours before the assay. Medium was aspirated off and cells washed with HBSS, before 1 mL transport medium, warmed to 37 °C was added. After 3 minutes, the transport medium was aspirated off and transport stopped by washing cells with ice cold HBSS three times. Cells were lysed by incubating at 37 °C in 5% w/v sodium dodecyl sulphate for 30 minutes. The amount of radiation in the lysates was measured by liquid scintillation

in disintegrations per minute which were used to calculate the amount of L-DOPA taken up per million cells in pmoles.

Protein purification

HEK293-LAT1 or HEK293SG-LAT1 cell pellets were retrieved from cryo-storage and thawed on ice in 5 mL lysis buffer per gram of wet biomass (10 % v/v glycerol; Dulbecco's phosphate buffered saline, pH 7; Pierce protease inhibitor tablets, no EDTA). The cell suspension was lysed by TissueRuptor (Qiagen) at approximately 24 000 rpm for 2 minutes followed by six cycles of sonication (20 secs on/off). Cell nuclei and debris were removed by centrifugation between 23,500 *g* for 20 minutes. The supernatant was then ultra-centrifuged at 206,000 *g* for 1.5 hrs to isolate the membrane fraction from the soluble cytosolic fraction. The membranes were suspended by dounce homogeniser for solubilization in TBS1 (1.5 % w/v n-dodecyl beta maltoside (DDM); 0.32 % w/v cholesteryl hemisuccinate (CHS); 0.1 % w/v lauryl maltose neopentyl glycol (LMNG); 20 mM Tris-Cl; 300 mM NaCl; 10 % w/v glycerol, pH 8). Solubilisation was performed overnight, concomitantly with V5 affinity gel (Biotools) incubation, 10 µL resin slurry was used for 1 mL solubilisation suspension. The fraction of the solubilization suspension not bound to the affinity gel, was removed by decanting the supernatant after centrifugation at 1500 *g* for 2 minutes. Resin was then washed in SEC1 buffer (0.02 % w/v DDM; 0.0013 % w/v LMNG; 0.00426 % w/v CHS; 100 mM Tris-Cl; 300 mM NaCl; 10 % w/v glycerol, pH 8) until A_{280} of used wash buffer was ~ 0.2. LAT1-CD98hc was eluted by incubating the washed resin with 400 µg mL^{-1} V5 peptide for 30 minutes. Further purification was performed by size exclusion chromatography on a Superdex 200 10/300 column. The

purified protein was concentrated using a 100 kDa cut-off polyethersulfone centrifugal filter and the pure protein concentration calculated using the molar extinction co-efficient at 280 nm in water, of 164750 M^{-1} cm^{-1}, calculated from the combined primary sequence of LAT1 and CD98hc by ExPASy ProtParam (Gill and von Hippel, 1989). In the final year V5 affinity gel was no longer available from Biotools and the Sigma version was used. Sigma's gel had at least 10 times less of capacity of the Biotools gel.

Determining optimal conditions for CD98hc deglycosylation

LAT1-CD98hc was purified from 6 g HEK293 LAT1 stably overexpressing cells and separately from 6.5 g of HEK293SG stably overexpressing cells, as described above. After final size exclusion chromatography step, LAT1-CD98hc containing samples were concentrated to 1 mg ml^{-1} for use in deglycosylation trials. Reaction conditions were set up as shown in Table 3, using 10 µL volumes. Deglycosylation enzymes and deglycosylation buffer were purchased from New England Biolabs.

Determining the effect of sodium aurothiomalate hydrate on the reduction of the inter-subunit disulphide bond of LAT1-CD98hc

2.6 x 10^6 HEK293-LAT1 cells were lysed in 300 µL RIPA or protein purification lysis buffer. RIPA lysis buffer was supplemented with 0, 1 or 2 mM sodium aurothiomalate hydrate (ATM) and the purification lysis buffer with 0, 1, 2, 5, 10 or 20 mM ATM. The amount of protein in the lysates was determined by DC assay and immunoblotting for LAT1-V5-His_6 was performed as described above. Densitometry was performed on the resulting blots using Image studio Lite 5 (LI-COR biosciences).

Table 3 - Experimental conditions trialed for deglycosylation of CD98hc.

	Enzyme/Incubation conditions	Buffer
LAT1-CD98hc from HEK293 cells/PNGase F		
1	500 units PNGase/27 °C/ 2 hrs	Purification buffer
2	500 units/PNGase/37 °C/1 hr	X1 glycoprotein denaturing buffer/X1 glyco2 buffer/0.7 % NP40
3	0 units PNGase/27 °C/2hrs	Purification buffer
LAT1-CD98hc from HEK293SG cells/EndoH		
1	0 units EndoH/4 °C /overnight	X1 glycobuffer 3/X1 glycoprotein denaturing buffer
2	1000 units EndoH/ 4 °C/ overnight	X1 glycobuffer3
3	1000 units EndoH/ 4 °C/ overnight	X1 glycobuffer 3/X1 glycoprotein denaturing buffer
4	1000 units EndoH/ 27 °C/ 2hrs	X1 glycobuffer 3/X1 glycoprotein denaturing buffer
5	1000 units EndoH/ 27 °C/ 2hrs	X1 glycobuffer3
6	1000 units EndoH/37 °C/1 hrs	X1 glycobuffer 3/X1 glycoprotein denaturing buffer
7	1000 units EndoH/37 °C/1 hrs	X1 glycobuffer3
8	2000 units EndoH/27 °C/6 hrs	X1 glycobuffer 3/X1 glycoprotein denaturing buffer
9	2000 units EndoH/27 °C/6 hrs	Purification buffer
10	2000 units EndoH/27 °C/6 hrs	X1 glycobuffer 3/X1 glycoprotein denaturing buffer
11	2000 units EndoH/27 °C/6 hrs	Purification buffer
12	4000 units EndoH/37 °C/6 hrs	X1 glycobuffer 3/X1 glycoprotein denaturing buffer
13	4000 units EndoH/37 °C/6 hrs	Purification buffer

The fraction of LAT1 in monomeric form was calculated by dividing the signal below the 45 kDa molecular weight marker by the sum of the signal below 45 kDa and above 100 kDa.

Optimisation of detergent concentration, detergent to protein ratio and DDM to CHS ratio in membrane solubilisation stage of protein purification

Membranes were prepared from HEK293SG-LAT1 cells as described above, with the addition of 1 mM ATM to the lysis buffer, then suspend in solubilisation buffers with the detergent concentrations shown in Table 4. For each of experimental condition, 407 mg of HEK293SG-LAT1 membranes were used. The detergent to protein ratio was varied by keeping constant the concentration of detergent at 0.9% w/v DDM, 0.06% w/v LMNG, 0.19% w/v CHS, while adjusting the solubilisation volume as required. To vary the DDM: CHS ratio as shown in Table 4. DDM and LMNG concentrations were kept constant at 0.9% w/v and 0.06% w/v respectively. Samples were agitated at 4 °C with 96 µL anti-V5 affinity gel overnight. LAT1-CD98hc was eluted from the resin using V5 peptide and analysed on a superdex200 10/300 GL size exclusion column.

Optimisation of size-exclusion buffer for protein purification

Cell membranes were isolated from HEK293SG-LAT1 cells as described above but in the presence of 1 mM ATM and solubilised in the modified TBS1 (0.9% w/v DDM, 0.06% w/v LMNG, 0.19% w/v CHS; 20 mM Tris-Cl; 300 mM NaCl; 10 % w/v glycerol, pH 8). After incubation with solubilized membranes, the V5 affinity gel was washed with SEC1 buffer supplemented with 50 mM leucine, LAT1-CD98hc eluted from the gel and analysed by size exclusion chromatography in the same buffer. A control sample was prepared using SEC1 without leucine. The effect of leucine on the thermal stability of the purified HAT was determined by applying heat stress at 60 °C

Table 4 - Experimental conditions tested during the optimization of the solubilization stage of the purification.

Effect of varying detergent concentration	
Condition	**Detergent concentration (% w/v)**
1	0.3 DDM, 0.02 LMNG, 0.06 CHS
2	0.6 DDM, 0.04 LMNG, 0.13 CHS
3	0.9 DDM, 0.06 LMNG, 0.19 CHS
4	1.2 DDM, 0.08 LMNG, 0.26 CHS
5	1.5 DDM, 0.1 LMNG, 0.32 CHS
Effect of varying DDM: CHS ratio	
Condition	**DDM/CHS (mg/mg)**
1	1.67
2	2.50
3	3.33
4	4.74
5	9.47
Effect of carrying detergent: protein ratio	
Condition	**DDM/protein (mg/mg)**
1	0.25
2	0.5
3	1
4	1.5
5	2

for 10 minutes before analysing by size exclusion high pressure liquid chromatography (SE-HPLC) as described below but with column equilibrated with SEC1 buffer without leucine.

In order to determine the optimal detergent concentration in the SEC buffer, LAT1-CD98hc samples were prepared in SEC buffers of increasing detergent concentrations, ranging from 5 – 15 times greater than SEC1 buffer detergent concentration, (see Table 5) while leucine concentration was kept constant at 50 mM This analysis was performed on the Agilent infinity 1260 high pressure liquid chromatography system using a BIO-SEC5 column (1000 $Å^3$, 4.3x300 mm)

equilibrated with SEC2 buffer (0.1 % w/v DDM; 0.02 % w/v CHS; 0.007 % w/v LMNG; 100 mM Tris-Cl; 300 mM NaCl; 10 % w/v glycerol, pH 8). Once the optimal detergent concentration had been determined another LAT1-CD98hc sample was prepared at the optimal concentration and the sample concentrated to 3 mg mL^{-1}. 20 µl samples were taken for analysis at 0.5; 1; 1.5; 2.1 and 2.9 mg/mL and these were analysed by SE-HPLC. The peak area of the major peak in the chromatogram was calculated by integration, plotted against protein concentration, and fit to a linear regression passing through the origin.

Table 5 - Experimental conditions tested during the optimization of the solubilization stage of the purification.

Condition	Detergent concentration (% w/v)
1	0.1 DDM; 0.02 CHS; 0.007 LMNG
2	0.15 DDM; 0.03 CHS;0.01 LMNG
3	0.2 DDM; 0.04 CHS; 0.01 LMNG
4	0.3 DDM; 0.06 CHS; 0.02 LMNG

Characterisation of the kinetic and thermodynamic stability of LAT1-CD98hc by SE-HPLC

LAT1-CD98hc was purified in SEC1 buffer and the fractions corresponding to the heterodimer were pooled and concentrated to 1 mg mL^{-1} immediately after size-exclusion and analysed by SE-HPLC. The SE-HPLC analysis was repeated after 3 and 7 days to determine the stability of purified LAT1-CD98hc at 4 °C over time. To determine the thermal stability of the HAT, in the presence or absence of 50 mM leucine in SEC1 buffer, 12 µL of purified protein at a concentration between 0.3 – 0.5 mg mL^{-1} was incubated at a range of temperatures for 10 mins. Samples in SEC1

buffer without leucine were heated to temperatures between 4 – 80 °C and samples in SEC1 buffer with leucine between 4 – 100 °C. Each sample was heated in duplicate or triplicate at the various temperatures. 9 µL of each sample was injected and analysed using the BIO-SEC5 HPLC column. The heterodimer eluted between 6.5 – 10 minutes or 15 – 20 minutes retention time, when the samples were run at 0.2 mL min^{-1} or 0.4 mL min^{-1} respectively. The peak height was normalized by dividing by the peak area and expressed as a fraction of the normalized peak height at 4 °C, which is here referred to as the relative peak intensity. Relative peak intensity was plotted against temperature and the data analysed by a non-linear regression to the Boltzmann sigmoidal function using GraphPad Prism 5. All SE-HPLC analysis was performed as described above.

Cryo-EM data collection and processing

Cryo-EM data were collected at the Medical Research Council's Laboratory of Molecular biology (LMB), Astbury Biostructure Laboratory (ABSL) at the University of Leeds and the Electron Biology Imaging Centre (eBIC) at the Diamond Light Source, Didcot. The quality of the data obtained with each collection was used to inform modifications to the sample preparation and or data collection in order to improve data quality. LAT1-CD98hc was purified as described above but with modification to the size exclusion buffer mentioned in Table 6 which also summarises the data collection parameters for each data set. Data processing was done in RELION versions 2.1 and or 3 (Figure 13) (Scheres, 2012b; Zivanov et al., 2018).

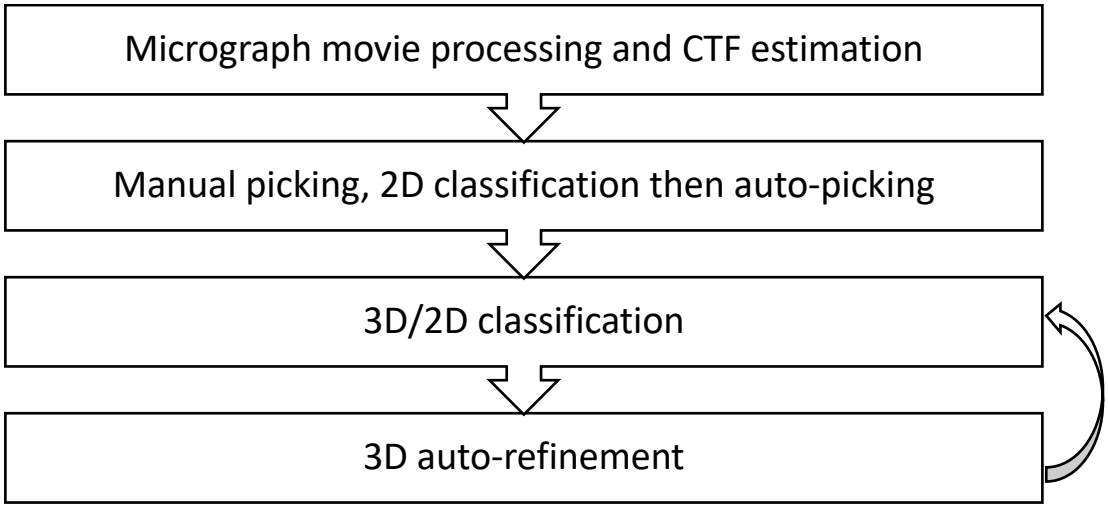

Figure 13 - General single particle cryo-EM data processing workflow.

Interpretation of Coulomb potential maps produced by single particle reconstruction

EM map resulting from processing of dataset 4, was tested for consistency with the crystal structure of the ectodomain of CD98hc (PDB ID: 2DH2) by docking the crystal structure into the EM map, using Chimera, after filtering the crystal structure to 12 Å. This was done by segmenting the map using the Segger (v1.9.4) tool with the map at a threshold of 0.00872 and the "Smoothing steps" parameter in Segger was set to 10 steps, while other options were set to default (Pintilie et al., 2010). An apo-out open model of LAT1 was docked into the map after segmenting at the same threshold but "Smoothing steps" set to 3. Several segments were grouped to form a single segment that contained the density at the centre of the larger lobe of the map. The model was fit after filtering to 12 Å. After docking CD98hc ectodomain, residues at the interface of the heterodimer were defined loosely as the residues in one monomer that were 10 Å from the other (Table 7)

Table 6 - Summary of cryo-EM data collection.

Cryo-EM data collection		
Data set	**Protein concentration/Buffer/Grid type**	**Microscope and other data collection parameters**
Exploratory Aug 2016	- 1.1 mg mL^{-1} - 0.1% DDM: CHS: LMNG and 10% glycerol - 1.1 mg ml^{-1} - 0.01% DDM: CHS: LMNG	Krios LMB,300 kV, K2 Gatan detector, 4 micrographs per sample, 1.3 Å/px,
1 Feb 2017	- 1.1 mg ml^{-1} - 0.1% DDM: CHS: LMNG and 50 mM leucine and 10% glycerol - Quantifoil 2/2	Krios 1 at ABSL, Leeds, 300 kV, Falcon III detector, 2452 micrographs, 1.07 Å/px, 2.25 e^- per frame
2 Apr 2017	- 1.1 mg mL^{-1} - 0.01% DDM: CHS: LMNG, 50 mM leucine, and 5% glycerol - Quantifoil 1.2/1.3	Krios 2 at ABSL, Leeds, 300 kV, K2 Gatan detector, 3349 micrograph movies, 1.07 Å/px, 40 frames, 2.18 $e^-/Å^2$ per frame
3 Aug 2017	- 1.4 mg mL^{-1} - 0.01% DDM: CHS: LMNG 50 mM leucine, and 5% glycerol - Quantifoil 1.2/1.3	Krios (M06) at eBIC, 300 kV, K2 Gatan detector, Volta phase plate, 1200 micrographs movies, 1.08 Å/px, 40 frames, 1.4 $e^-/Å^2$ per frame
4 Sep 2017	- 2.3 mg mL^{-1} - 0.01% DDM: CHS: LMNG, and 0% glycerol - Quantifoil 1.2/1.3	Krios (M06) at eBIC, 300 kV, K2 Gatan detector, Volta phase plate, 2390 micrographs movies, 1.06 Å/px, 40 frames, 1.27 $e^-/Å^2$ per frame

Table 7 - Predicted dimer interface residues based on EM density map docking of CD98hc ectodomain crystal structure and apo-out open LAT1 model.

Putative HAT interface residues		
	LAT1	**CD98hc ectodomain**
Residue number	73, 75, 76, 77, 78, 79, 80, 81 ,82, 164, 225, 226, 227, 228, 229, 230, 231, 235, 236, 237, 242, 245, 300, 301, 302, 303, 304, 305, 306, 307, 309, 310,314, 318	109, 110, 111, 112, 113, 114, 115, 427, 428, 429, 430, 431, 432, 433, 434, 435, 436, 437, 438, 439, 455, 456, 457, 458, 459, 460, 461, 527, 528

The sequence of LAT1 and LAT2 (Uniprot ID: Q9UHI5) were aligned and the conservation of residues at the predicted interface of LAT2 and CD98hc ectodomain as well as the residues used in the crosslinking experiments performed for the validation of the docking of LAT2 and CD98hc ectodomain by Rosell *et al.*, 2014 (Table 8). Based on the sequence analysis, residues in LAT1 corresponding to those used in crosslinking LAT2 to CD98hc were identified and used as distance restraints for the docking of LAT1 and CD98hc ectodomain (PDB ID 2DH2) using the ClusPro server (Figure 14) (Kozakov et al., 2017).


```
{"required":1,"groups":[{"required":3,"restraints":
[{"type":"residue","dmax":14.3,"dmin":
3.5,"rec_chain":"A","rec_resid":"220","lig_chain":"A","lig_resid":"4
12"},{"type":"residue","dmax":10.5,"dmin":
6.3,"rec_chain":"A","rec_resid":"244","lig_chain":"A","lig_resid":"5
05"},{"type":"residue","dmax":10.5,"dmin":
6.3,"rec_chain":"A","rec_resid":"450","lig_chain":"A","lig_resid":"5
05"}]},{"required":2,"restraints":[{"type":"residue","dmax":
14.3,"dmin":
3.5,"rec_chain":"A","rec_resid":"220","lig_chain":"A","lig_resid":"1
51"},{"type":"residue","dmax":14.3,"dmin":
3.5,"rec_chain":"A","rec_resid":"325","lig_chain":"A","lig_resid":"1
51"},{"type":"residue","dmax":17.5,"dmin":
3.5,"rec_chain":"A","rec_resid":"220","lig_chain":"A","lig_resid":"1
95"},{"type":"residue","dmax":15.5,"dmin":
3.5,"rec_chain":"A","rec_resid":"324","lig_chain":"A","lig_resid":"1
95"},{"type":"residue","dmax":14.3,"dmin":
3.5,"rec_chain":"A","rec_resid":"401","lig_chain":"A","lig_resid":"4
87"}]}]}
```


Figure 14 - Distance restraints as used in docking of LAT1 apo-out open model with CD98hc ectodomain crystal structure using the ClusPro server. Constraints shown in json format as used in docking, the outward open model of LAT1 was designated the receptor and the crystal structure of the ectodomain of CD98hc the ligand.

A two-body multibody refinement was performed using the final 3D auto-refinement from dataset 4. The density presumed to correspond to the ectodomain of CD98hc was defined as body 1 and the micellar density, body 2. Density maps for mask creation were created by segmenting the 12 Å map using Segger into two densities corresponding to each body to be refined, the map segments were Gaussian filtered using the "Volume Filter" tool and resampled using "vop" command onto the same grid as the 12 Å map. These map segments were then low pass filtered to 20 Å and 11 Å soft edges added, in RELION 3 to create the masks used in the refinement Figure 15. The "body.star" file was setup as described by Nakane *et al.*, 2018. Principle component analysis was performed on the orientations of both bodies and the "eigen movies" for the first three eigen vectors were written out as a series of volumes in MRC format, describing the relative motions of the two bodies as described by these vectors. The "Volume series" tool of Chimera was used to visualise the movies and the "Fit in map" tool used to fit CD98hc ectodomain crystal structure and the outward open conformation of LAT1 in each of the volumes before saving each as a pdb file to be used for ensemble analysis using Chimera's "MD movie" tool.

Table 8 - Residues predicted at the interface of LAT2 and CD98hc ectodomain from in silico docking and the corresponding residues in LAT1.

Similarity scoring was done using Jalview, the greater the value of the score, the greater the similarity between the residues at that position. Identical residues are not assigned a score. The Consurf score increases with decreasing variability at that position between orthologues, indicating the degree of conservation.

LAT2	LAT1	Similarity score	LAT1 Consurf Score	<10 Å in LAT1 EM structure
K63	T73	7	9	No
G64	G74		9	No
E67	K77	7	1	No
F155	F161		4	No
P157	P167		6	Yes
N221	F231	6	3	Yes
F223	F233		8	Yes
L239	Y248	7	8	No
L297	L306		5	Yes
N300	E309	7	1	Yes
A301	A310		9	Yes
A303	A312		9	No
M384	I393	9	6	No
Y385	F394	9	2	No
Y390	F399	9	5	No
F393	F402		7	No
F440	V449	7	5	No
L442	F451	8	5	No
W443	W452		2	No

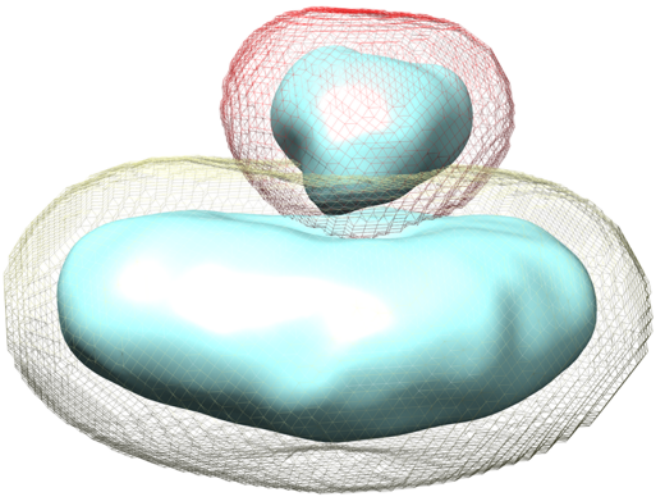

Figure 15 - Soft masks used for multibody refinement. The density map from the final 3D auto-refinement is shown in cyan, threshold 0.00871. The mask for body 1 is shown as a mesh surface in red and the mask for body 2 as a mesh surface in yellow.

Statistical tests

Statistical tests were performed in GraphPad 7. T-tests were done for pairwise comparison were tested using two tailed t-tests and one-way ANOVA performed for multiple comparisons. Linear regression analysis was performed for LAT1 model docking data presented in Chapter 3.

Chapter 3 - Sequence analysis, comparative modelling and docking of LAT1

Structural modelling of LAT1 has relied greatly on its bacterial homologues, this chapter reports novel insights into the role membrane lipids the in function of LAT1, gained from exploiting the published structure of a eukaryotic transporter of the LeuT-fold. Also, in this chapter are insights on inhibitor binding by docking of homology models of LAT1 in the outward facing open and inward facing occluded conformations.

PREDICTION OF MODULATORY EFFECT AND BINDING OF CHOLESTEROL TO LAT1 BY SEQUENCE ANALYSIS AND COMPARATIVE MODELLING

Crystal structures of the *Drosophila melanogaster* dopamine transporter were solved in the outward open conformation with cholesterol (site I) and CHS (site II) bound (Penmatsa et al., 2013; Wang et al., 2015). Residues at the interface with cholesterol at site I were, V34, L37, L38, I41 on transmembrane helix (TM) 1, W266, L270, Y273, L276, L277 on TM 5, and L347, I351 and I358 on TM 7. The interface of binding site II and CHS was composed of residues L73, A74, L66, Y69 on TM2, Y342, L346, L350, A354, F357 on TM7, and Y518 and W519 on TM11 (Penmatsa et al., 2013; Wang et al., 2015). Alanine was substituted for valine at position 74 in the construct used for crystallization. It was presumed to facilitate crystallization by thermodynamically stabilizing the transporter. When aligned to the sequence of human LAT1, 91% of the residues in binding site I were conserved, with either identical residues or ones of similar physicochemical properties. 70% of residues in binding site II were conserved (Figure 16).

If the residues conserved between human LAT1 and dDAT, at dDAT's interfaces with cholesterol and CHS in the crystal structures were required for the

function of LAT1, then they would also be conserved among the orthologues of LAT1. To test this hypothesis an alignment of 8 LAT1 orthologues from different species, including *H. sapiens*, domesticated species such as *C. familarus* and *B. taurus* and model organisms such as *M. musculus* and *D. rerio* was performed. Residues in both putative cholesterol binding sites were conserved across the orthologues suggesting functional relevance (Figure 17).

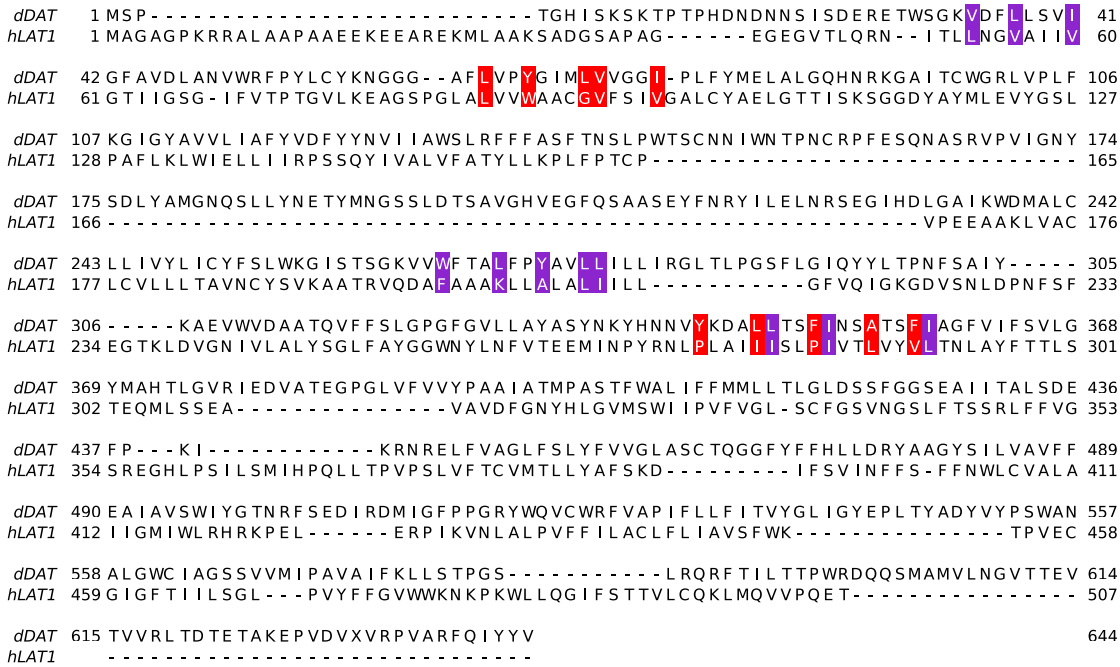

Figure 16 - Sequence alignment of dDAT and LAT1. The sequence of human LAT1 was aligned with the sequence of dDAT. Residues that were observed interacting with cholesterol in the crystal structures of dDAT were annotated, purple and red for binding sites I and II respectively. Annotation and similarity scoring were done using Jalview. Image adapted from Dickens et al., 2017.

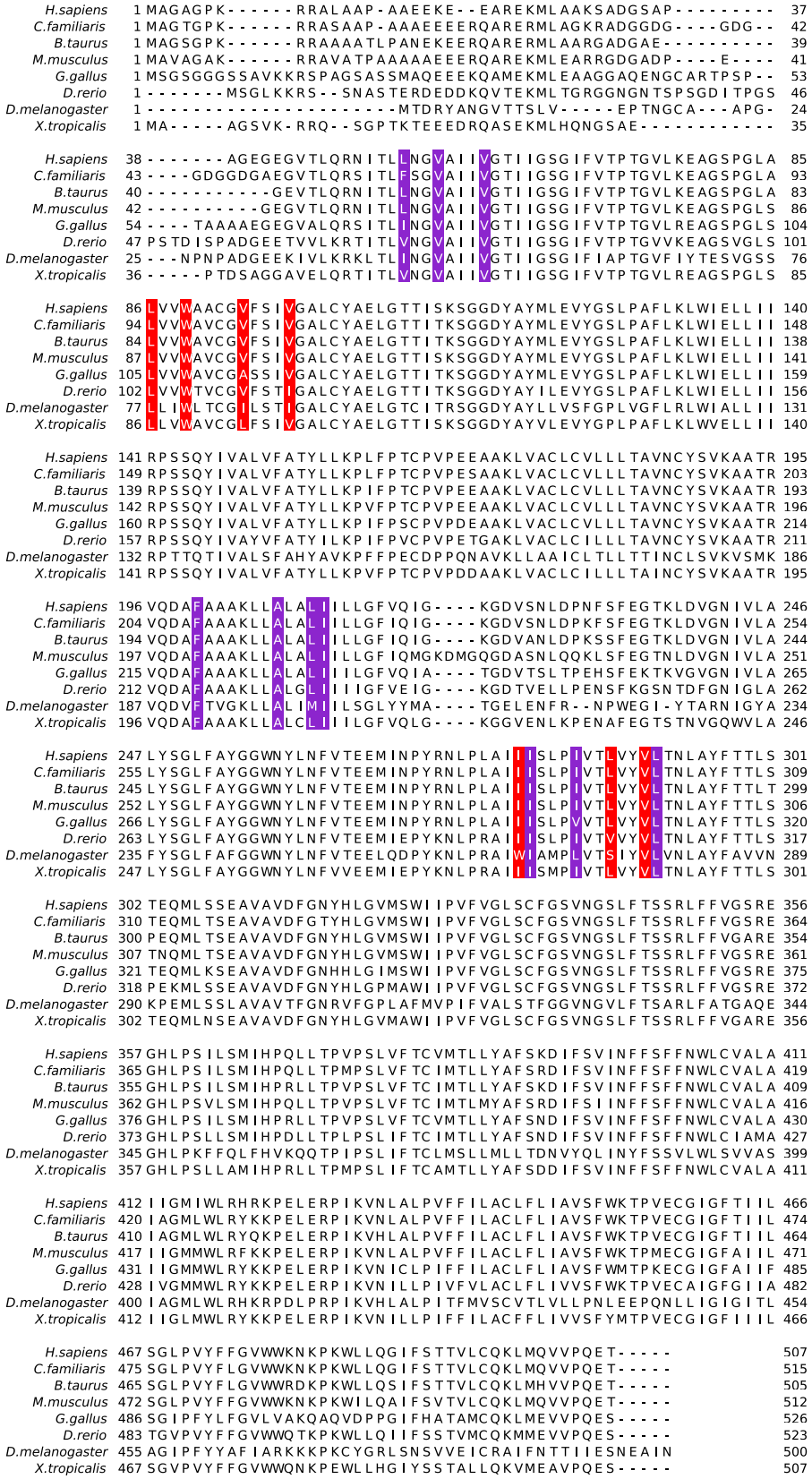

Figure 17 - Sequence alignment of LAT1 orthologues. LAT1 sequences from 7 different organisms were aligned with the human sequence and residues of the putative cholesterol binding sites were annotated, purples and red respectively for site I and II respectively. Annotation and similarity scoring were done using Jalview. Image adapted from Dickens et al., 2017.

Another question was whether these conserved residues were located in LAT1 in a manner similar to that of dDAT, forming similar putative binding sites for cholesterol. To address this, 10 homology models per template of LAT1 were generated using MODELLER based on sequence alignments to and the structures of *E. coli* AdiC in the apo outward facing conformation and the alanine bound inward facing and occluded structure of the APC transporter from *G. Kaustophillus*, PDB IDs 5J4I and 5OQT respectively (Figure 9; Figure 10). The model with lowest overall DOPE (Discrete Optimized Protein Energy) score was then further improved by ModRefiner. The DOPE score is statistical potential derived from experimental structures deposited in the PDB, it is a measure of how close to the native fold a predicted structure is, the lower the score the closer to the native fold (Shen and Sali, 2006). ModRefiner optimises the global fold of predicted structures by subjecting them to an atomic level energy minimization, and as a result the global DOPE score and stereochemistry of the outward facing open and inward facing occluded conformations were improved (Table 9) (Xu and Zhang, 2011). The local quality of the models was assessed by plotting DOPE per residue score or DOPE score profile, smoothed over a 15 residues window, against the alignment position. Both the best models of outward facing and occluded conformation of LAT1 had DOPE score profiles similar to their templates, indicating the quality alignments used in the modelling were good. There were some regions of high DOPE score relative to the template, namely alignment positions 216 – 229 (A175 – I188) in the inward facing model and alignment positions 93 – 106 (C92 – L106), 191 – 195 (K191 – R195) in the outward open conformation (Figure 18). The conserved residues composing the proposed cholesterol binding sites, L53, V56, V60, F200, A207, L210, I211, I280, I284,

and L291 in site I and L86, W89, V94, V98, I279, L287, and V290 in site II, are adjacent to some of these high local DOPE score regions in the models of LAT1 generated (Figure 19) thus limiting the conclusions that could be drawn from the models particularly with respect to the docking of cholesterol. The models do allow for the inference that the proposed binding site residues are similarly organised and located as in dDAT (Figure 19).

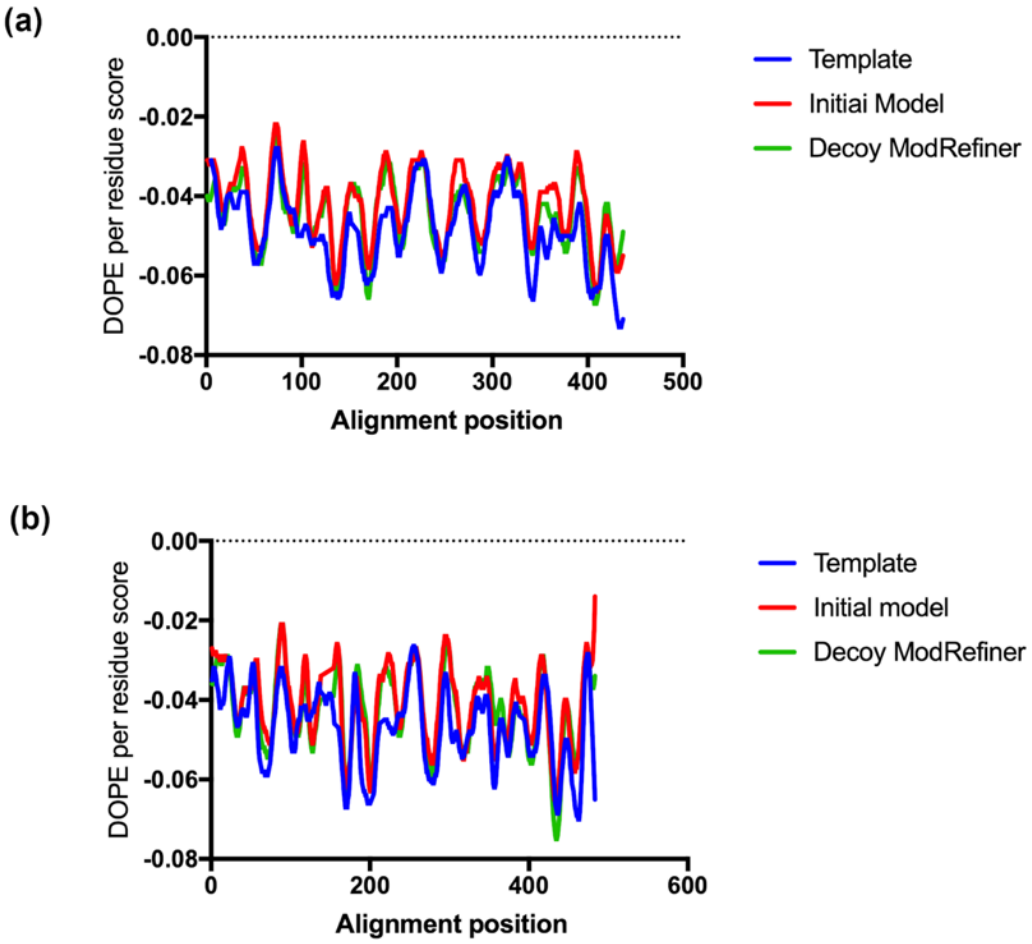

Figure 18 – Quality assessment of local structure prediction for LAT1 models before and after refinement by ModRefiner. The DOPE score profile of the outward open model is shown in a) and that of the inward facing conformation in b). The outward facing open conformation of LAT1 was modelled using EcAdiC and the inward facing occluded conformation GkApcT as templates and their DOPE score profiles are also given for comparison.

Table 9 - Global DOPE scores and dihedral angle analysis for homology modelling.

Ramachandran plot analysis values are given as number of residues in favoured/ allowed/outlier regions of the Ramachandran plots.

Outward facing open conformation		
Model	**DOPE score**	**Ramachandran Plot Analysis (%)**
EcAdiC	-64233.848	
Initial model	-62046.527	94.7/3.6/1.8
ModRefiner model	-65038.004	97/2.4/0.6
Inward facing occluded conformation		
GkApcT	-73368.617	
Initial model	-62435.633	94/3.6/2.4
ModRefiner model	-64841.848	95.9/2.1/1.9

Given the similarity in fold and conservation of residues in the cholesterol binding site, it was reasonable to determine what effect, if any, membrane cholesterol had on the function of LAT1 in cells. Total cholesterol depletion protocols using methyl-β-cyclodextrin in HEK293 cells stably overexpressing LAT1, were recently established to determine the effect of cholesterol depletion on the kinetics of LAT1 mediated L-DOPA uptake (Dickens et al., 2017). After cholesterol depletion, the V_{max} of LAT1 mediated transport decreased significantly ($P<0.05$) from 13,925 ± 923 to 8,506 ± 684 pmoles/million cells/min. The K_m however did not change significantly, from 200 ± 78 μM before depletion to 148 ± 22 μM after (Dickens et al., 2017). Control experiments were setup to ensure that these observed changes were not due to cholesterol depletion induced changes in the localization of LAT1-CD98hc at the plasma membrane. Another possible explanation for the reduced activity of LAT1 observed in these experiments are changes in membrane fluidity, which cholesterol is known to regulate (Mouritsen and Zuckermann, 2004). Based on the structural homology shared with dDAT as explored here, the preferred hypothesis is

that cholesterol allosterically modulates the transporter, increasing the activity of the HAT without significantly changing its affinity for substrate L-DOPA. It is also possible that if LAT1-CD98hc interacts with cholesterol in the plasma membrane, it does not do so via the dDAT homologous sites noted. To explore additional sites that may interact, the sequence of LAT1 was searched for Cholesterol Recognition/Interaction Amino Acid Consensus (CRAC) and CRAC-like motifs (CARC). Thirty-one such motifs were identified with some overlap between many of them (Table 10). Using the model of the outward open conformation of LAT1, and visual inspection it was suggested that 8 of the predicted CRAC/CARC motifs were plausible membrane cholesterol binding sites. These were neither located on intra– or extracellular loops nor were they in the core of the protein, where presumably membrane cholesterol could not access them. The putative interaction sites identified were located at positions 382/385 – 391, 182/185 – 191, 195 – 205/206 and 210 – 221, in the primary sequence (Figure 20). Interestingly positions 195 – 205/206 and 210 – 221, overlap with dDAT homologous binding site I residues A207, L210 and I211.

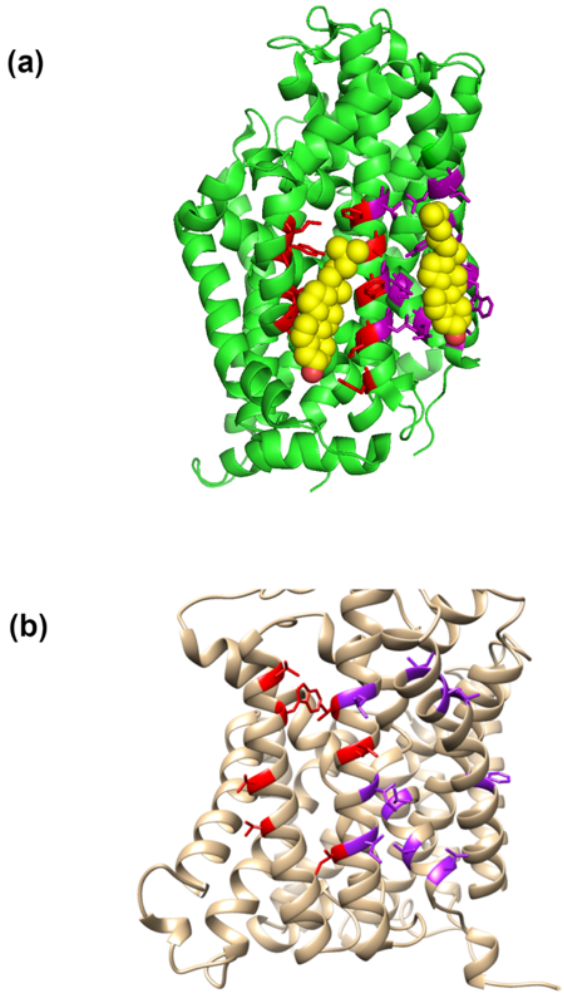

Figure 19 - Putative cholesterol binding sites on 3D model of LAT1. Residues in binding site I are shown in purple and those for site II are shown in red. a) Crystal structure of dDAT (PDB ID: 4PXF) with bound cholesterol molecules shown in spheres. b) Homologous residues on outward open conformation model of LAT1. Adapted from Dickens et al., 2017.

Table 10 - CRAC/CARC motifs identified in the primary sequence of LAT1.

Potentially membrane cholesterol accessible motifs are highlighted with colours corresponding to those used to annotate their sequence on the out open conformation of LAT1 in Figure 20.

Fuzzpro search pattern	Position	Sequence
[LV]-X(1,5)-Y-X(1,5)-[RK]	385 - 391	LLYAFSK
	382 - 391	VMTLLYAFSK
	185 - 191	VNCYSVK
	182 - 191	LTAVNCYSVK
	151 - 158	VFATYLLK
	150 -158	LVFATYLLK
[RK]-X(1,5)-Y-X(1,5)-[LV]	141 - 148	RPSSQYIV
	141 - 150	RPSSQYIVAL
	141 - 151	RPSSQYIVALV
	112 - 121	KSGGDYAYML
	112 - 123	KSGGDYAYMLEV
[RK]-X(1,5)-F-X(1,5)-[LV]	391 - 396	KDIFSV
	348 - 352	RLFFV
	195 - 205	RVQDAFAAAKL
	195 - 206	RVQDAFAAAKLL
	158 -166	KPLFPTCPV
[LV]-X(1,5)-F-X(1,5)-[RK]	471 - 479	VYFFGVWWK
	469 - 479	LPVYFFGVWWK
	449 - 453	VSFWK
	446 - 453	LIAVSFWK
	386 - 391	LYAFSK
	385 - 391	LLYAFSK
	349 - 355	LFFVGSR
	339 - 348	VNGSLFTSSR
	227 - 237	LDPNFSFEGTK
	214 - 221	LGFVQIGK
	213 - 221	LLGFVQIGK
	210 - 221	LIILLGFVQIGK
	196 - 204	VQDAFAAAK
	150 - 158	LVFATYLLK
	148 - 158	VALVFATYLLK
	127 - 132	LPAFLK

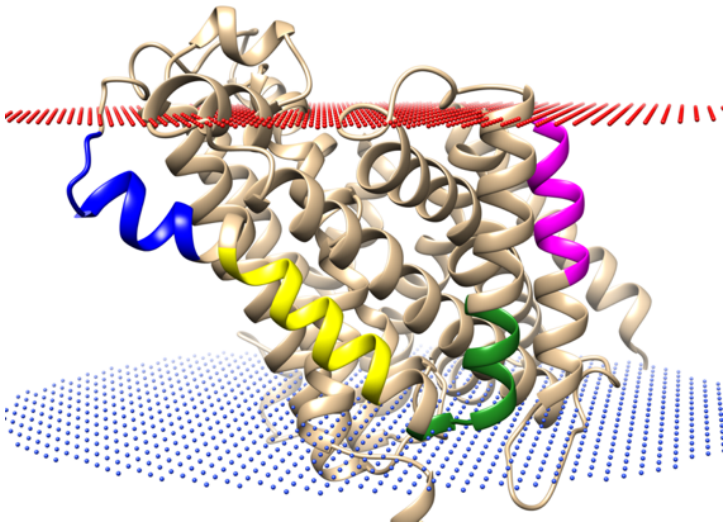

Figure 20 - Putative CRAC/CARC motifs visualized on model outward facing conformation of LAT1. Sequences identified by pattern searching LAT1 that are membrane embedded and thus membrane cholesterol accessible are highlighted on structure in blue (position 210 – 221), yellow (position 195 – 206), green (position 181 – 191) and magenta (position 382 – 385). The red and blue lattices demarcate the predicted extracellular facing and intracellular facing parts of the plasma membrane, respectively.

EXPLORING LAT1 INHIBITOR BINDING BY *IN SILICO* DOCKING INTO OUTWARD FACING AND INWARD FACING MODELS OF THE TRANSPORTER

There have been significant efforts and successes in the development of potent high affinity LAT1 inhibitors as potential chemotherapeutics (Oda et al., 2010; Huttunen et al., 2016; Kongpracha et al., 2017; Napolitano et al., 2017b). So far, these efforts have been mostly based on the screening of synthetic compounds, designed to mimic known substrates of LAT1, through mostly *cis*-inhibition transport assays. Since the poor-quality regions of the two structural models of LAT1 are outside the substrate binding site of the transporter, they provided an opportunity to characterize, *in silico,* the molecular mechanisms of some of the reported inhibitors, (Figure 18). Two cavities corresponding presumably to the substrate binding site of the transporter were visible in the models (Figure 21). The cavity at the core of the outward facing conformation was accessible from the extracellular facing side

whereas in the inward facing conformation, the cavity was occluded from both the extracellular and intracellular sides, which is consistent with the conformations of the templates used in the modelling of either conformations (Kowalczyk et al., 2011; Jungnickel et al., 2018).

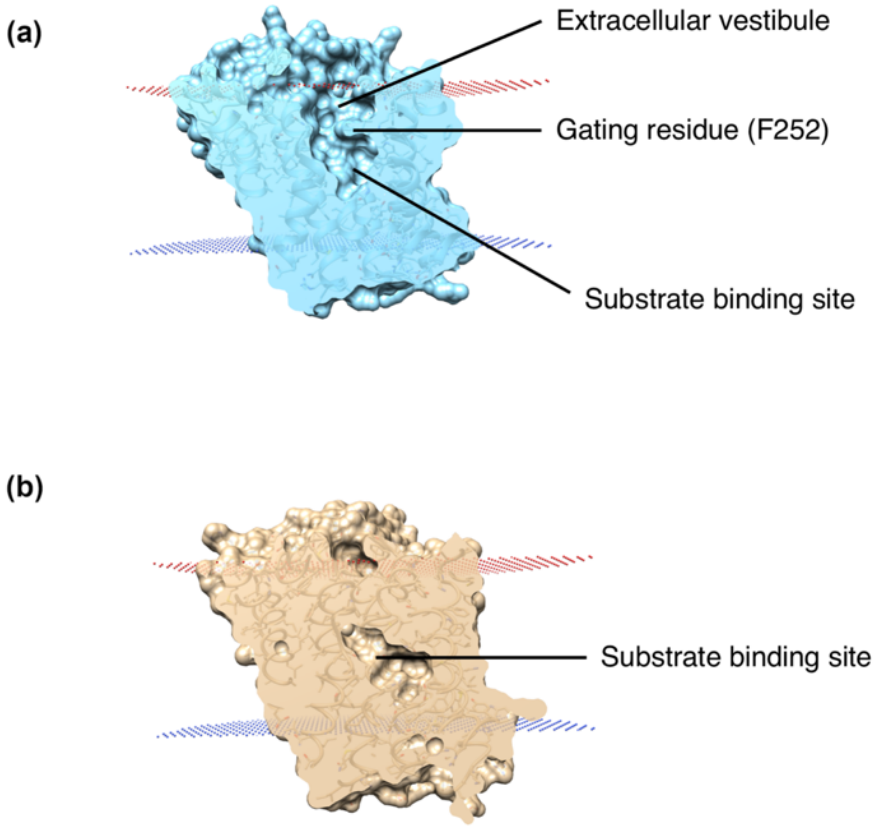

Figure 21 - Slice through models of the outward facing open and inward facing occluded conformations of LAT1. The red and blue lattices demarcate the predicted extracellular facing and intracellular facing parts of the plasma membrane, respectively. a) The outward open conformation has a large cavity with two parts, demarcated by F252. b) A large central cavity is visible in the inward occluded conformation and is closed off from the extracellular side by several residues including F252.

Previously reported, putative substrate binding site residues, T62 – S67, I139, I140, V148, F252 – G255, S342, S401, F402, and W405, were located mostly in the lower part of the cavity proximal to extracellular vestibule, in the model of the outward open conformation and in the cavity of the inward occluded conformations

(Figure 22b & d) (Geier et al., 2013). F252 in the model of the outward open conformation, was positioned to act as a gating residue, opening or occluding the putative substrate binding site from the extracellular space in a similar manner to W202 in AdiC and F231 in GkApcT, which is consistent with the observation that this position is conserved between LAT1, AdiC and GkApcT (Figure 22c & d) (Gao et al., 2010; Jungnickel et al., 2018). The arrangement of these putative substrate binding site residues was compared by structural alignment to the experimentally validated *in silico* model of LAT1 in the outward open conformation from the Schlessinger lab (Chien et al., 2018). The two models had a Cα-RMSD of 0.68 Å and some differences in the putative binding site residues (Figure 22a & b). Worth noting was the sidechain of F252, which is in a different conformation in the two models, with the control model having the sidechain facing away from the opening of the cavity (Figure 22b). The inward facing occluded and outward facing open models have a higher Cα-RMSD of 1.37 Å and some differences in the residues of the putative substrate binding site particularly F252 – F255. The side chain of F252 has a similar conformation in both models, that is facing toward the cavity, but in the inward occluded conformation, the top half of TM6 is shifted more toward the opening of the cavity rendering it inaccessible from the extracellular side (Figure 22c & d). The Cα-RMSD of F252 – F255 on TM6 between the inward facing occluded conformation and the outward open conformation is 2.40 Å, compared to 1.36 Å between the outward open model and the control model.

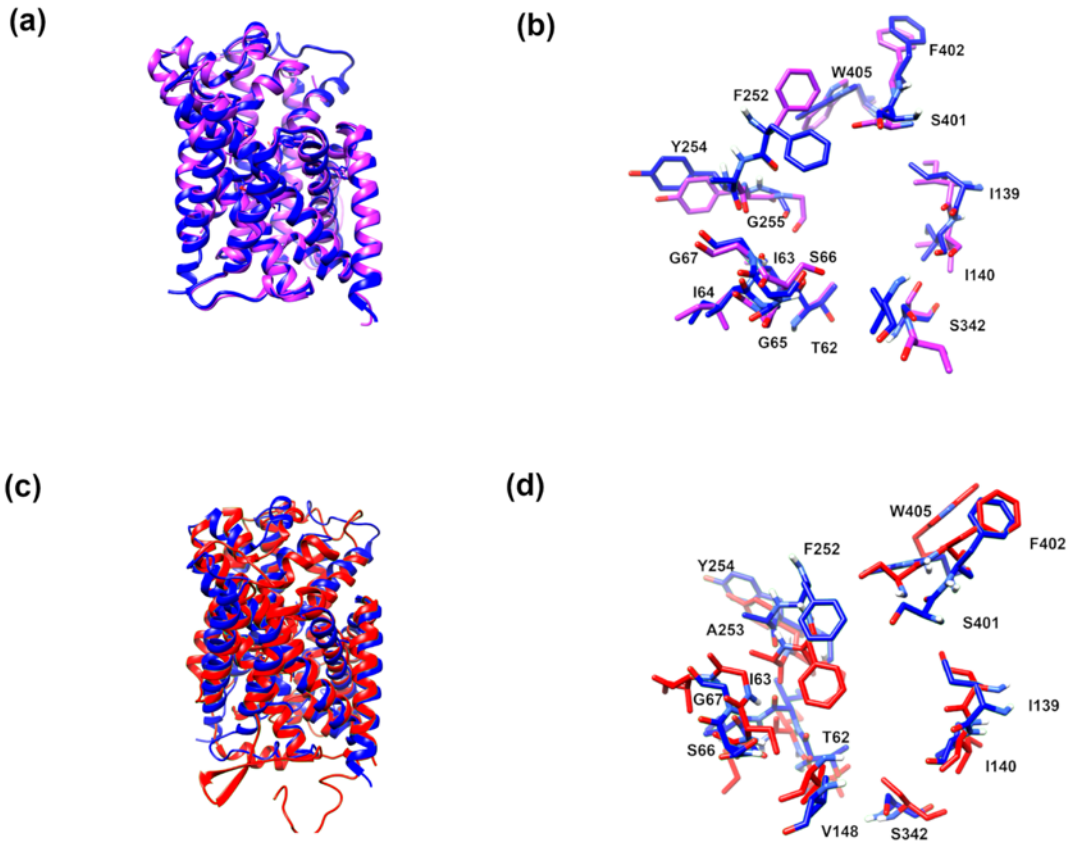

Figure 22 - Alignment of LAT1 homology models and their putative binding site residues. a) Aligned models of LAT1 in the outward facing open conformation. Control model is shown in purple and my model in blue. Binding site residues in each model are aligned and shown in (b). c) Aligned models of LAT1 in the inward facing occluded (red) and my outward facing open (red) conformations. Binding site residue conformations are aligned and shown in (e).

As further validation of the models, known substrates of LAT1 as well as inhibitors, JPH203, SKN203 and KMH233, were docked into the putative substrate binding sites of the two new models and the control model (Table 11; Figure 23). There was an evident correlation between the predicted binding free energy/score from the docking of a LAT1 ligand and its molecular weight with R^2 values of 0.61 ($P<0.05$), 0.64 ($P<0.05$) and 0.44 ($P<0.05$) for the control, outward open and inward occluded models respectively (Table 11; Figure 23). For all three models the R^2 was lowered by the inclusion T_3, which appears to be an outlier. Without T_3 in in the linear

regression, the R^2 values are 0.97 (P<0.0001), 0.94 (P<0.0001) and 0.91 (P<0.0001) for the control, outward open and inward occluded models respectively. T_3 has the highest molecular weight of all the ligands but not the most favourable predicted binding free energy. This is because T_3 has three iodine atoms (A_r = 126) in its structure, each of which has an atomic weight (A_r) much higher than the C (A_r = 12), N (A_r = 14), O (A_r = 18) atoms that make up the other ligands, with the exception of JPH203 and SKN103 which also have Cl (A_r = 35) and methionine which has S (A_r = 32) (Figure 2.2). The observed correlation maybe because the higher molecular weight ligands, with the exception of T_3, have more atoms and therefore potentially more interactions with LAT1, thermodynamically favouring their binding. The linear fits of the docking scores from both the control and out open model are similar indicating that the two models are of similar predictive power with regard to the predicted free binding energies of LAT1 ligands and thus presumably the binding modes of these ligands. Although following a similar trend to the out open models, the inward occluded model has better scores for all the ligands docked except KM233 which does not dock at the substrate binding site in this conformation (Table 11). Overall both the out open and inward occluded models of LAT1 appear sufficiently plausible to explore structure activity relationships between LAT1 and some of its inhibitors.

Table 11 - Predicted binding energies of LAT1 ligands at the putative substrate binding sites of homology models in the outward facing and the inward facing conformations.

An experimentally validated model of the outward open conformation from the Schlesinger lab was used as a control.

Predicted free energy of binding/Score (kcal mol^{-1})				
Ligand	**MW (Da)**	**Control**	**Outward open**	**Inward occluded**
BCH	155.197	-5.4	-5.7	-5.8
Histidine	155.155	-5.2	-5.2	-6.4
Phenylalanine	165.19	-5.6	-5.6	-6.5
Tryptophan	204.23	-6.8	-6.8	-8.0
Leucine	131.17	-5.2	-4.4	-5.1
Isoleucine	131.17	-4.6	-4.6	-5.5
Methionine	149.21	-4.4	-4.0	-4.5
Valine	117.151	-4.3	-4.2	-5.3
Kynurenine	208.22	-6.3	-6.4	-6.8
Triiodothyronine (T_3)	650.977	-7.3	-7.5	-6.9
JPH203	472.32	-10.6	-10.7	-12.3
KM233	587.6	-11.2	-10.6	
SKN103	481.37	-10.7	-9.8	-12.9

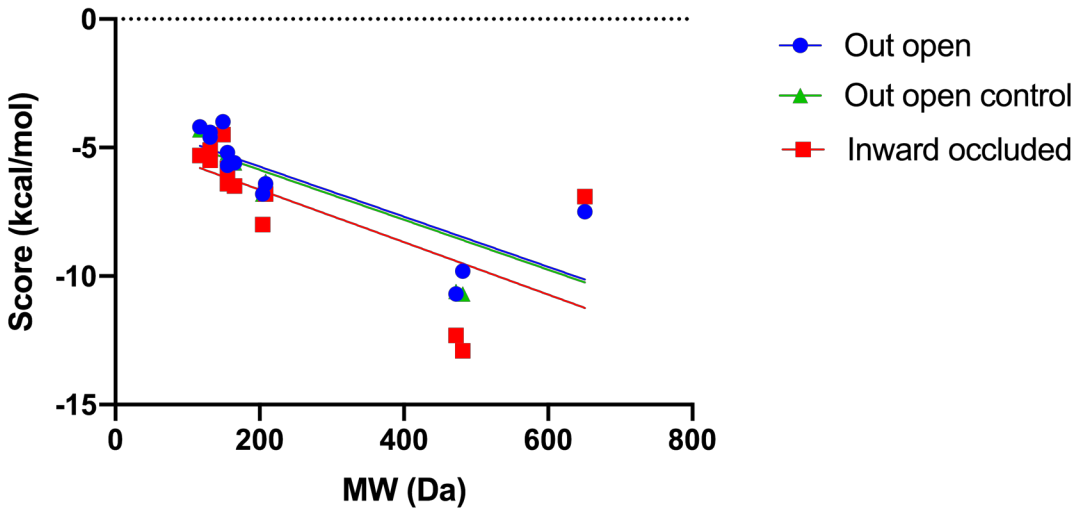

Figure 23 - Trends in molecular weight and predicted binding energy. The predicted binding energies/scores of 10 know substrates and 3 synthetic inhibitors to the outward open and inward occluded conformations of LAT1 were plotted against their molecular weight. Linear regression was performed and the fitted lines are shown. R^2 values for regression are 0.97 (P<0.0001), 0.94 (P<0.0001) and 0.91 (P<0.0001) for the control, outward open and inward occluded models respectively.

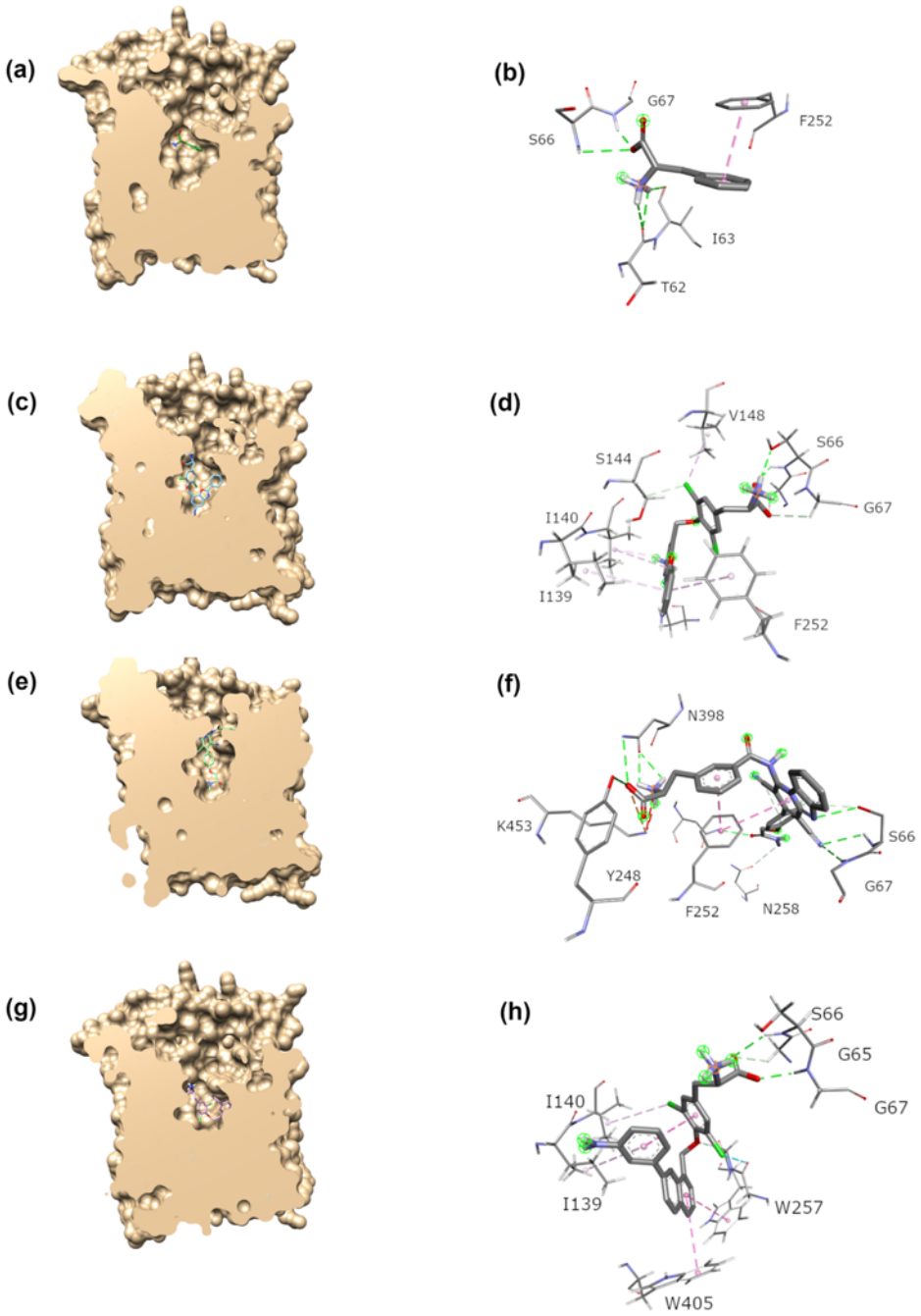

Figure 24 - Ligand docking onto outward open model of LAT1. a) Slice through of surface of model with phenylalanine (green) docked at the putative binding site shown as sticks. b) Residues in the model interacting with phenylalanine. c) Slice through of surface of model with JPH203 (cyan) docked at the putative binding site shown as sticks. d) Residues in the model interacting with JPH203. e) Slice through of surface of model with KMH233 (green) docked at the putative binding site shown as sticks. f) Residues in the model interacting with KMH233. g) Slice through of surface of model with SKN103 (purple) docked at the putative binding site shown as sticks. h) Residues in the model interacting with SKN103. Electrostatic attractions are shown with dashed dark orange lines, H bonds are shown with dashed green lines and Van der Waals (VdW) interaction with pink dashed lines.

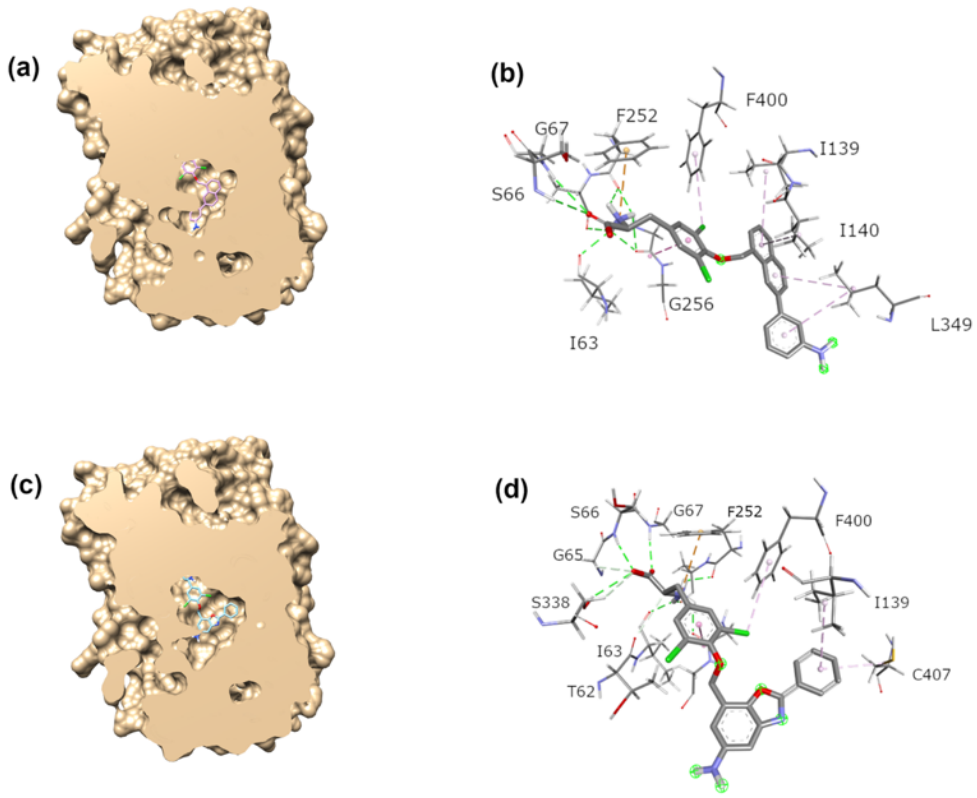

Figure 25 - Inhibitor docking onto inward open model of LAT1. a) Slice through of surface of model with SKN103 (purple) docked at the putative binding site shown as sticks. b) Residues in the model interacting with SKN103. c) Slice through of surface of model with JPH203 (cyan) docked at the putative binding site shown as sticks. d) Residues in the model interacting with JPH203. Electrostatic attractions are shown with dashed dark orange lines, H bonds are shown with dashed green lines and VdW interaction with pink dashed lines.

Consistent with previous reports, H-bonding between the backbone of G65, G67, T62 and I63 and the sidechain of S66 with the amino acid functional groups of the ligands of LAT1, such as phenylalanine, was predicted from the docking poses in both the outward open and inward occluded conformations with the exception of KMH233 (Figure 24; Figure 25) (Geier et al., 2013). KMH233's amino acid moiety was bound to a pocket on the extracellular side of F252. It was recognised by K453, which was predicted to electrostatically attract the carboxyl of the amino acid via its positively charged side chain, and also bound by N398 and Y248 via hydrogen

bonding with their sidechains. KMH233 was also predicted to bind to the outward open conformation by hydrogen bonding with G65, S66 and N404 as well as π-π stacking and t-stacking with F252 (Figure 24e & f). The numerous interactions between KMH233 may explain why this ligand binds strongly and with specificity to LAT1 (Table 12) (Huttunen et al., 2016). The predictions that this ligand may interact strongly via electrostatic interaction and hydrogen bonding with residues in the extracellular vestibule, by hydrogen bonding and VdW interactions with the extracellular gate (F252) and residues across it, are consistent with observation that KM233 is not a transported ligand of LAT1. This binding pose may preclude conformational change from the outward open to an occluded state thereby sterically hindering the movement of F252 – F255 to the inward occluded conformation (Huttunen et al., 2016). KMH233 is also the only inhibitor that could not be docked onto the inward occluded model, which suggests that it cannot bind to this conformation and therefore cannot be transported by LAT1.

JPH203 and SKN103 were predicted to bind to the substrate binding site in both the outward open and inward occluded conformations. In addition to H bonding with G65 – G67 and S144, JPH203 was predicted to interact with the outward open conformation via π-alkyl interactions with F252 and I140 (Figure 25b). In the inward occluded model, SKN103 was predicted to interact with LAT1 via H bond with G55 – G66, F252, A253, G255, and S338 in addition to π-alkyl interactions with F400, I139, I140, and L349 (Figure 25d). The prediction of a more extensive H bonding network and VdW interactions between SKN103 and the inward occluded conformation compared to the outward open conformation, may explain the difference in the predicted free binding energies between the two models, -12.9 and -9.8 kcal mol^{-1}

respectively. JPH203 also has had a higher predicted binding free energy to the inward occluded conformation, -12.3 kcal mol^{-1}, than the outward open conformation -10.6 kcal mol^{-1}. Of the three inhibitors considered here, JPH203, has highest affinity, as inferred from IC50 calculations and this may be because it binds and interacts more extensively with the inward occluded conformation in LAT1's transport cycle (Table 12).The predicted interactions of JPH203 and SKN103 with LAT1, suggest similar binding affinity for the two inhibitors (Oda et al., 2010; Kongpracha et al., 2017). Both JPH203 and SKN103 interacted with more residues in the binding site than those typically involved in the interaction of LAT1 and its transported substrates such as phenylalanine and BCH, which may explain not only their higher affinity of the transporter but also leave open the question of whether these interactions preclude their transport either sterically or by stabilising intermediates in the transport cycle of LAT1.

In the inward open model, F252 interacts with NH_3^+ of the amino acid of the substrates, including JPH203 and SKN103 by a π-cation bond (Figure 25). This interaction may be important to the recognition of a LAT1 substrate, stabilizing the inward occluded conformation as well as facilitating transport. The distance (<6 Å) and geometry between the amino group of the substrate alanine and the face of the benzene side chain of the extracellular gating residue F231 in the GkApcT structure, on which the inward occluded model was based, allows for such a π-cation interaction (Jungnickel et al., 2018). This supports the hypothesis that this interaction is important for the formation of this conformation and thus substrate transport. When the corresponding gating residue in the predicted model of LAT2, F242 was mutated to the valine, transport activity decreased while mutation to tryptophan at

the same position results in increased activity relative to the wild type, suggesting a role for the aromatic nature of the residue in this gating position (Hinz et al., 2015). Interestingly π-π stacking was observed between phenylalanine and F252 in the outward open conformation, an interaction that has been suggested to explain the apparent preference for aromatic side chains over alkyl ones in LAT1 substrates, a preference also consistent with the trend observed in the predicted binding free energies of the substrates (Ylikangas et al., 2013; Chien et al., 2018).

Table 12 - LAT1 transport inhibitors and their IC50s

LAT1 inhibitor	**IC50 (μM) (transport inhibition)**
KMH233	18.2 ± 1.2 (Huttunen et al., 2016)
SKN203	1.98 ± 1.07 (Kongpracha et al., 2017)
JPH203	0.14 (Oda et al., 2010)

CONCLUSION

As of December, 2017, there were twenty-three solute carrier structures deposited in the Protein Data Bank, less than half of which are from mammalian organisms. Due to this small number of experimental structures, for high value pharmacological targets such as LAT1 where structural information is essential, much of the structure function work has relied on homology models (Reviewed by Bai, Moraes and Reithmeier, 2017; Singh and Ecker, 2018). The bacterial homologues of LAT1, EcAdiC and MjApcT, have been the most exploited for the purposes of homology modelling of the transporter usually in the outward open conformation, yielding much information about the structure-activity relationship of LAT1 and leading to development of potent inhibitors (Geier et al., 2013; Augustyn et al., 2016;

Zur et al., 2016; Napolitano et al., 2017b; Chien et al., 2018; Palazzolo et al., 2018). Conversely, knowledge gained from other crystal structures of LeuT-fold transporters such as the dDAT and SERT has been under-utilized for the understanding of LAT1 function. The activities of both the dDAT and SERT transporters have been shown to be modulated by membrane cholesterol and when solved, their structures revealed cholesterol binding sites (Penmatsa et al., 2013, 2015; Coleman et al., 2016). A combination of sequence analysis and structure prediction supported the hypothesis that LAT1 interacts with and is modulated by membrane cholesterol possibly through sites homologous to dDAT and or through CRAC/CARC motifs in the transporter's transmembrane domains. LAT1 mediated uptake of L-DOPA has indeed been shown to be modulated by membrane cholesterol, but whether this is by direct interaction remains undetermined (Dickens et al., 2017). The interaction of cholesterol and cholesterol hemisuccinate with dDAT stabilized the outward open conformation, reducing conformational heterogeneity; something that could facilitate structural study of LAT1.

In the case of dDAT and SERT, high affinity inhibitors were also key to stabilizing the transporters in a single conformation making them more amenable to crystallization (Penmatsa et al., 2013, 2015; Coleman et al., 2016). Several inhibitors of LAT1 have been reported, namely KMH233, SKN103 and JPH203, and the binding mode of these has been here explored by docking to predictive models of LAT1 in the outward open and inward occluded conformation (Oda et al., 2010; Huttunen et al., 2016; Kongpracha et al., 2017). All three inhibitors were found in the substrate binding site of the outward open conformation, in a manner similar to transported substrates with exception of KM233. KM233 was also the only inhibitor that did not

dock to the substrate binding site of the inward occluded conformation and because of its interaction with the extracellular gate residue, F252, and residues across it in the substrate binding site, the inhibitor probably prevents formation of the inward occluded conformation and thus cannot be transported. JPH203 and SKN103 docked to the inward occluded conformation as substrates but had predicted binding free energies higher than those of transportable substrates, leaving it an open question whether they are transported by LAT1. As far as stabilising a particular conformation for the purpose of structural characterisation, KM233 seems like the best candidate between the three inhibitors explored here, although it has lowest affinity of the three as inferred from IC50 calculations.

Here I have elaborated upon several hypotheses that are open to experimental testing. Namely, LAT1 interacts with cholesterol via specific residues; the inhibitors of LAT1 studied here are most likely competitive inhibitors; KM233 is not a transportable ligand of LAT1; and JPH203 and SKN103 are most likely substrates of LAT1. The first one can be tested by solving the structure of LAT1 in the presence of cholesterol, but solving the structure of LAT1 has so far remained elusive. An alternative approach would be a combination of the cholesterol depletion followed uptake assay experiments used by Dickens *et al.*, 2017 and mutagenesis of the proposed cholesterol binding site residues. Whether the inhibitors of LAT1 are competitive inhibitors or not, can be inferred by determining the effect of the inhibitors on the V_{max} and K_m of LAT1 mediated transport, a competitive inhibitor should alter the V_{max} but not K_m of the transporter. Trans-stimulation assays in cells or proteoliposomes would be useful for determining whether these inhibitors are transported substrates or not.

Chapter 4 - Overexpression, purification and biophysical characterisation of LAT1-CD98hc

This chapter reports development of an expression system and purification protocol for the production of LAT1-CD98hc. Biochemical characterisation of the thermal and kinetic stability of the complex in detergent and the impact of ligand binding on these is also explored.

LAT1 OVEREXPRESSION AND STABLE CELL-LINE DEVELOPMENT

The suspension adapted and N-acetylglucosaminyltransferase I deficient, HEK293SG expression system was chosen for its capacity for natively folded, mammalian membrane protein over-expression with simplified endoglycosylase sensitive glycosylation (Reeves et al., 2002; Chaudhary et al., 2012; Goehring et al., 2014). Cells were transfected with a pcDNA3.1 plasmid for LAT1-V5-His_6 fusion protein expression. G418 selection was used to isolate a heterogeneous pool of cells with stably integrated expression vector in their genomes. Forty-eight clones were isolated as described in the Methods Section and screened by immunoblotting for the LAT1-V5-His_6 fusion protein. Once identified, the highest expressing clone was expanded up and assayed for the function of the exogenous LAT1. A HEK293-LAT1 cell-line was used as a positive control and HEK293SG cells as a control for endogenous transporter meditated up take. HEK293SG-LAT1 accumulated more L-DOPA than the HEK293SG control (48.0 ± 12.1 vs 12.7 ± 3.8 pmol/1 x 10^6 cells; p value <0.01) and HEK293-LAT1 cells (48.0 ± 12.1 vs 31.9 ± 5.3 pmol/1 x 10^6 cells; p value <0.01), which expressed less of the fusion protein as determined by immunoblotting (Figure 26). This result was indicative of functional LAT1-V5-His_6 in the HEK293SG cell-line. The smeared signal of CD98hc from the HEK293-LAT1 cell-line, compared with the 6 discrete bands from the HEK293SG-LAT1 cell-line in Figure 26a, is consistent

with data in the literature (Reeves et al., 2002), showing that the heavy chain of the HAT is glycosylated and that HEK293SG cells produce simplified glycosylation.

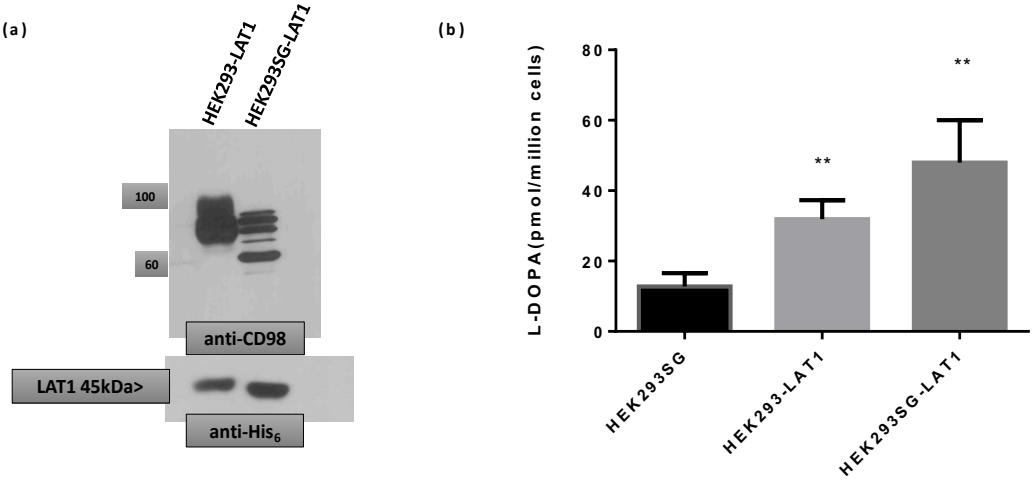

Figure 26 - Stable over-expression of functional LAT1-CD98hc in HEK293SG cells. (a) Immunoblotting following SDS-PAGE in reducing conditions was used to detect LAT1-V5-His_6 in the highest expressing HEK293SG single cell derived clone. CD98hc was up regulated in response to LAT1 overexpression and displayed a simplified glycosylation pattern in HEK293SG-LAT1 relative to HEK293-LAT1. (b) The function of the HAT was assayed by L-DOPA accumulation in the various cell-lines. Both HEK293-LAT1 and HEK293SG-LAT1 cell lines accumulated more L-DOPA in three minutes than the control cell-line, consistent with LAT1 overexpression (error bars are SD; n = 3).

STABILIZATION AND PURIFICATION OF LAT1-CD98hc

Once the expression and function of LAT1-V5-His_6 had been established, the HEK293SG-LAT1 cells were grown in 1.0 and 1.5 L suspension culture flasks. An immunoaffinity purification workflow developed using the HEK293-LAT1 cell-line (Figure 27a), was applied for purification of the HAT from the new cell-line. The work flow was assessed at each step by immunoblotting (Figure 27b) and modified as necessary to optimize the process as described in detail below. The first lysis step was modified by the introduction of ATM to inhibit the reduction of the disulphide bond that covalently attaches the light chain to the heavy chain, stabilizing the heteromeric complex. Small scale experiments showed that including 1 mM ATM,

reduced the proportion of total LAT1 in a monomeric state on non-reducing SDS-PAGE, from 42% to 9%. Concentrations greater than 1 mM resulted in no further reduction in the proportion of HAT in a monomeric state (Figure 28).

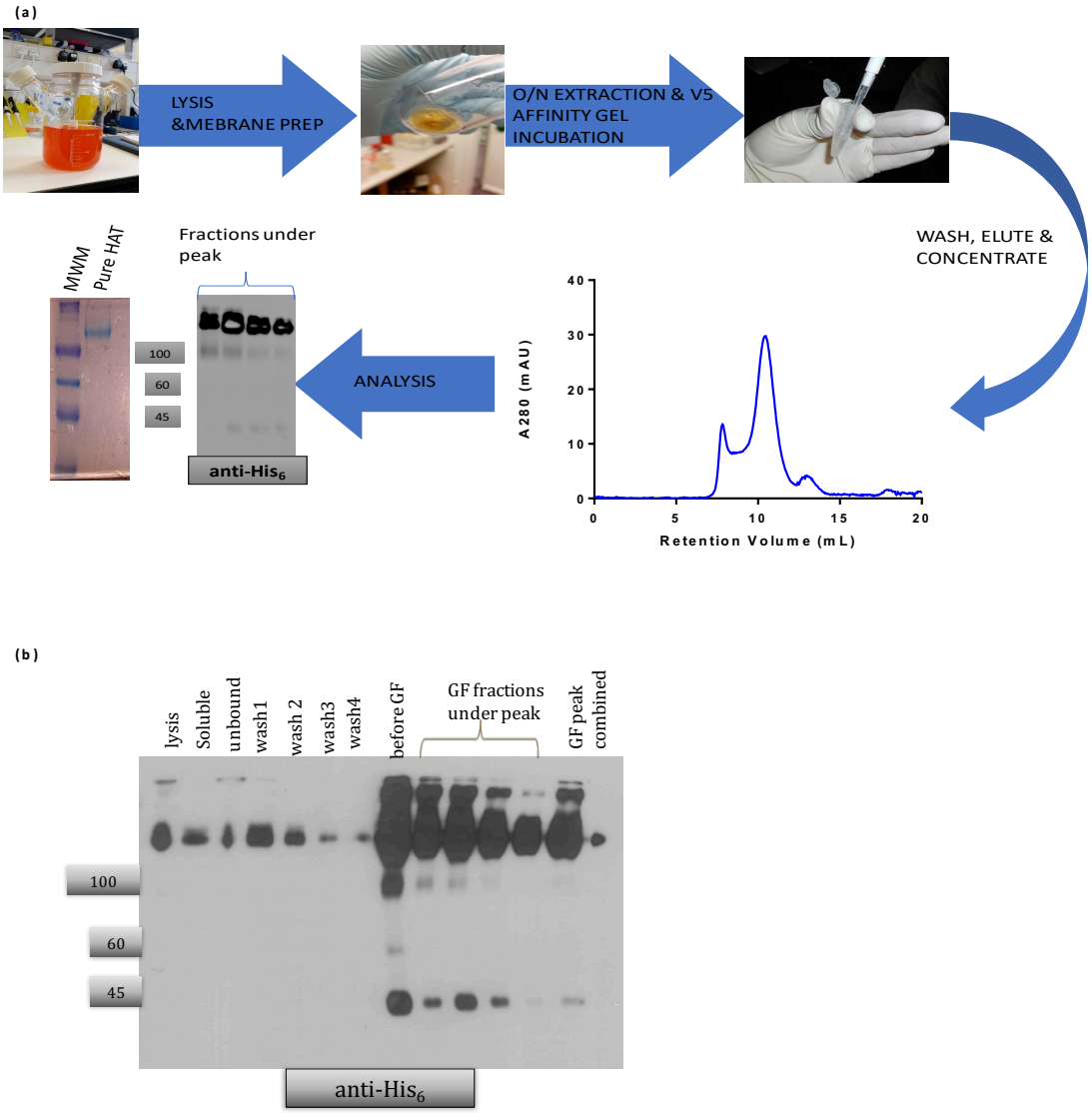

Figure 27 - Immuno-affinity purification of LAT1-CD98hc. (a) The HAT was purified by immunoaffinity precipitation as illustrated by this work flow. The peak eluted at 10.5 mL was analysed by immunoblotting for LAT1-V5-His_6 and the degree of purity by SDS-PAGE in non-reducing conditions followed by Coomassie staining. (b) The efficiency of each step of the purification was assessed by immunoblotting for LAT1-V5-His_6. Molecular weights are in kDa.

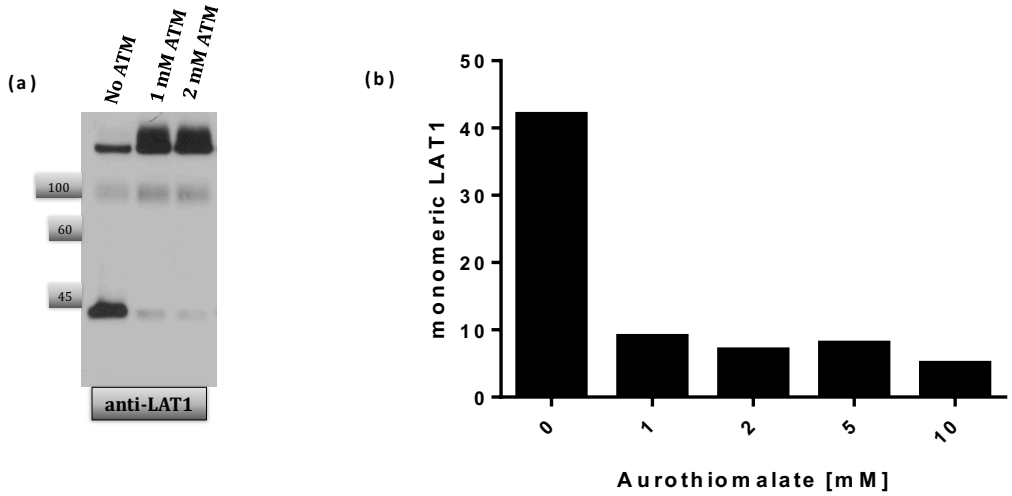

Figure 28 - The effect of ATM in lysis buffer on reduction of the HAT disulphide bond. (a) Lysates prepared in various concentrations of ATM were analysed by immunoblotting for LAT1-V5-His_6 in non-reducing conditions. (b) The fraction of LAT1 in monomeric state after non-reducing SDS-PAGE was calculated by densitometry.

DEGLYCOSYLATION OF PURIFIED LAT1-CD98hc

Complex glycosylation is often a source of biochemical heterogeneity which can hinder structural study but sometimes removing it destabilises the protein of interest (Nettleship, 2012). With this in mind, the glycosylation state of CD98hc was characterised and a deglycosylation strategy developed. Immunoblotting of CD98hc co-purified with LAT1 from HEK293 showed a diffuse band between 60 - 100 kDa; this band has been replaced by at least 6 distinct bands (Figure 29) after treatment of the purified protein with PNGase F, an amidase that is most effective for removing almost all N-linked oligosaccharides from glycoproteins, at 37 °C and 27 °C for 1 hr and 2 hrs respectively. The higher molecular weight bands were missing or fainter in the sample incubated at 37 °C compared to 27 °C. LAT1-CD98hc purified from HEK293SG cells, when run on SDS-PAGE and Coomassie stained, had a similar pattern of 6 distinct bands between 60 – 100 kDa and a band less than 45kDa consistent with

the light chain of the HAT (Figure 29b). When LAT1-CD98hc purified from HEK293SG cells was incubated with EndoH enzyme, at 4 °C for 16 hrs or at 27 or 37 °C for less than 6 hrs there was some apparent deglycosylation when compared to the control sample, the largest molecular weight band disappeared and two new bands less than 60 kDa appeared. The density of the 5th largest band appeared reduced as well (Figure 29c). Incubation for 6 hrs at 27 °C or 37 °C reduces the number of bands visible to two that are less than 60 kDa, and are absent from the untreated control sample (Figure 29c). The apparently similar efficiency of deglycosylation between the native and denatured samples is consistent with the glycans being solvent accessible (Figure 29c; Figure 5).

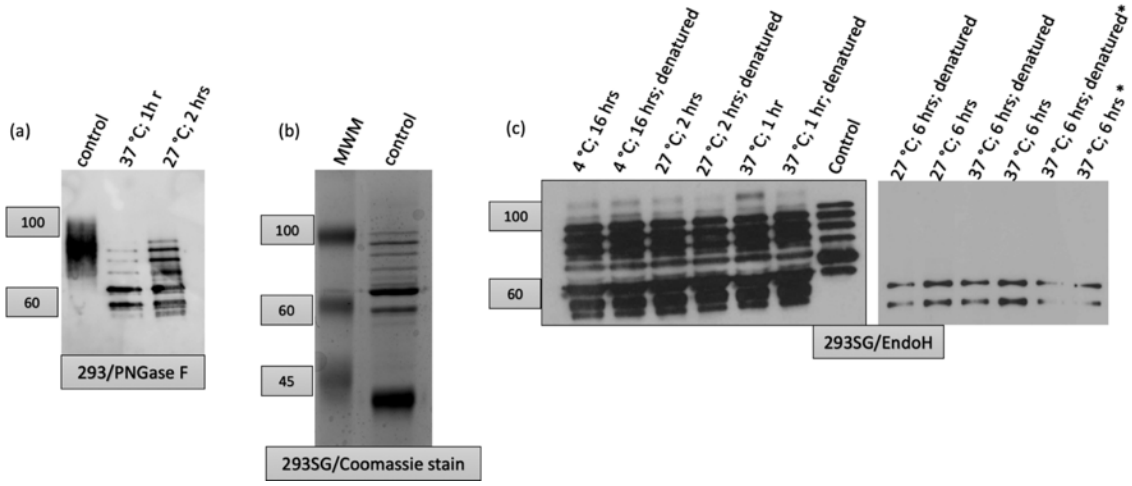

Figure 29 - Analysis of CD98hc glycosylation using purified LAT1-CD98hc and deglycosylase enzymes, PNGase F and Endo H. (a) Immunoblot with anti-CD98hc polyclonal antibody of LAT1-CD98hc purified from HEK293 cells and treated with 500 units PNGase F for 1 or 2 hrs at 37 °C and 27 °C respectively. (b) LAT1-CD98hc purified from HEK293SG-LAT1 cells, analysed by SDS-PAGE in reducing conditions and Coomassie stained. This sample was used in the EndoH experiment and served as a negative control. Molecular weights (MWM) are given in kDa (c) Immunoblots with anti-CD98hc antibody in reducing conditions of LAT1-CD98hc purified from HEK293SG cells, after incubation with 2000 or 4000(*) units EndoH in the conditions indicated.

OPTIMISATION OF LAT1-CD98hc PURIFICATION BY IMMUNOAFFINITY PRECIPITATION

Lipid membrane solubilization begins at detergent concentrations in excess of the critical micelle concentration (Le Maire et al., 2000). Optimization is necessary to achieve efficient of solubilization, without compromising stability of the protein detergent complex of interest (Privé, 2007). As a starting point, the conditions reported by Meury et al., 2014 for the solubilisation of LAT2-CD98hc from *P. pastoris*, were used for HEK293SG-LAT1 cell membranes. Membranes were prepared and solubilised overnight in a mixture of DDM, LMNG and CHS micelles (5:1 DDM to CHS and 3:1 CHS to LMNG) at a DDM concentration of 1.5 % w/v. Given that DDM has a low CMC, 0.0009% w/v, 1.5 % w/v is well in excess of the CMC and is 0.5 % more than is typical used for membrane solubilization therefore the optimal detergent concentration was sought by solubilising cell membranes and immuno-precipitating LAT1-CD98hc in decreasing concentrations of detergent, from 0.3 – 1.5 w/v. The analysis of the efficiency of solubilisation was performed by size-exclusion chromatography as described in Chapter 2 (Figure 30a). The peak height between 10.3 - 10.5 mL retention volume, corresponding to pure HAT dimer, increased from 30.15 to 69.65 mAU, as the DDM concentration was lowered from 1.5 to 0.9 % w/v, respectively. Below DDM concentration 0.9 % w/v, the peak height decreased as detergent concentration decreased. Based on this result, subsequent solubilization and purification experiments were performed at 0.9 % w/v DDM.

Another parameter selected for optimization was the DDM:CHS ratio. CHS appears to be important for the purification LAT1-CD98hc (Figure 30b). DDM:CHS ratios of 3.3 and greater, had no effect on the peak height between 10.3 - 10.5 mL

retention volume, compared to the control ratio of 4.74. Ratios less than 3.3 resulted in reduced peak height (Figure 30c). Based on the results of this experiment the DDM:CHS ratio was maintained at 4.74.

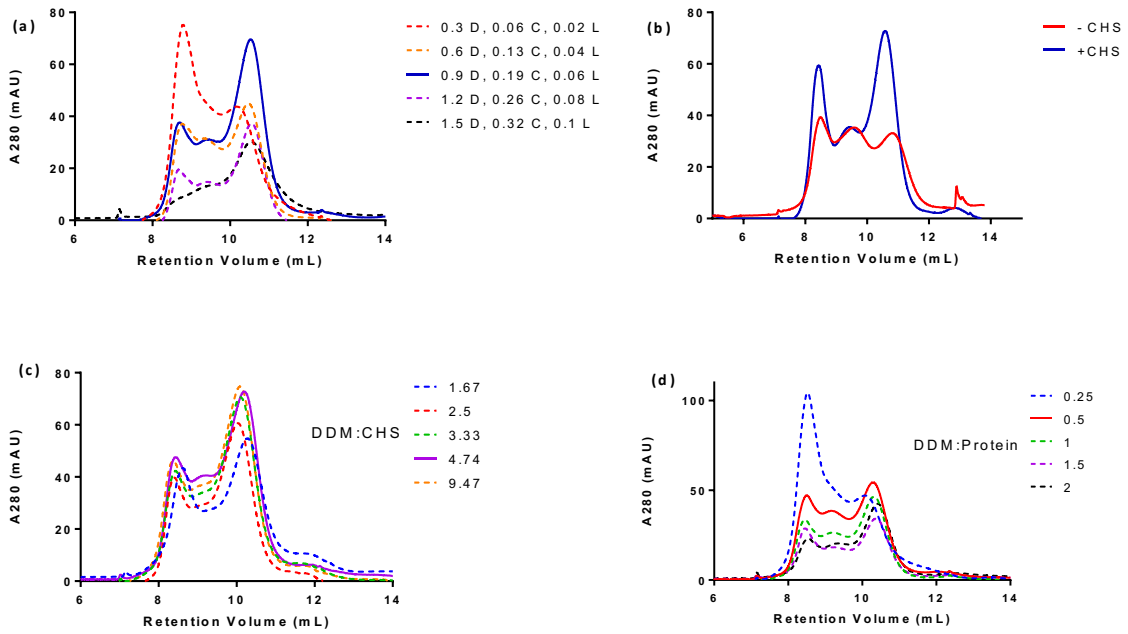

Figure 30 - Optimization of membrane solubilization step of LAT1-CD98hc purification. Detergent concentration (a), DDM:CHS (c) and detergent to protein ratio (d) were varied as described in the methods and the effects of LAT1-CD98hc analysed by size exclusion chromatography. The chromatogram of the chosen as being to be optimal is illustrated by the unbroken line in each of graph. (b) The size exclusion chromatography of LAT1-CD98hc purified in the presence or absence of CHS in the membrane solubilisation and SEC1 buffer.

The final solubilisation parameter selected for optimisation was the DDM: Protein ratio. This was done by keeping the detergent concentration constant at 0.9 % DDM while varying the solubilisation volume. A ratio of 0.5, which was also the control ratio, was found to be the optimal condition for LAT1-CD98hc purifcation (Figure 30d).

OPTIMIZATION OF SIZE-EXCLUSION BUFFER FOR PURIFICATION

The initial buffer condition used for washing V5 affinity resin, elution of LAT1-CD98hc and preparative size exclusion chromatography was refered to as SEC1 buffer (0.02 % w/v DDM; 0.0013 % w/v LMNG; 0.00426 % w/v CHS; 100 mM Tris-Cl; 300 mM NaCl; 10 % w/v glycerol; pH 8). It yielded 100 µg from 1 L of suspension culture. The SEC1 DDM concentration, double the CMC, was chosen in order to keep the HAT stable in solution by preventing disintegration of the protein-detergent complex. LAT1-CD98hc was kinetically stable in the buffer for 7 days at 4 °C with no detectable aggregation or denaturation by size exclusion high performance liquid chromatography (SE-HPLC) (Figure 33a). The T_m of the HAT in SEC1 buffer was 47 °C (Figure 33c). Optimisation was undertaken in an attempt to improve the yield per litre as well as the thermal and conformational stability of LAT1-CD98hc.

Leucine was chosen for the determination of the effect of including ligand in the buffers used for protein purification. The inclusion of 50 mM leucine in the purification buffers resulted in a 39% increase in the peak height at 10.4 mL by size exclusion chromatography (Figure 31a). To determine whether this increase was due to increased stability of LAT1-CD98hc, samples of HAT purified in the presence and absence of leucine were heat stressed at 60 °C for 10mins then analysed by SE-HPLC. Figure 31b shows increased monodispersity in the presence of leucine and a 14% ($p < 0.001$) higher relative peak intensity in the presence of leucine, indicative of a thermal stabilising effect. Addition of 4 mM leucine did not have a significant effect on the relative peak intensity compared to no ligand control while the same concentration of kynurenine increased the relative peak intensity by 9% ($p<0.01$). There was no significant difference in relative peak intensity between 50 mM leucine

and 4 mM kynurenine. When determined, the T_m of LAT1-CD98hc was 10 °C higher in the presence of leucine (Figure 31). 50 mM leucine was included in all purification buffers from this point unless otherwise stated.

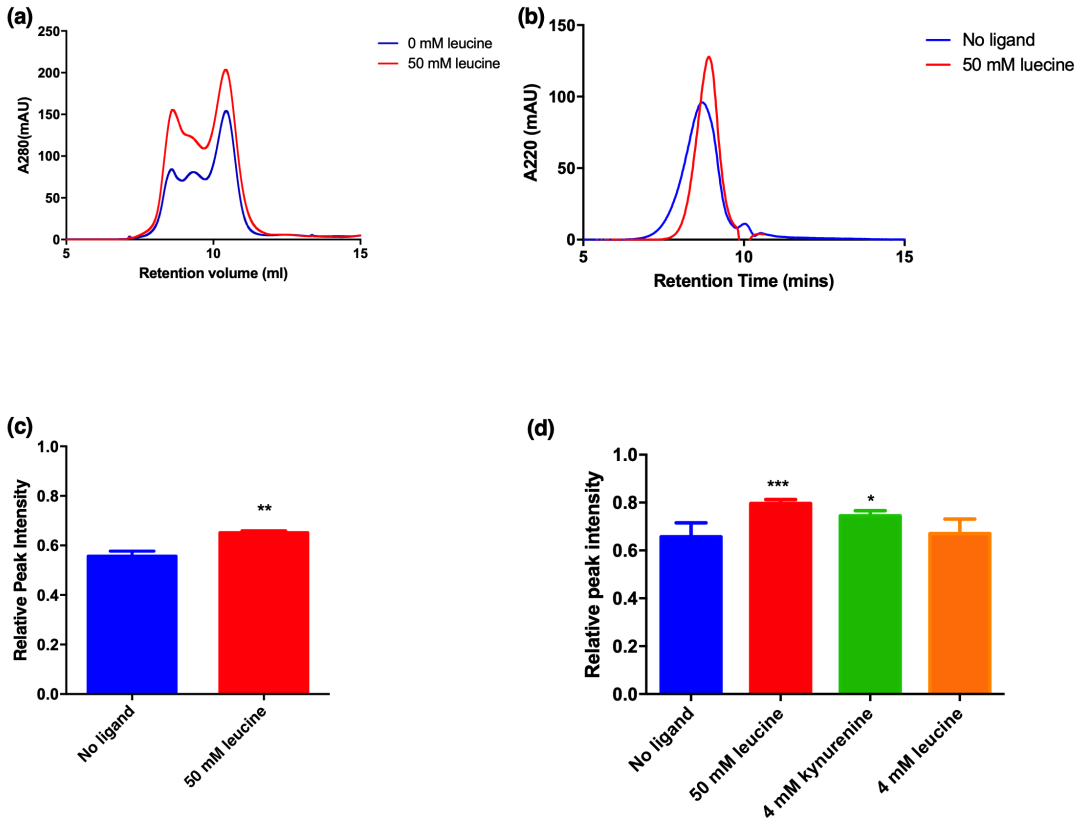

Figure 31 - The effect of leucine on the yield and thermal stability of LAT1-CD98hc. (a) Protein purification was performed in the presence of 50 mM leucine at each stage of the purification. (b) The effect of leucine on the thermal stability of LAT1-CD98hc was determined by heating stressing, at 60 °C for 10 minutes followed by SE-HPLC analysis. (c) The effect of the heat stress on the purified HAT, in the absence or presence of leucine was quantified by calculating the relative peak intensity (n = 3). (d) The stabilising of effect of leucine at 50 mM was compared to that at 4 mM for both leucine and another substrate kynurenine (n=5).

Despite the improvement in the thermal stability of the HAT heterodimer in the presence of leucine, a significant fraction of the HAT was present in higher oligomeric states so further optimization was attempted. Costa et al., 2013 reported similar oligomerization when detergent solubilising LAT2-CD98hc, a difficulty Meury et al., 2014 overcame by modifying the solubilisation conditions and introducing CHS

into the purification. The SEC buffer detergent concentrations employed by Meury et al., 2014, referred to here as SEC2 (0.1 % w/v DDM; 0.02 % w/v CHS; 0.007 % w/v LMNG; 100 mM Tris-Cl; 300 mM NaCl; 10 % w/v glycerol, pH 8), were chosen as the starting point for further optimisation of the SEC buffer. Purification using SEC2 buffer resulted in an increased HAT yield per litre from 100 to 300 µg. LAT1-CD98hc was eluted in 4 different SEC buffers with increasing concentrations of detergent followed by SE-HPLC analysis 1, 1.5, 2 and 3 times greater than SEC2. There was observed a 30 % increase in relative peak intensity between condition 1 and 3 but only a further 3 % increase in condition 4 (Figure 32b). Although increases in peak intensity were observed with increasing detergent concentrations, SEC2 buffer was used for cryo-EM to limit background from detergent.

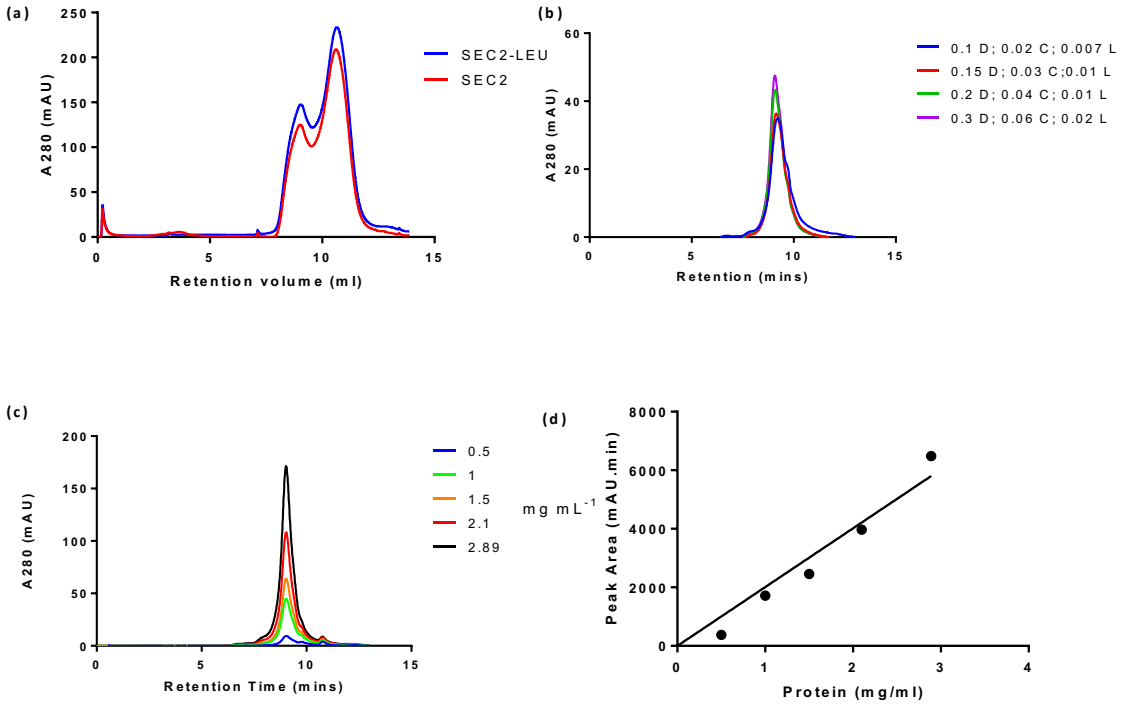

Figure 32 - Optimization of the buffer for size-exclusion chromatography. (a) Size exclusion chromatogram of HAT in SEC with and without leucine (b) LAT1-CD98hc was eluted off the V5 affinity gel in SEC buffers of varying detergent concentrations and analysed by SE-HPLC to determine the optimal SEC detergent concentration. To determine the stability of the HAT at concentration between 0 – 3 mg mL^{-1}, 20 µL of sample in condition 2, at was analysed by SE-HPLC various protein concentrations and the major peak area plotted against sample concentration(c).

The stability of LAT1-CD98hc as its concentration increased was determined by analysing samples of equal volume at various concentrations by SE-HPLC (Figure 32c). Peak area increased linearly as protein concentration increased which is consistent with a sample stable independent of concentration (Figure 32d).

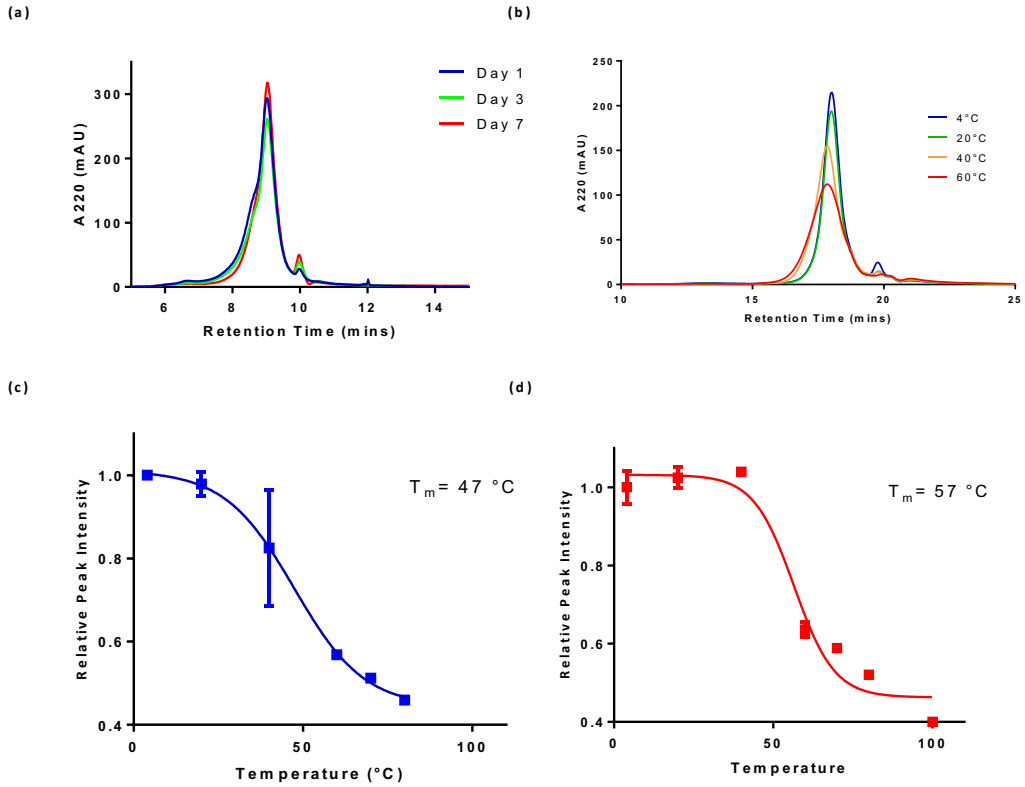

Figure 33 - Characterization of LAT1-CD98hc kinetic and thermal stability by SE-HPLC. (a) Stability of LAT1-CD98hc at 4 °C was monitored for 7 days after purification by SE-HPLC. (b) The chromatograms of the HAT after heating for 10 minutes at the indicated temperatures. Thermal profiles of LAT1-CD98hc in SEC1 buffer in the absence (c) or presence (d) of 50 mM leucine.

CONCLUSION

Progress in the structure determination of human membrane proteins has been hampered in part by the inefficiency of heterologous expression for their production. By using mammalian expression systems such as the HEK293SG system, the difficulty of human membrane protein production has been reduced. However lower yields when compared to heterologous expression mean that, particularly for

the purpose of structural study, protein production remains labour intensive and a major bottleneck. I successfully overexpressed LAT1-CD98hc in HEK293SG cells. The yields per L of cell culture were between, 0.1 – 0.3 mg, depending of the detergent concentration used in the size exclusion buffer. CHS is known to stabilise detergent solubilised membrane proteins by two mechanisms, that is by either binding directly to the membrane protein and, or by modulating the geometry of the protein-detergent complex to better mimic the cell membrane (O'Malley et al., 2011). The work with purified LAT1-CD98hc is consistent with the modulation of the transporter's activity by membrane cholesterol and the presence of putative cholesterol/CHS binding sites on LAT1. The presence of simplified glycans on CD98hc represent potential for further optimisation to improve homogeneity of the sample without potentially compromising yield.

Protein crystallography and cryo-EM can be used in parallel and can be complementary to each (Vinothkumar and Henderson, 2010; Lander et al., 2012). The sample requirement for for homogeneous and stable sample similar in both techniques, but buffer composition, amount of sample and the requirement for crystals are significant differences (Vinothkumar, 2015). The optimisation reported here has so far focused on preparing samples homogeneous and stable enough to work with both techniques but further optimisation was required for cryo-EM. The presence of glycerol and detergent concentrations 10x higher than the CMC of DDM, will most likely contribute to the background noise of any cryo-EM micrographs that may be obtained using LAT1-CD98hc samples in the conditions reported here so far (Thompson et al., 2016). Work toward a structure by cryo-EM single particle analysis is described in the next chapter.

Chapter 5 - LAT1-CD98hc structure determination by single particle cryo-EM

This chapter details the results of efforts toward solving the structure of LAT1-CD98hc using single particle cryo-electron microscopy. Cryo-EM was used to inform further optimisation of the sample preparation described in Chapter 4. Single particle processing of collected cryo-EM data yielded a low-resolution structure that was interpreted by docking the crystal structure of CD98hc ectodomain and a homology model of LAT1. Further single particle analysis revealed previously unreported flexibility in the interaction of CD98hc ectodomain and LAT1.

OPTIMISATION OF SAMPLE PREPARATION, IMAGE PROCESSING AND CRYO-EM DATA COLLECTION

LAT1-CD98hc was prepared, for initial cryo-EM experiments in the buffers optimised and used during biochemical characterisation. Namely, size exclusion buffers 1 & 2 (SEC1 and SEC2), both containing 50 mM leucine, 100 mM TrisCl, 300 mM NaCl and 10 % glycerol at pH 8 but with SEC1 having only x1 the critical micelle concentration of DDM with LMNG and CHS (15:5:3) and SEC2 having 10 times that concentration of the detergent mix. For cryo-grid preparation “in-house” grids, and a custom-built guillotine used for plunge freezing in a humidified cold room (4 °C). Grids were imaged on a 300 kV Titan Krios with a Gatan K2 camera and the images produced were subjected to down sampling to an Å/px size of 2.3 then contrast transfer correction was applied (Figure 34). No large aggregates were visible in the micrographs, while small particles consistent with the image collection parameters

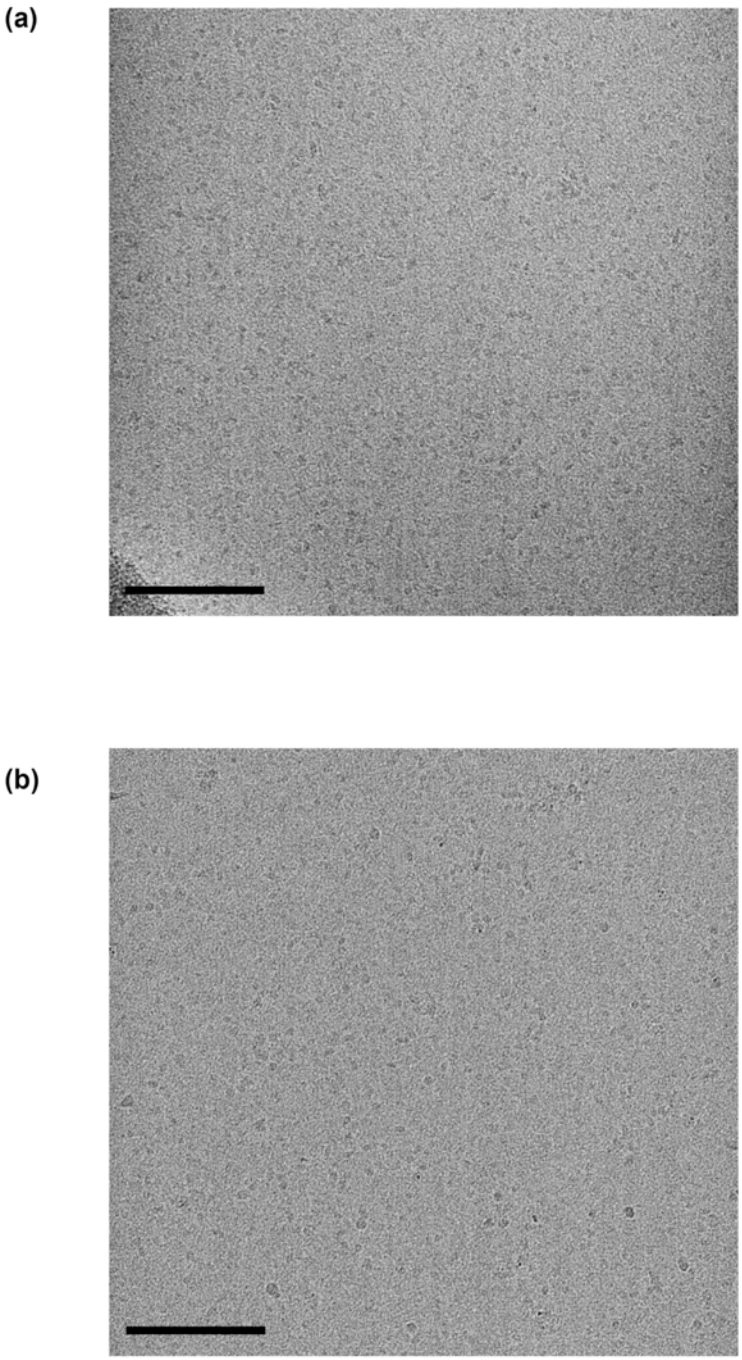

Figure 34 - Exploratory cryo-EM micrographs of LAT1-CD98hc purified in SEC2 (a) or SEC1 (b) buffer obtained at the LMB. Samples were concentrated to 1.1 mg mL^{-1} before application to cryo-grid, blotting and plunge freezing. Images were subject to 2x2 binning and CTF correction, scale bar shown is 100 nm.

and molecular weight of the HAT (123 kDa) were visible and appear evenly distributed on the grid. The small number of micrographs did not allow for further processing but was sufficient to motivate further work at the Astbury Biostructure Laboratory in Leeds.

The first large dataset was collected at the University of Leeds from sample purified in SEC2 buffer, as this had given the higher yield of pure HAT. 2,452 micrograph movies were collected. These were whole frame aligned for beam induced motion correction using Motion Cor 2.1, then CTF estimation and correction was performed on aligned movies without dose weighting using gCTF (Zhang, 2016; Zheng et al., 2017). The resulting images were similar to those obtained from the LMB, with evenly distributed particles, although a gradient in the ice thickness was visible (Figure 35). 2000 particles were manually picked and submitted to reference free 2D classification in RELION 2.1 and 2D classes characteristic of the HAT were used as references for auto picking the entire micrograph set, yielding 373,916 particles. After several rounds of 2D classification, almost all the particles had been discarded as they were either carbon or ice contaminates. 2D classes that were consistent with the HAT, when further classified, yielded what appeared to be projections of protein-detergent complexes (Figure 36b) as well as potentially empty detergent micelles (Figure 36a) in almost equal amounts. The geometry of the DDM:CHS micelles was consistent with small angle x-ray and neutron scattering experiments that predicted an oblate ellipsoid geometry for DDM micelles (Lipfert et al., 2007; O'Malley et al., 2011). Based on the observed abundance of empty micelles, the detergent concentration was subsequently lowered to the lowest practical concentration, x1 CMC of DDM. The limited number of distinct HAT orientations represented in the particle set and the small number particles, precluded single particle 3D reconstruction of the HAT.

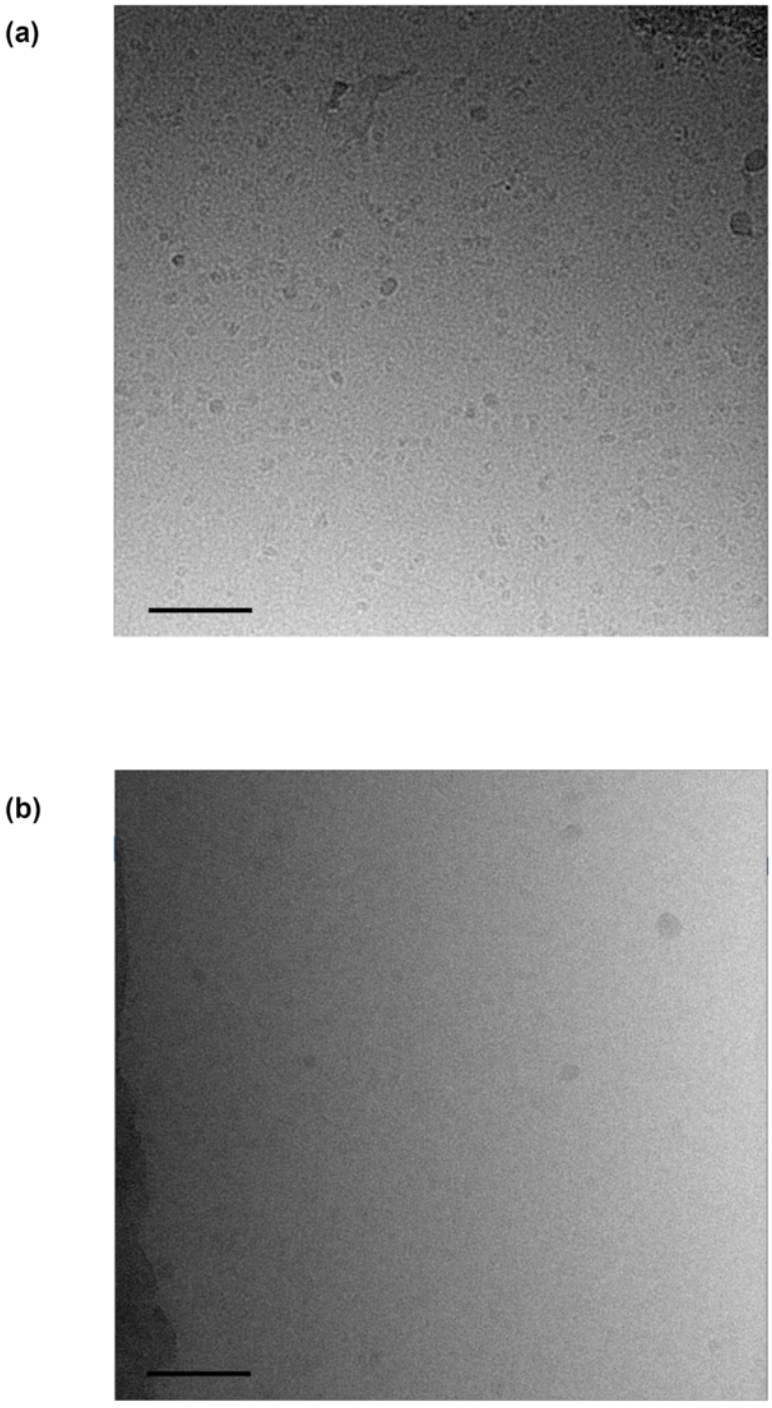

Figure 35 - Representative aligned micrograph movies of first large dataset of LAT1-CD98hc in SEC2 at (a) ~3.6 and (b) ~2 μM defocus. Sample was concentrated to 1.1 mg ml^{-1} before application to a Quantifoil 2/2 grid, blotting and plunge freezing using a Vitribot instrument. Micrograph movies were aligned for beam induced motion correction then CTF corrected. Scale bar given is 60 nm.

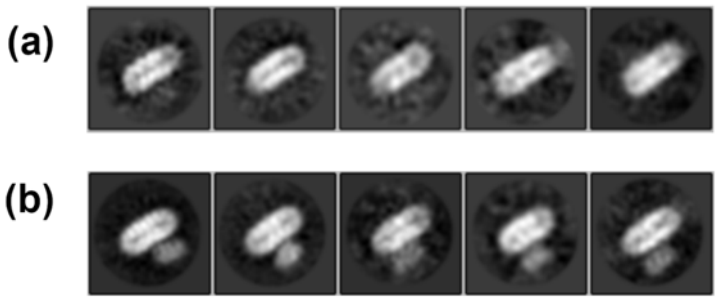

Figure 36 - 2D classes of empty detergent micelles and protein detergent complexes from the first large dataset of LAT1-CD98hc in SEC2. (a) Side view projections of oblate ellipsoid detergent micelles. (b) 2D classes characteristic of a HAT protein detergent complex, with small soluble density and large ellipsoidal detergent belt. Particle box size was 200 Å with a mask diameter of 180 Å.

A second dataset was collected with x1 CMC DDM and 5 % glycerol, as glycerol is known to contribute to background scattering, reducing the signal to noise ratio (Thompson et al., 2016). The improvement in contrast was obvious and most likely due to the lower glycerol. However, the particle distribution on the grid was not ideal, with most of the particles clustering near the carbon support (Figure 37). The ice appeared to increase in thickness closer to the carbon support. The same sample conditions were used to prepare new grids and where the ice thickness, particle distribution and contrast was improved by changing the blotting parameters and collecting data using a Volta phase plate respectively (Figure 38). The improvement in image quality gained from reducing glycerol allowed for generation of an initial 3D model by stochastic gradient descent in RELION 2.1, 3D classification and 3D auto-refinement. The quality of the resulting 3D reconstructions did not allow for a satisfactory docking of the crystal structure of CD98hc's ectodomain and although the phase plate improved the contrast, the background signal was also boosted minimising the gains in contrast.

SINGLE PARTICLE RECONSTRUCTION AND EM DENSITY MAP INTERPRETATION

Another dataset was collected using a VPP but with sample prepared in glycerol free SEC buffer at x1 CMC DDM and a higher protein concentration of 2.3 mg mL^{-1}. The contrast was improved compared to the previous phase plate data with 5 % glycerol, and there were more particles per image (Figure 39). After whole frame beaming induced motion correction and CTF correction, 1388 particles were manually picked in RELION 3 and subjected to reference free 2D classification to yield 2D classes for use as auto picking references. The 2D references were used to auto pick 374,941 particles, giving an average of 157 particles per micrograph. Using a previously generated initial 3D model low-pass filtered to 60 Å, 3D classification using all the particles was done with 2 classes in order to remove "junk" while reducing risk of discarding poorly represented orientations of the HAT. After visual inspection, 191,445 particles that were in one of the two classes were chosen and subjected to reference free 2D classification to yield 100 classes, the majority of which were protein detergent complex. After 2D classification of this particle set and a 3D classification of the particles making up the best 2D classes (Figure 40), 77,423 particles remained and were used in a 3D auto-refinement yielding a 3D single particle reconstruction at 12 Å after post-processing and a B factor sharpening of -1200 (Figure 41f). The 3D reconstruction was docked with the 2.1 Å crystal structure of CD98hc ectodomain using the "fit to segment" tool in Chimera. The cross-correlation between the map and crystal structure was 0.77, also 96% and 98% of crystal structure's atoms and backbone respectively were included inside the EM map after docking suggesting that the results of the 3D reconstruction are consistent with the crystal structure. The large lobe of the 3D reconstruction had an "empty"

ring like channel presumably demarcating the boundary between the detergent micelle and the transmembrane domains of the HAT (Figure 41a – d). This “empty” channel is presumably due to flexibility in the hydrophobic tails of the detergent monomers, which in principle should face towards and stabilise the hydrophobic domains of the protein in the protein detergent complex. The quality of the dataset as indicated by the maximum resolution frequency distribution is sufficient for achieving a sub-nanometre resolution single particle reconstruction, with ~99% of the micrographs falling between 2.5 – 5 Å, and the diversity of projection orientations, suggested that flexibility within the sample itself limited the resolution, despite improvements gained through optimization (Figure 42).

The apo-out open model of LAT1 was docked into a segment of the density in the larger lobe of the density map, with 99% of all the model’s atoms included inside the map there was still some unoccupied density which may be explained by the transmembrane domain of CD98hc (Figure 41b). The distance between the C164 in the outward open model of LAT1 and G109 substituted for C210 (Uniprot ID: P08195-1) in the ectodomain structure after docking was 17 ± 2 Å, that is from the N atom of one residue to that of the other (Figure 47). Both positions are located on loops and are therefore presumably flexible. Figure 43 shows a model of an alternative conformation of the linker region, residues 109 – 112, of CD98hc, demonstrating the C109 in CD98hc and C164 in LAT1 can be brought into sufficient proximity for the disulphide bond to form in the model of the HAT based on the 12 Å EM map. The placement of a model of LAT1 in the micellar density was a substantial improvement over the previously reported 21 Å structure of a HAT, allowing for structural characterization of the quaternary structure of LAT1-CD98hc.

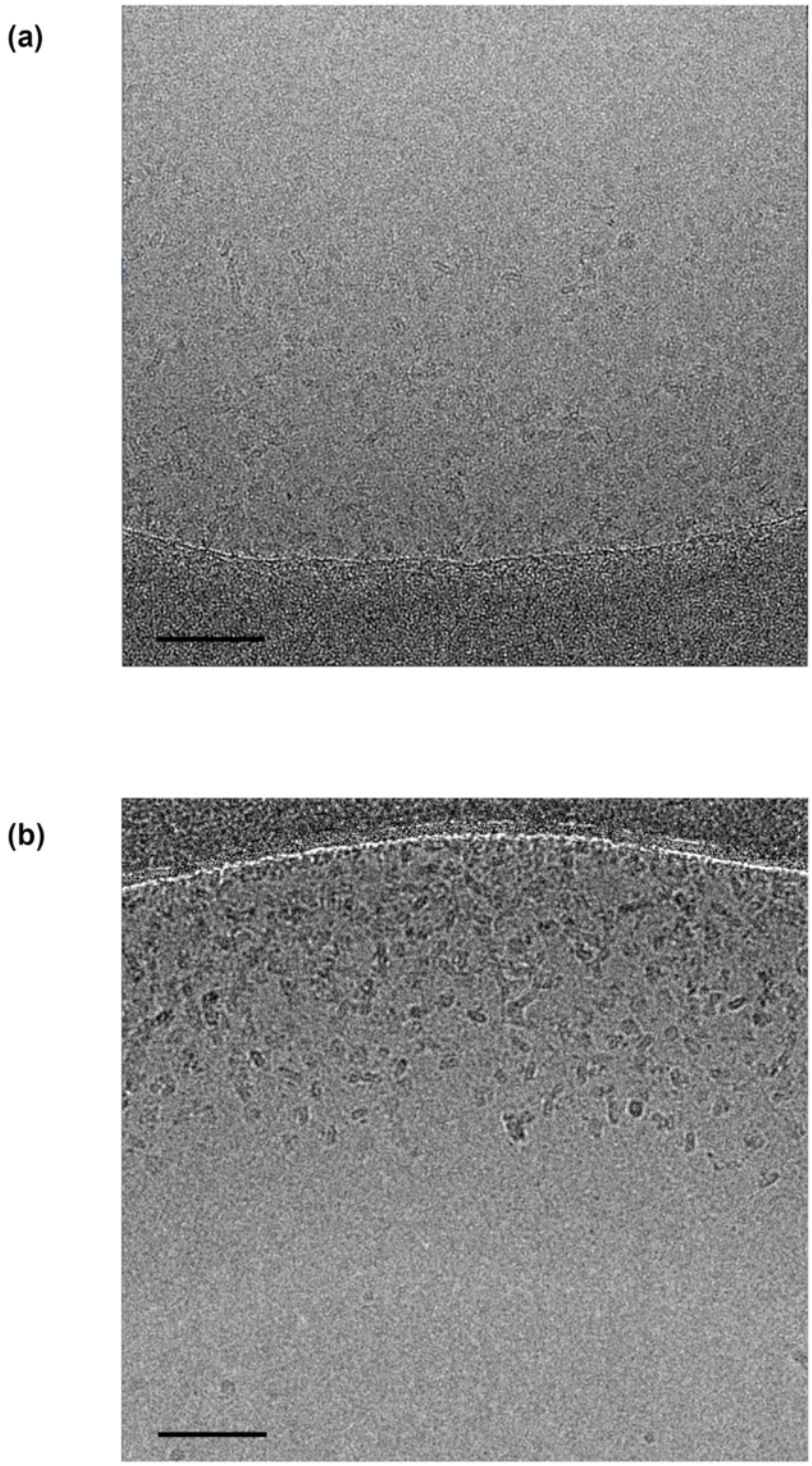

Figure 37 - Representative aligned micrograph movies of LAT1-CD98hc in 5% glycerol and x1 CMC of DDM at (a) ~1.2 and (b) ~3.4 μM defocus. Sample was prepared with lower glycerol and detergent before concentrating to 1.1 mg ml^{-1}, application to a Quantifoil 1.2/1.3 cryo-grid, blotting and plunge freezing using a Vitribot instrument. Micrograph movies were aligned for beam induced motion correction then CTF corrected. Scale bar given is 60 nm.

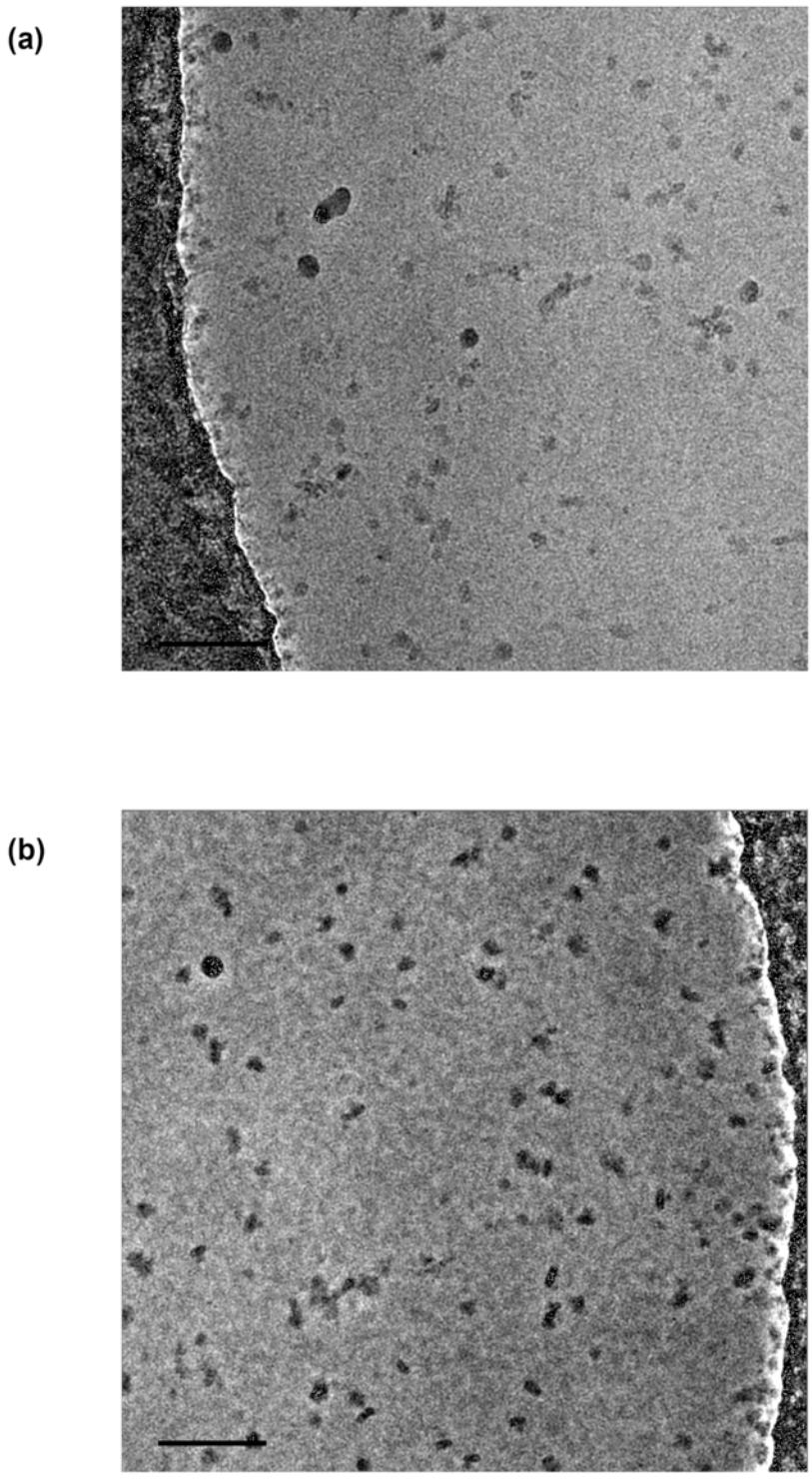

Figure 38 - Impact of Volta phase plate data on image contrast of LAT1-CD98hc in 5% glycerol and x1 CMC of DDM. Sample was prepared with lower glycerol and detergent before concentrating to 1.4 mg ml^{-1}, application to a Quantifoil 1.2/1.3 cryo-grid, blotting and plunge freezing using a Vitribot instrument. Micrograph movies were aligned for beam induced motion correction then CTF corrected. Images (a) and (b) are from movies recorded at ~1.9 and ~0.1 μM defocus respectively. Scale bar given is 60 nm.

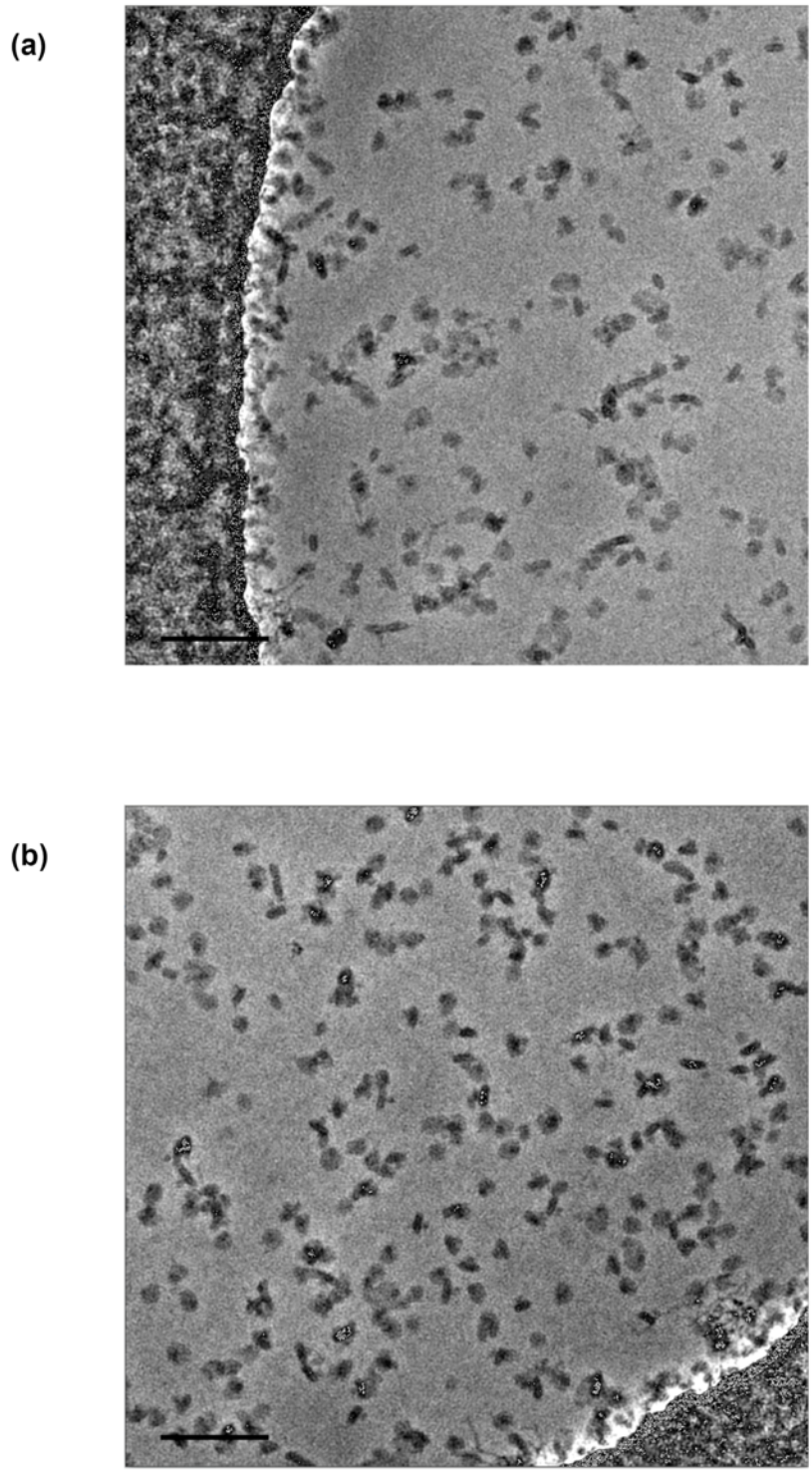

Figure 39 - Representative aligned micrographs movies of LAT1-CD98hc in glycerol free buffer at x1 CMC of DDM collected using Volta phase plate. Sample was concentrated to 2.3 mg ml $^{-1}$ before application to a Quantifoil 1.2/1.3 cryo-grid, blotting and plunge freezing using a Vitribot instrument. Micrograph movies were aligned for beam induced motion correction then CTF corrected. Images (a) and (b) are from movies captured at ~1.1 and ~0.1 μM defocus respectively. Scale bar given is 60 nm.

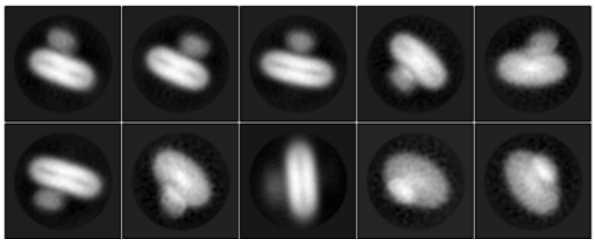

Figure 40 - Representative 2D classes from glycerol free sample collected using Volta phase plate. A variety of projections of the protein detergent complex visible amongst the 2D classes. Particle box size was 200 Å with a mask diameter of 180 Å.

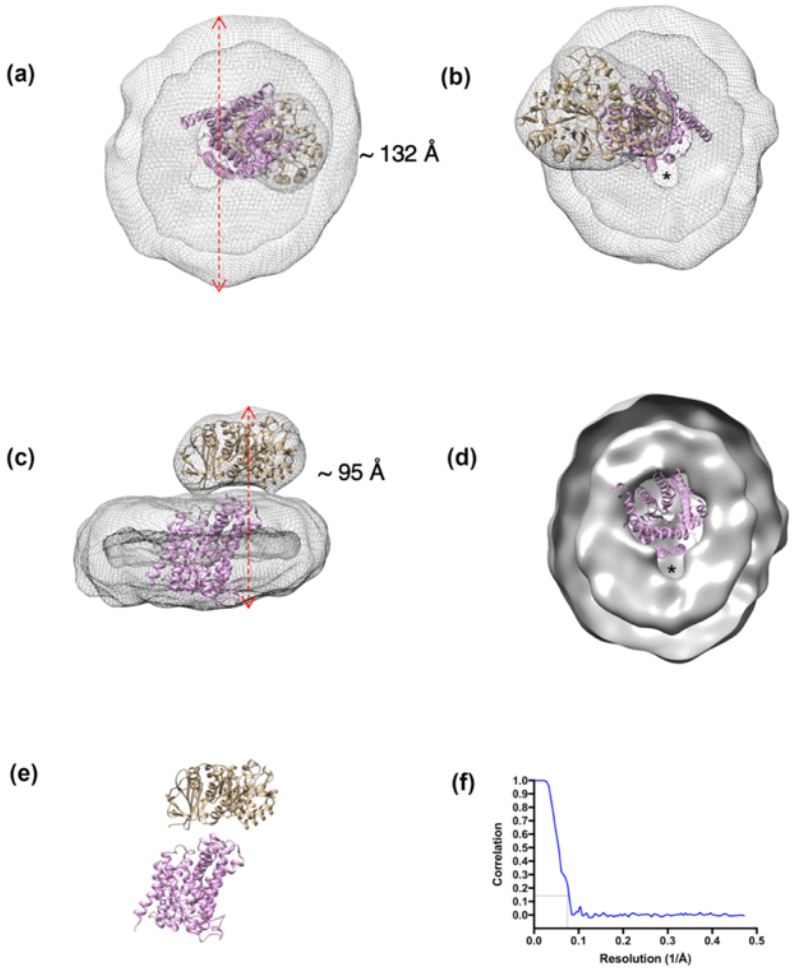

Figure 41 - 12 Å reconstruction of apo-LAT1-CD98hc in glycerol-free buffer. Coulomb potential map of 3D reconstruction of LAT1-CD98hc protein-detergent complex shown as a mesh surface in a – c and the ectodomain crystal structure of CD98hc and outward open model of LAT1 shown as tan and pink ribbons respectively in a – e. (a) is rotated 180 ° in the plane of the page with respect to (b) a bottom and top view of the protein-detergent complex. (c) Side view of the docked EM map. (d) Top view of a cross section through the long axis of the larger lobe, show as a grey surface, illustrating the quality of the docking of the LAT1 model in the EM map. Dimensions of EM map marked by red arrows and the distances given in Å. Unoccupied density adjacent to the LAT1 model indicated by * in b and d. (e) Models LAT1-CD98hc ectodomain without EM density map (f) Fourier shell correlation vs 1/Å with dotted black line to show spatial frequency at correlation 0.143, which was ~12 Å.

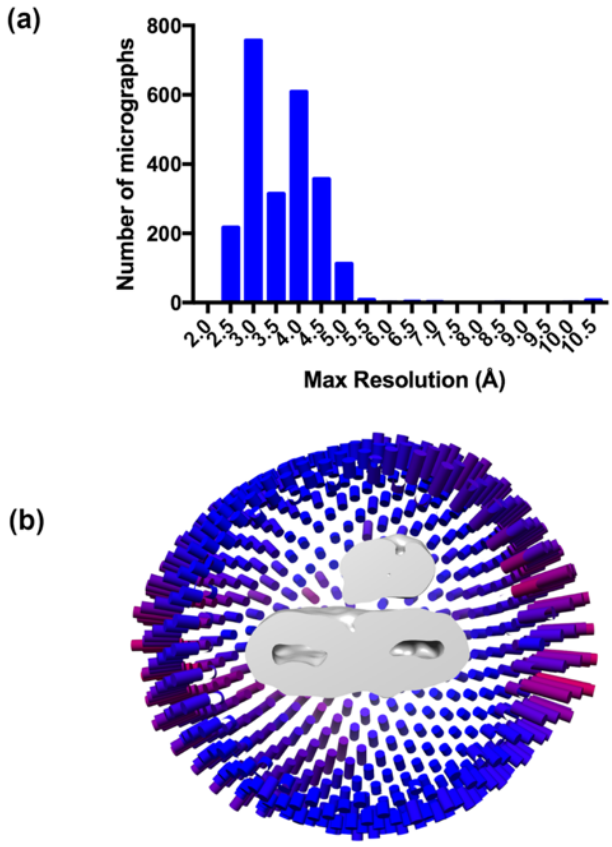

Figure 42 - Quality of dataset 4 and orientation distribution of 2D projections used in single particle reconstruction of LAT1-CD98hc to 12 Å. (a) Histogram of the frequency distribution of micrographs in dataset 4 across different maximum resolutions bins. (b) Orientation distribution of LAT1-CD98hc projections from dataset 4 used in the 3D reconstruction of 12 Å EM map of the protein-detergent complex.

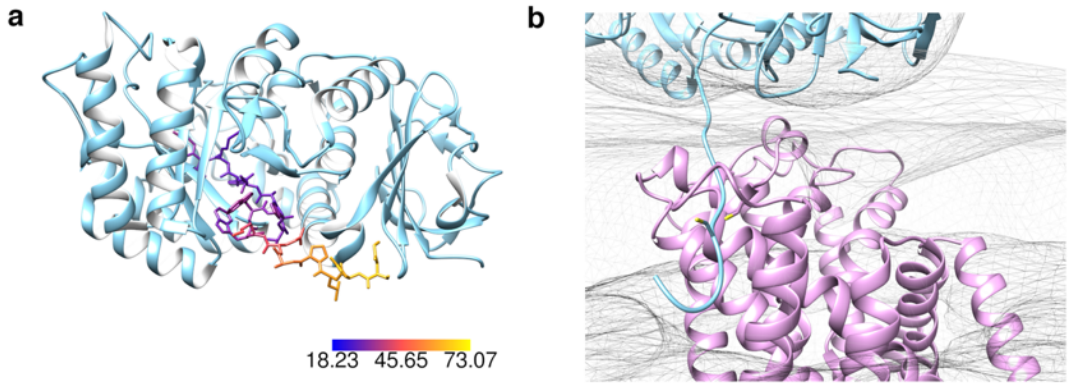

Figure 43 - Modelling conformations of residues 109 – 112 of the CD98hc ectodomain crystal structure (PDB ID 2DH2), where disulphide bond forming C210 in CD98hc is located. (a) Crystal structure of CD98hc, residues 109 – 112 coloured by Cα B factor. B factor scale is in $Å^2$. (b) CD98hc ectodomain (blue) and outward open conformation of LAT1 (purple) docked in 12 Å map (mesh). C109 (sticks) of CD98hc brought >5 Å of C164 (sticks) LAT1.

The extracellular face of LAT2 and the ectodomain of CD98hc have been postulated to interact extensively and the residues at the interface have been predicted (Rosell et al., 2014). In the EM map, LAT1 and the ectodomain of CD98hc do not interact in a manner similar to LAT2 even though sequence analysis showed that putative interaction residues are conserved or substituted for similar ones in LAT1 (Figure 44). Out of 19 of these residues only 6 were <10 Å of CD98hc ectodomain, in the docked EM map (Table 8; Figure 44). As a means of independent validation, LAT1 in the outward open conformation and CD98hc ectodomain were docked using ClusPro, with distance restraints inferred from cross-linking experiments of LAT2 and CD98hc ectodomain (Rosell et al., 2014). All the predicted docking poses did not place CD98hc in better proximity to the predicted interface residues and some were implausible as they placed CD98hc ectodomain in regions of LAT1 predicted to be membrane embedded. The evidence from the interpretation of the EM map and protein-protein docking suggests that LAT1 does not interact with CD98hc in a similar fashion to LAT2, in fact the EM docking suggests limited interaction between LAT1 and CD98hc ectodomain and therefore CD98hc ectodomain may adopt various conformations with respect to LAT1.

In order to explore possible flexibility between the two subunits, 3D multibody auto-refinement was performed using the final 3D auto-refinement that produced the 12 Å map as a starting point, followed by principle component analysis as described by Nakane *et al.*, 2018. Principal component analysis (PCA) of the variance in rotations and translations of the two bodies defined in the multibody refinement was accounted for by motion along 12 eigen vectors/principle components, with the first three accounting for 42.7% of variance (Figure 46a).

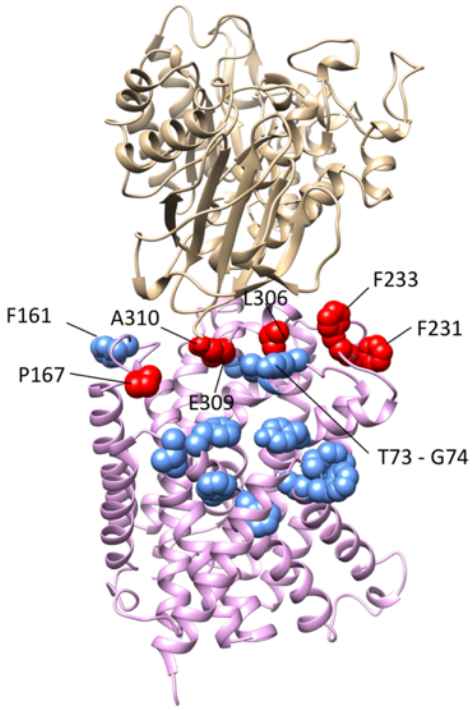

Figure 44 – Putative LAT1-CD98hc interface residues. LAT1 (pink ribbon) residues predicted based on homology with LAT2, to interact with CD98hc ectodomain are shown as blue spheres. The orientation of CD98hc ectodomain (tan ribbon) to LAT1 was predicted based rigid body docking into the 12 Å EM of the complex. Residues within <10 Å of CD98hc ectodomain are shown as red spheres. (See also *Table 8*)

A volume series, consisting of 10 volumes per component, were written out for the first 3 components, allowing for visualization of the molecular flexibility between the two bodies. The crystal structure of CD98hc ectodomain and outward open model of LAT1, were docked in each volume of the series allowing for modelling of the flexibility described by the volume series in molecular terms (Figure 45;Figure 46). Component 1, described 18.7% of the variance, showed mostly translation but also some rotation of CD98hc ectodomain and LAT1 in opposite directions along parallel planes, perpendicular to the plane of the long axis of the complex (Figure 46b; Movie 1). The second largest component, which described 13.7% of the variance, showed a rocking motion i.e. forward downward but slanted motion in CD98hc ectodomain and a downward backward motion in LAT1, with the effect of bringing the C domain of CD98hc closer to LAT1 while lifting the A domain away

(Figure 46c; Movie 2). The third component showed an upward and downward motion in CD98hc ectodomain and a slight twisting motion in LAT1 bringing the two closer and further apart from each other (Figure 46d: Movie 3). The flexibility described by the principle component analysis was consistent with transient or limited interaction between LAT1 and CD98hc ectodomain, which is contrary the prediction of extensive interaction based on homology to LAT2. The distance between residues that were positive in LAT2-CD98hc cross-linking experiments were tracked across each frame of the eigen movies for vectors 1 – 3. All residues tracked being > 18 Å apart, outside the range of the cross-linkers (3.5 – 14.3 Å) used by Rosell *et al.*, 2014 (Figure 47). However, Gly505 and Ser487 in CD98hc, are located on a linking loop comprised of residues with relatively high temperature factors in the crystal structure of the ectodomain, while Gly220 and Ser324 in the LAT1 homology model are likely to be flexible. They are also located on loops and therefore these residues may be within the range of the cross-linkers in some conformations. This distance analysis also highlights the dynamic LAT1-CD98hc interaction with residues being displaced by as much as 5 Å between various conformations of the HAT.

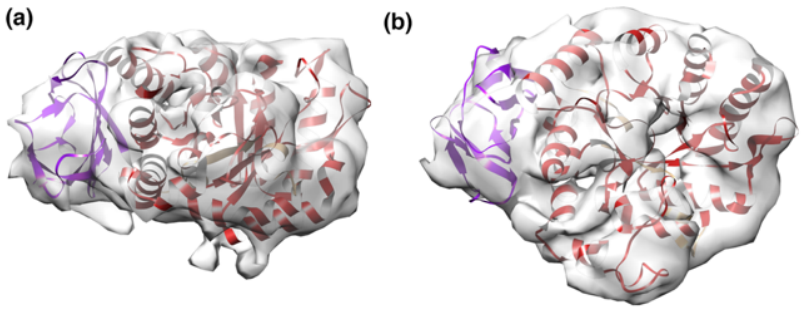

Figure 45 - CD98hc ectodomain crystal structure docked in improved EM map density. Both a) and b) show crystal structure (PDB ID) 2DH2 docked the density corresponding to CD98hc ectodomain which had an improved resolution (~9 Å) after multibody refinement. Densities corresponding to A and C domains of the ectodomains were visually distinguishable increasing confidence in the interpretation of the map by docking. b) is rotated 90 ° anti-clock wise in the plane perpendicular to that of the page, relative to a).

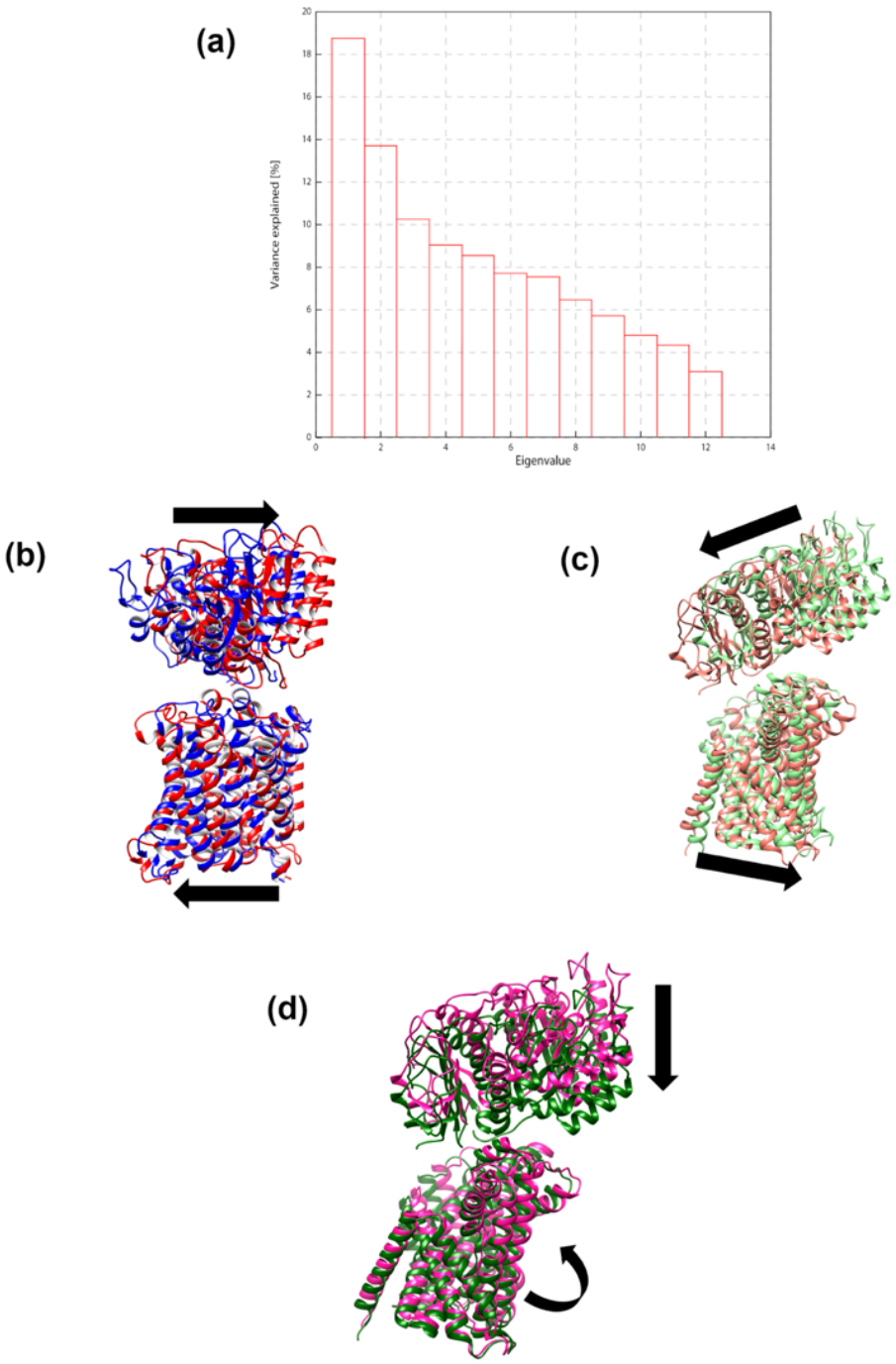

Figure 46 - Molecular dynamics of LAT1-CD98hc in solution. a) PCA of relative orientations of EM densities corresponding to CD98hc ectodomain and the transmembrane domains of CD98hc and LAT1, after two body 3D auto-refinement. Molecular flexibility along eigen vectors 1 (b), 2 (c), and 3 (d). Structures in (c) and (d) are rotated approximately 90 ° anti-clockwise relative to (b) in the plane perpendicular to the page. The black arrows indicate the direction of motion from the first to the last EM density map of volume series showing motion/flexibility along the given Eigen vector.

Table 13 - Residues cross-linked in order to validate in silico docking of LAT2 and CD98hc ectodomain crystal structure.

Distance restraints were obtained from Rosell et al., 2014. The estimated distance between these residues and residues in CD98hc ectodomain were calculated from docking of the volume series of PCs 1 – 3 for LAT1 to the nearest Å.

CD98hc	LAT2	LAT1	Distance LAT2 from cross-linking (Å)	Average LAT1 distance from cryo-EM (Å)
S151	C210	G220	13.4	25 ± 2
	A315	S324	14.9	32 ± 2
S195	C210	G220	17.5	20 ± 2
	A315	S324	15.5	31 ± 2
S412	C210	G220	11.5	36 ± 2
S487	G392	S401	12.9	34 ± 1
G505	A235	V244	8.4	23 ± 1
	S441	S450	8.1	32 ± 1

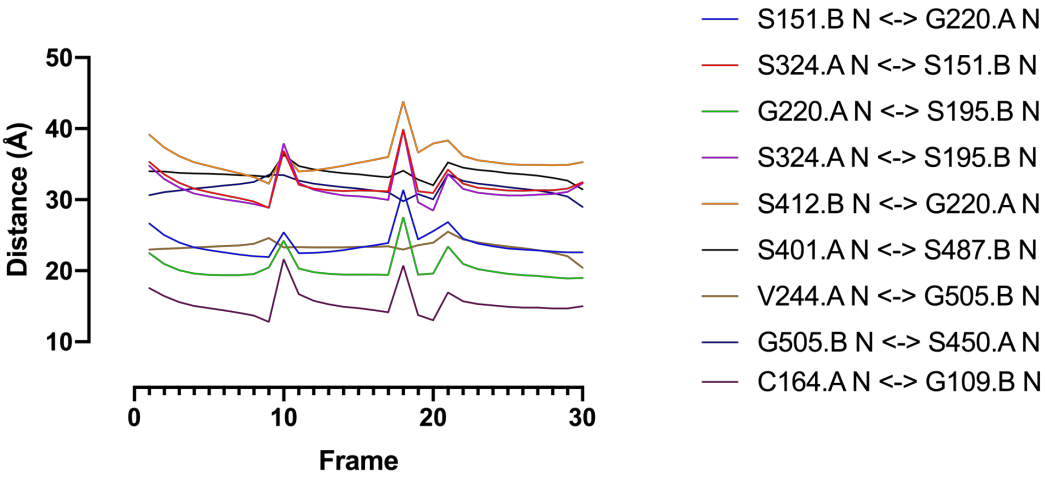

Figure 47 - Distances between residues predicted to be in close proximity based on homology to LAT2. The distance between the N atoms of residues in CD98hc ectodomain, designated chain B and LAT1, designated chain A, were measured across conformations predicted based on docking of the two structure in the frames of "eigen movies" of eigen vectors 1,2 and 3 from the principle component analysis of the variance discovered in the multibody refinement of LAT1-CD98hc at 12Å.

CONCLUSION

A high resolution structure of a HAT such as LAT1-CD98hc remains elusive despite efforts toward achieving this goal (Fort et al., 2007; Costa et al., 2013; Meury et al., 2014; Rosell et al., 2014). Here I report the first attempt at single particle analysis of LAT1-CD98hc using cryo-EM. Cryo-EM micrographs of LAT1-CD98hc in vitreous ice showed particles of a size consistent with the 123 kDa complex in detergent. Excess detergent and glycerol interfered with the single particle reconstruction as empty detergent micelles were mistaken for protein detergent complexes and glycerol reduced the signal to noise ratio of the particles. The elimination of glycerol from the sample and lowering of detergent concentration, also improved grid preparation and Volta phase plate data collection, producing a data set from which a 12 Å structure of LAT1-CD98hc in detergent was solved. The reconstruction was validated by docking the 2.1 Å crystal structure of CD98hc ectodomain. This map was sufficiently detailed to allow for docking of a predicted model of the outward open conformation of LAT1. There was little density in the EM map between LAT1 and CD98hc ectodomain suggesting transient interactions between the two. Multibody refinement using RELION 3, followed by principal component analysis of the rotations and translations of LAT1 and CD98hc ectodomain, revealed variance within the particles that had been assumed to be of the same conformation. The flexibility described by the first three eigen vectors of the PCA visualised showed CD98hc ectodomain barely interacts with LAT1 and is most likely tethered to LAT1 by interactions between the transmembrane domain of CD98hc and the conserved disulphide bond.

An interaction interface between CD98hc ectodomain and LAT2 was proposed on the basis of docking and cross-linking experiments by Rosell *et al.*, 2014. LAT2 shares 52% sequence identity with LAT1 and residues at this interface are conserved and therefore it was assumed that LAT1 interacted with CD98hc ectodomain in a similar manner to LAT2. EM maps reported here and the subsequent interpretation of them, do not support this hypothesis. Only 31.6 % of the putative interacting residues in LAT1 are < 10 Å away from CD98hc ectodomain and all of the residues successfully cross-linked in order to validate the results of *in silico* docking of LAT2 and CD98hc ectodomain, were greater >18 Å apart in each member of the LAT1-CD98hc ectodomain model ensemble generated from the cryo-EM data presented here.

Chapter 6 - General discussion & future outlook

This chapter serves a final discussion of the main novel finding of this study which are:

- LAT1-CD98hc is modulated and stabilised by cholesterol through putative cholesterol binding sites in LAT1. This part of the study was published in "Modulation of LAT1 (SLC7A5) transporter activity and stability by membrane cholesterol" Scientific Reports volume 7, Article number: 43580 (2017)
- Inhibitors of LAT1, JPH203, KMH233 and SKN103, are competitive inhibitors of the transporter and JPH203 and SKN103 are potentially transported substrates while KMH233 may sterically hinder transition from the outward open conformation to any of the occluded conformations and thus may not be a transported substrate.
- Cryo-EM of detergent solubilised LAT1-CD98hc shows limited interaction between CD98hc ectodomain and LAT1 and thus flexibility between the two domains. The interaction of the two is not consistent with modelling of the interaction with LAT2.

LAT1-CD98hc is one of the rare heterodimeric solute carrier transporters in the human genome and plays key roles in normal and disease physiology as outlined in the introduction of this thesis. Understanding the structural details of this amino acid transporter's organisation and function was the overarching aim of the research reported here. The cloning of LAT1 was reported in 1998, since and before then there have been significant efforts to understand the transporter's structure and function (Kanai et al., 1998; Mastroberardino et al., 1998). There also has been significant progress in the structural biology of SLC transporters, particularly the solution of the

structures of bacterial homologues of LAT1, EcAdiC and GkApcT, as well as structural analogues of eukaryotic origin such as dDAT (Gao et al., 2010; Penmatsa et al., 2013; Bai et al., 2017; Jungnickel et al., 2018). Sequence alignment of LAT1 and dDAT suggested that the two cholesterol/CHS binding sites observed in the crystal structures of dDAT were conserved in LAT1. The residues identified were found conserved across several LAT1 orthologues consistent with functional importance. Homology modelling of LAT1's structure revealed a similar organisation of these residues in the tertiary structure, lending further credence to the hypothesis of LAT1/cholesterol interaction via these conserved residues. The hypothesis was tested experimentally by transport assay and cholesterol depletion in cells expressing LAT1. It was shown that cholesterol depletion lowered V_{max} but not K_m of LAT1 mediated transport and thus it was concluded cholesterol was acting as an allosteric modulator of LAT1 transport (Dickens et al., 2017). Additional putative binding site were identified by sequence motif searching for CRAC/CARC motifs. This study adds to a growing body of knowledge about the role of lipid bilayers in the functions of specific membrane proteins within them. This may have implications for research, particularly for *in vitro* and *in silico* experiments that seek to model the functions of membrane proteins. For example, lipids have proved to be important for the preservation of function of solubilized membrane proteins and for their crystallization (Banerjee et al., 1995; Guan et al., 2006; Phillips et al., 2009; Laganowsky et al., 2014). Drug design may also be impacted as lipids could act as templates for the design of allosteric modulators of membrane protein function for the treatment of disease.

LAT1 mediated transport plays a major role in the survival and progression of a variety of cancers and as result this activity has been the focus of chemotherapeutic drug development. The binding modes of three LAT1 specific inhibitors was explored here using models of LAT1 in the outward facing conformation and in the inward facing occluded conformation. SKN103 and JPH203 bound to both conformations and had extensive interaction networks compared typical substrates, an observation consistent with their predicted binding energies and affinity as inferred from IC_{50} calculations. The predicted binding energies were higher for the inward occluded conformation compared to the outward open. Their binding in a similar manner to substrates to both transporter conformations suggest they may be transportable but their favourable binding to one conformation raises the possibility that they may inhibit transport by stabilising this favoured conformation, stalling the transporter cycle. The design and screening of conformation specific drugs is becoming common for the targets like G-protein coupled receptors but is still to be extended to transporter drug design. These are question for further research. The inhibitor KMH233 behaved atypically and bound only to the outward open conformation by binding to a novel putative amino acid binding site. The binding pose of KMH233 was such that it would sterically hinder conformational change from the outward open to the inward open conformation, disrupting the transport cycle. The two different inhibition modes described here could form a basis for more nuanced inhibitor design for LAT1, increasing the urgency for experimental validation of these models specifically through X-ray crystallography or single particle cryo-EM.

Membrane proteins are often present in cells, in small quantities insufficient for structural study (Ostermeier and Michel, 1997). Although there are solutions to

this problem, membrane proteins remain recalcitrant to characterisation by structural techniques such as protein crystallography and cryo-electron microscopy (Kang et al., 2013; Vinothkumar, 2015). The paucity of membrane proteins in cellular material is often addressed by heterologous or overexpression of the protein of interest. *Escherichia coli* is the most popular organism for heterologous expression and has worked well with small soluble proteins and the soluble domains of membrane proteins. However, prokaryotic expression systems like *E.coli,* prove less efficient or fail to express membrane proteins larger than 35 kDa, with more than 6 transmembrane helices, regardless of the organism of origin (Terpe, 2006; Nettleship et al., 2010; Bernaudat et al., 2011). Additionally, post translational processing such as disulphide bond formation and glycosylation, tend to be inefficient or completely absent in these systems, leading to expression of unfolded and or non-functional proteins (Terpe, 2006). Yeast are an alternative to bacterial expression that can provide similar, albeit with reduced flexibility and ease in manipulation, the requisite expression capacity and processing to produce larger membrane proteins that are correctly folded and functional (Nettleship et al., 2010). *Saccharomyces cerevisiae* and *Pichia pastoris* are two species of yeast commonly used in the production of eukaryotic proteins including transmembrane proteins (Joubert et al., 2010; Ahmad et al., 2014). Like yeast, insect cells such as those from *Spodoptera frugiperda*, are capable of post-translational modifications such as glycosylation, but differ from higher eukaryotes in the exact nature of this glycosylation and in membrane lipid composition, meaning the native fold and functionality of the expressed transmembrane protein is only more likely but not guaranteed (Nettleship, 2012). The insect baculoviral system is more time consuming and expensive compared to

yeast, due to the requirement for virus production, titration, the optimisation of the insect cell transduction before expression, and because of the cost of growth medium used in the culture of the insect cells. Given the disadvantages of insect cell expression compared to yeast cell expression, in a situation where near native glycosylation is essential, mammalian expression systems such the Chinese hamster (CHO) and human embryonic kidney cell-lines (HEK293) are preferable (Dalton and Barton, 2014; Büssow, 2015). Membrane protein production in mammalian cells, can be technically demanding, as well as labour and resource intensive, relative to heterologous expression in bacteria or yeast, and often results in lower protein yields (Chaudhary et al., 2012; Klepsch et al., 2011). However once successfully overexpressed, the resulting protein is often correctly folded, post-translationally modified and thus most likely biochemically active. These advantages often outweigh the challenges, and strategies for streamlining expression and increasing yields are being developed, as a result mammalian protein production for the structural study of human membrane proteins is increasingly becoming popular in structural biology (Chaudhary et al., 2012; Aricescu and Owens, 2013; Goehring et al., 2014; Lin et al., 2015). A protocol for stable mammalian expression and purification of detergent solubilised LAT1-CD98hc was developed and optimised. The requirement for CHS in the purification buffers during and after membrane solubilisation was consistent with the hypothesis detailed above, that's the modulation of LAT1 by direct interaction with cholesterol. The addition of ATM to the lysis buffer was a small but important modification to the purification protocol as it maximised the amount of purified HAT with the disulphide bond. Although already reported in the literature, it will be used regularly in the purification of proteins with structural disulphide bonds

from mammalian cells (Kao et al., 2010; Trexler-Schmidt et al., 2010; Koterba et al., 2012).

After further sample optimisation, informed by cryo-EM data collection and processing, a 12 Å structure of LAT1 was achieved allowing for the docking of the crystal structure of CD98hc ectodomain and the outward open conformation of LAT1. Given the low SNR ratio of cryo-EM data which requires averaging techniques to improve, and the uncertainty of orientation assignment between the 2D projections from the data during 3D reconstruction, the final map must be validated to ensure it is representative of the structure under investigation (Frank, 2006). Tilt pair analysis, which requires collecting a subset of micrographs at two goniometer angles generating 2D projections related to each by a known angle. These can be used to determine the accuracy of orientation assignment of 2D projections in the final map by comparing the angle between matching projections in the final EM map (Rosenthal and Henderson, 2003; Rosenthal, 2016). Also, if known consistency between an independently determined structure of the same particle or part of it, such as crystal structure, may be used to assess the quality of the of the final map (Frank, 2006; Henderson et al., 2012; Rosenthal, 2016). The latter approach was taken here as no tilt pair data was collected. The crystal structure of CD98hc ectodomain docked into the 12 Å EM structure. From the structure reported here it is obvious that detergent solubilised LAT1-CD98hc is not a dimer of heterodimers even though one of the reported crystal structures of CD98hc ectodomain is a dimer (PDB ID 2DH3) and a LAT1 dimer has been suggested on the basis of homology to EcAdiC (Fort et al., 2007; Napolitano et al., 2017a). The orientation of CD98hc ectodomain in the docking, in fact precludes a CD98hc dimer and LAT1 as it would

clash with the plasma membrane. There is also no extensive interaction between the CD98hc ectodomain and LAT1 as was described for LAT2-CD98hc by Rosell *et al.*, 2014. Residues at the predicted interface of LAT2 and CD98hc were found to be mostly conserved in LAT1 but less than half of them were less 10 Å away from each other in the cryo-EM model LAT1-CD98hc ectodomain. 3D auto refinement of the CD98hc ectodomain and micellar density was performed on them as two independent rigid bodies followed by PCA of their relative rotations and translations. This revealed continuous motion between the two subunits. The flexible motion of CD98hc relative to LAT1 is consistent with limited or transient interaction between the ectodomain and LAT1. A similar conclusion was reached from the work reported by Pfeiffer *et al.*, 1998, using mutagenesis and co-immunoprecipitation. The idea that LAT1 and LAT2 may interact differently with CD98hc is not a new one. Bröer *et al.*, 2001 put forward, based experiments with truncated versions of CD98hc and various light chains, including LAT1 and LAT2, that CD98hc is modular requiring different modules to interact with different light chains. These experiments showed that, for the recognition of LAT1, the cytosolic N terminus and transmembrane domain of CD98hc were sufficient for the association of CD98hc and LAT1 whereas LAT2 required the complete ectodomain domain. Rosell *et al.*, 2014 stated that the extracellular vestibule to the substrate binding site was accessible in the model of CD98hc ectodomain and LAT2 proposed but it unclear whether the binding of CD98hc reduced the volume open to the solvent. This is of interest as it may offer in part a molecular mechanism for the LAT1 selectivity of inhibitors such as JPH203, which may be too large to access the substrate binding site of LAT2 due to the

placement of CD98hc. Even more interesting is the prospect of exploiting this difference heavy-light chain interaction for rational drug design.

The structural characterisation of proteins to atomic or near atomic resolution, requires a biochemically homogenous and monodisperse samples (Newby et al., 2009). Membrane protein samples which meet these conditions are challenging to prepare due to the lipid bilayer embeddedness and amphipathic character of these membrane protein systems. In order to apply techniques common for soluble protein purification, such as affinity and size exclusion chromatography, the membrane protein or complex in question must first be extracted from its lipid bilayer and simultaneously solubilised in aqueous buffer while maintaining its functional, native fold. This is often achieved by the use of surfactants such as detergent or amphipathic polymers such as styrene maleic acid (SMA) (Lin and Guidotti, 2009; Hattori et al., 2012; Stroud et al., 2018). Detergents are small amphipathic molecules that above a certain concentration, the critical micelle concentration, form aggregates in aqueous solution referred to as micelles. In detergent micelles, the hydrophobic tails of the detergent are sequestered away from the aqueous environment external to the micelle, forming a hydrophobic core at the centre, while the hydrophilic head groups keep the micelles soluble by interacting with the solvent (Linke, 2009). The amphipathic structure of detergent monomers is analogous to that of phospholipids and as a result, detergents are capable of interacting with and solubilising phospholipid membranes and the proteins embedded in them. The hydrophobic core of the micelle mimics the hydrophobic centre of a phospholipid bilayer, interacting with the transmembrane domains of the detergent solubilised membrane proteins (Le Maire et al., 2000).

Detergents vary in the composition of the head and tail groups and thus vary in their efficacy in membrane protein solubilisation and stabilisation. They are informally classified as being either harsh or mild, depending on whether they are more likely to destabilise or stabilise the native fold of a membrane proteins during membrane solubilisation. Long chain hydrophobic tailed detergents, usually 10 – 12 carbons, with polar head groups such as maltose or glucose, such as n-dodecyl β-D-maltoside or n-octyl-β-D-glucoside, are considered mild and are widely used in structural studies of membrane proteins. Detergents also differ in the extent to which they co-extract membrane proteins and their bound lipids with some even enriching for particular lipids. For example, the zwitterionic detergent, CHAPS (3-((3-cholamidopropyl) dimethylammonio)-1-propanesulfonate), has been shown to solubilise 4 times more lipids than triton-X100, while enriching the phospholipid, phosphatidylethanolamine (Banerjee et al., 1995). Despite these generalisations and rules of thumb, the choice of detergent for the purification of a given membrane protein or complex, which is an important one because it determines the stability and functional state of the purified sample as well as the ease or difficulty with which the protein can be structurally characterised, it is difficult to predict *a priori* a suitable detergent or sometimes cocktail of detergents and additives. Therefore significant effort is often spent on screening detergents and optimising purification conditions (Arachea et al., 2012; Champeil et al., 2016). In this study the effect of detergent solubilisation on the structure of LAT1-CD98hc was not explored. Biochemical and biophysical characterisation of the HAT in lipid environments such as in nanodiscs, may shed light on the interaction CD98hc and LAT1 since it has been hypothesised that CD98hc ectodomain interacts with the

plasma membrane (Fort et al., 2007). This putative membrane interaction may play a role in the role of CD98hc in the transport cycle of LAT1.

A high-resolution structure of LAT1-CD98hc remains crucial for further understanding the function of the transporter and for placing some of the insight gleaned here and in other similar efforts on sound experimental footing. The state of the art cryo-EM appears sufficiently advanced for the determination of a structure of this complex but heterogeneity in the sample remains a challenge. Expressing a fusion construct of LAT1 and BRIL or T4 lysozyme to increase the mass of the complex, and potentially help with projection alignments may be necessary (Thal et al., 2018). The deletion of CD98hc's ectodomain using CRISPR Cas9 is also another modification that could be made. It would give an opportunity to reproduce the experiments of Bröer *et al.*, 2001 in a better model system and if successful would remove the heterogeneity of due the ectodomain's flexibility. Despite some work towards it, we could not collect data with ligand bound. Towards this goal, testing of the hypotheses generated from the homology modelling and docking is necessary. KMH233, if it indeed only interacts with the outward open conformation and stabilises it, and also given its affinity and solubility, would be a suitable candidate for cryo-EM data collection of ligand bound LAT1-CD98hc. The solution of a high-resolution structure of LAT1-CD98hc may require a combination of all three but it is goal worth of pursuing.

References

Adhikary, S. and Eilers, M., (2005) Transcriptional regulation and transformation by Myc proteins. *Nature Reviews Molecular Cell Biology*, [online] 68, pp.635–645. Available at: http://www.nature.com/articles/nrm1703 [Accessed 18 Apr. 2018].

Ahmad, M., Hirz, M., Pichler, H. and Schwab, H., (2014) Protein expression in Pichia pastoris: recent achievements and perspectives for heterologous protein production. *Applied microbiology and biotechnology*, [online] 9812, pp.5301–17. Available at: https://link.springer.com/content/pdf/10.1007%2Fs00253-014-5732-5.pdf [Accessed 23 Oct. 2018].

Altan, B., Kaira, K., Watanabe, A., Kubo, N., Bao, P., Dolgormaa, G., Bilguun, E.-O., Araki, K., Kanai, Y., Yokobori, T., Oyama, T., Nishiyama, M., Kuwano, H. and Shirabe, K., (2018) Relationship between LAT1 expression and resistance to chemotherapy in pancreatic ductal adenocarcinoma. *Cancer Chemotherapy and Pharmacology*, [online] 811, pp.141–153. Available at: http://link.springer.com/10.1007/s00280-017-3477-4 [Accessed 29 Nov. 2017].

Angert, I., Burmester, C., Dinges, C., Rose, H. and Schröder, R.R., (1996) Elastic and inelastic scattering cross-sections of amorphous layers of carbon and vitrified ice. *Ultramicroscopy*, [online] 633–4, pp.181–192. Available at: https://www.sciencedirect.com/science/article/pii/0304399196000368 [Accessed 4 Jan. 2019].

El Ansari, R., Craze, M.L., Diez-Rodriguez, M., Nolan, C.C., Ellis, I.O., Rakha, E.A. and Green, A.R., (2018a) The multifunctional solute carrier 3A2 (SLC3A2) confers a poor prognosis in the highly proliferative breast cancer subtypes. *British Journal of*

Cancer, [online] 1188, pp.1115–1122. Available at: http://www.nature.com/articles/s41416-018-0038-5 [Accessed 28 Mar. 2018].

El Ansari, R., Craze, M.L., Miligy, I., Diez-Rodriguez, M., Nolan, C.C., Ellis, I.O., Rakha, E.A. and Green, A.R., (2018b) The amino acid transporter SLC7A5 confers a poor prognosis in the highly proliferative breast cancer subtypes and is a key therapeutic target in luminal B tumours. *Breast Cancer Research 2018 20:1*, [online] 201, p.21. Available at: https://breast-cancer-research.biomedcentral.com/articles/10.1186/s13058-018-0946-6 [Accessed 28 Mar. 2018].

Arachea, B.T., Sun, Z., Potente, N., Malik, R., Isailovic, D. and Viola, R.E., (2012) Detergent selection for enhanced extraction of membrane proteins. *Protein Expression and Purification*, [online] 861, pp.12–20. Available at: http://ac.els-cdn.com/S1046592812002343/1-s2.0-S1046592812002343-main.pdf?_tid=b18e795a-9239-11e7-a413-00000aab0f02&acdnat=1504616395_3e43af69b598fa064a83843dc8cbe422 [Accessed 5 Sep. 2017].

Aricescu, A.R. and Owens, R.J., (2013) Expression of recombinant glycoproteins in mammalian cells: towards an integrative approach to structural biology. *Current Opinion in Structural Biology*, [online] 233, pp.345–356. Available at: http://dx.doi.org/10.1016/j.sbi.2013.04.003.

Ashkenazy, H., Abadi, S., Martz, E., Chay, O., Mayrose, I., Pupko, T. and Ben-Tal, N., (2016) ConSurf 2016: an improved methodology to estimate and visualize evolutionary conservation in macromolecules. *Nucleic Acids Research*, [online] 44. Available at: https://academic.oup.com/nar/article-

abstract/44/W1/W344/2499373 [Accessed 12 Feb. 2019].

Augustyn, E., Finke, K., Zur, A.A., Hansen, L., Heeren, N., Chien, H.-C., Lin, L., Giacomini, K.M., Colas, C., Schlessinger, A. and Thomas, A.A., (2016) LAT-1 activity of meta-substituted phenylalanine and tyrosine analogs. *Bioorganic & Medicinal Chemistry Letters*, [online] 2611, pp.1–6. Available at: http://dx.doi.org/10.1016/j.bmcl.2016.04.023.

Bai, X., Moraes, T.F. and Reithmeier, R.A.F., (2017) Structural biology of solute carrier (SLC) membrane transport proteins. *Molecular Membrane Biology*, [online] 341–2, pp.1–32. Available at: https://www.tandfonline.com/doi/full/10.1080/09687688.2018.1448123 [Accessed 16 Apr. 2018].

Bai, X., Rajendra, E., Yang, G., Shi, Y. and Scheres, S.H., (2015) Sampling the conformational space of the catalytic subunit of human γ-secretase. *eLife*, [online] 4, p.e11182. Available at: https://elifesciences.org/articles/11182 [Accessed 24 Dec. 2017].

Banerjee, P., Joo, J.B., Buse, J.T. and Dawson, G., (1995) Differential solubilization of lipids along with membrane proteins by different classes of detergents. *Chemistry and Physics of Lipids*, [online] 771, pp.65–78. Available at: http://linkinghub.elsevier.com/retrieve/pii/000930849502455R.

Barth, R.F., H Vicente, M.G., Harling, O.K., Kiger, W., Riley, K.J., Binns, P.J., Wagner, F.M., Suzuki, M., Aihara, T., Kato, I. and Kawabata, S., (2012) Current status of boron neutron capture therapy of high grade gliomas and recurrent head and neck cancer. *Radiation Oncology*, [online] 71, p.146. Available at: http://ro-journal.biomedcentral.com/articles/10.1186/1748-717X-7-146 [Accessed 16 Apr.

2018].

Bernaudat, F., Frelet-Barrand, A., Pochon, N., Dementin, S., Hivin, P., Boutigny, S., Rioux, J.-B., Salvi, D., Seigneurin-Berny, D., Richaud, P., Joyard, J., Pignol, D., Sabaty, M., Desnos, T., Pebay-Peyroula, E., Darrouzet, E., Vernet, T. and Rolland, N., (2011) Heterologous expression of membrane proteins: choosing the appropriate host. *PloS one*, [online] 612, p.e29191. Available at: https://dx.doi.org/10.1371/journal.pone.0029191 [Accessed 22 Oct. 2018].

Brenner, S. and Horne, R.W., (1959) A negative staining method for high resolution electron microscopy of viruses. *Biochimica et Biophysica Acta*, [online] 34C, pp.103–110. Available at: https://www.sciencedirect.com/science/article/pii/0006300259902379 [Accessed 4 Jan. 2019].

Bröer, A., Friedrich, B., Wagner, C.A., Fillon, S., Ganapathy, V., Lang, F. and Bröer, S., (2001) Association of 4F2hc with light chains LAT1, LAT2 or y+LAT2 requires different domains. *The Biochemical journal*, [online] 355Pt 3, pp.725–31. Available at: http://www.biochemj.org/bj/355/bj3550725.htm [Accessed 22 Oct. 2014].

Büssow, K., (2015) Stable mammalian producer cell lines for structural biology. *Current Opinion in Structural Biology*, [online] 32Table 1, pp.81–90. Available at: http://linkinghub.elsevier.com/retrieve/pii/S0959440X15000299.

Campbell, M.G., Cheng, A., Brilot, A.F., Moeller, A., Lyumkis, D., Veesler, D., Pan, J., Harrison, S.C., Potter, C.S., Carragher, B. and Grigorieff, N., (2012) Movies of ice-embedded particles enhance resolution in electron cryo-microscopy. *Structure (London, England : 1993)*, [online] 2011, pp.1823–8. Available at: http://dx.doi.org/10.1016/j.str.2012.08.026 [Accessed 10 Jan. 2019].

Cantor, J.M. and Ginsberg, M.H., (2012) CD98 at the crossroads of adaptive immunity and cancer. *Journal of cell science*, [online] 125Pt 6, pp.1373–82. Available at: http://jcs.biologists.org/cgi/doi/10.1242/jcs.096040.

Champeil, P., Orlowski, S., Babin, S., Lund, S., le Maire, M., Møller, J., Lenoir, G. and Montigny, C., (2016) A robust method to screen detergents for membrane protein stabilization, revisited. *Analytical biochemistry*, [online] 511, pp.31–5. Available at: http://ac.els-cdn.com/S0003269716301932/1-s2.0-S0003269716301932-main.pdf?_tid=13f43530-923a-11e7-afe1-00000aab0f6c&acdnat=1504616561_d7e45327e406be317ef18915ed23a386 [Accessed 5 Sep. 2017].

Chaudhary, S., Pak, J.E., Gruswitz, F., Sharma, V. and Stroud, R.M., (2012) Overexpressing human membrane proteins in stably transfected and clonal human embryonic kidney 293S cells. *Nature protocols*, [online] 73, pp.453–66. Available at: http://www.pubmedcentral.nih.gov/articlerender.fcgi?artid=3613139&tool=pmcentrez&rendertype=abstract [Accessed 7 Aug. 2014].

Cheng, Y. and Walz, T., (2009) The advent of near-atomic resolution in single-particle electron microscopy. *Annual review of biochemistry*, [online] 781, pp.723–42. Available at: www.annualreviews.org [Accessed 8 Jan. 2019].

Chien, H.-C., Colas, C., Finke, K., Springer, S., Stoner, L., Zur, A.A., Venteicher, B., Campbell, J., Hall, C., Flint, A., Augustyn, E., Hernandez, C., Heeren, N., Hansen, L., Anthony, A., Bauer, J., Fotiadis, D., Schlessinger, A., Giacomini, K.M. and Thomas, A.A., (2018) Reevaluating the Substrate Specificity of the L-Type Amino Acid Transporter (LAT1). *Journal of Medicinal Chemistry*, [online] 6116, pp.7358–7373. Available at: http://pubs.acs.org [Accessed 30 Jul. 2018].

Chiu, W., (1986) Electron Microscopy of Frozen, Hydrated Biological Specimens. *Annual Review of Biophysics and Biophysical Chemistry*, [online] 151, pp.237–257. Available at: http://www.annualreviews.org/doi/abs/10.1146/annurev.bb.15.060186.001321 [Accessed 9 Jan. 2019].

Cho, H.-J., Hyun, J.-K., Kim, J.-G., Jeong, H.S., Park, H.N., You, D.-J. and Jung, H.S., (2013) Measurement of ice thickness on vitreous ice embedded cryo-EM grids: investigation of optimizing condition for visualizing macromolecules. *Journal of Analytical Science and Technology*, [online] 41, p.7. Available at: http://jast-journal.springeropen.com/articles/10.1186/2093-3371-4-7 [Accessed 9 Jan. 2019].

Choi, D.W., Kim, D.K., Kanai, Y., Wempe, M.F., Endou, H. and Kim, J.-K., (2017) JPH203, a selective L-type amino acid transporter 1 inhibitor, induces mitochondria-dependent apoptosis in Saos2 human osteosarcoma cells. *The Korean journal of physiology & pharmacology : official journal of the Korean Physiological Society and the Korean Society of Pharmacology*, [online] 216, pp.599–607. Available at: http://www.ncbi.nlm.nih.gov/pubmed/29200902 [Accessed 12 Dec. 2017].

Coleman, J.A., Green, E.M. and Gouaux, E., (2016) X-ray structures and mechanism of the human serotonin transporter. *Nature*, [online] pp.1–17. Available at: http://www.nature.com/doifinder/10.1038/nature17629.

Cormerais, Y., Giuliano, S., LeFloch, R., Front, B., Durivault, J., Tambutté, E., Massard, P.-A., de la Ballina, L.R., Endou, H., Wempe, M.F., Palacin, M., Parks, S.K. and Pouyssegur, J., (2016) Genetic Disruption of the Multifunctional CD98/LAT1 Complex Demonstrates the Key Role of Essential Amino Acid Transport in the Control of mTORC1 and Tumor Growth. *Cancer research*, [online] 7615, pp.4481–

92. Available at: http://cancerres.aacrjournals.org/cgi/doi/10.1158/0008-5472.CAN-15-3376 [Accessed 11 Apr. 2017].

Costa, M., Rosell, A., Álvarez-Marimon, E., Zorzano, A., Fotiadis, D. and Palacín, M., (2013) Expression of human heteromeric amino acid transporters in the yeast Pichia pastoris. *Protein expression and purification*, [online] 871, pp.35–40. Available at: http://www.ncbi.nlm.nih.gov/pubmed/23085088 [Accessed 22 Oct. 2014].

d'Amico, A., (2015) Review of clinical practice utility of positron emission tomography with 18F-fluorodeoxyglucose in assessing tumour response to therapy. *La Radiologia medica*, [online] 1204, pp.345–51. Available at: http://link.springer.com/10.1007/s11547-014-0446-4 [Accessed 11 Apr. 2018].

Dalton, A.C. and Barton, W.A., (2014) Over-expression of secreted proteins from mammalian cell lines. *Protein Science*, [online] 235, pp.517–525. Available at: http://doi.wiley.com/10.1002/pro.2439.

Danev, R. and Baumeister, W., (2016) Cryo-EM single particle analysis with the Volta phase plate. *eLife*, [online] 5MARCH2016. Available at: https://elifesciences.org/articles/13046 [Accessed 9 Dec. 2018].

Danev, R., Tegunov, D. and Baumeister, W., (2017) Using the volta phase plate with defocus for cryo-em single particle analysis. *eLife*, [online] 6, pp.1–9. Available at: https://elifesciences.org/articles/23006 [Accessed 14 Jan. 2019].

DeBerardinis, R.J., Lum, J.J., Hatzivassiliou, G. and Thompson, C.B., (2008) The biology of cancer: metabolic reprogramming fuels cell growth and proliferation. *Cell metabolism*, [online] 71, pp.11–20. Available at: http://www.cell.com/cell-metabolism/pdf/S1550-4131(07)00295-1.pdf [Accessed 13 Apr. 2018].

DeBerardinis, R.J., Mancuso, A., Daikhin, E., Nissim, I., Yudkoff, M., Wehrli, S. and Thompson, C.B., (2007) Beyond aerobic glycolysis: transformed cells can engage in glutamine metabolism that exceeds the requirement for protein and nucleotide synthesis. *Proceedings of the National Academy of Sciences of the United States of America*, [online] 10449, pp.19345–50. Available at: http://www.pnas.org/content/pnas/104/49/19345.full.pdf [Accessed 18 Apr. 2018].

Devés, R. and Boyd, C.A., (2000) Surface antigen CD98(4F2): not a single membrane protein, but a family of proteins with multiple functions. *The Journal of membrane biology*, [online] 1733, pp.165–77. Available at: https://link.springer.com/content/pdf/10.1007%2Fs002320001017.pdf [Accessed 30 Oct. 2018].

Dickens, D., Chiduza, G.N., Wright, G.S.A., Pirmohamed, M., Antonyuk, S. V. and Hasnain, S.S., (2017) Modulation of LAT1 (SLC7A5) transporter activity and stability by membrane cholesterol. *Scientific Reports*, [online] 7October 2016, p.43580. Available at: http://www.nature.com/articles/srep43580.

Dickens, D., Webb, S.D., Antonyuk, S., Giannoudis, A., Owen, A., Rädisch, S., Hasnain, S.S. and Pirmohamed, M., (2013) Transport of gabapentin by LAT1 (SLC7A5). *Biochemical Pharmacology*, [online] 8585, pp.1672–1683. Available at: http://dx.doi.org/10.1016/j.bcp.2013.03.022.

Drulyte, I., Johnson, R.M., Hesketh, E.L., Hurdiss, D.L., Scarff, C.A., Porav, S.A., Ranson, N.A., Muench, S.P. and Thompson, R.F., (2018) Approaches to altering particle distributions in cryo-electron microscopy sample preparation. *Acta Crystallographica Section D: Structural Biology*, 746, pp.560–571.

Dubochet, J., Adrian, M., Lepault, J. and McDowall, A.W., (1985) Emerging techniques: Cryo-electron microscopy of vitrified biological specimens. *Trends in Biochemical Sciences*, [online] 104, pp.143–146. Available at: https://www-cell-com.liverpool.idm.oclc.org/action/showPdf?pii=0968-0004%2885%2990150-1 [Accessed 5 Jan. 2019].

Elmlund, H., Elmlund, D. and Bengio, S., (2013) PRIME: probabilistic initial 3D model generation for single-particle cryo-electron microscopy. *Structure (London, England : 1993)*, [online] 218, pp.1299–306. Available at: http://dx.doi.org/10.1016/j.str.2013.07.002 [Accessed 9 May 2017].

Elorza, A., Soro-Arnáiz, I., Meléndez-Rodríguez, F., Rodríguez-Vaello, V., Marsboom, G., de Cárcer, G., Acosta-Iborra, B., Albacete-Albacete, L., Ordóñez, A., Serrano-Oviedo, L., Giménez-Bachs, J.M., Vara-Vega, A., Salinas, A., Sánchez-Prieto, R., Martín del Río, R., Sánchez-Madrid, F., Malumbres, M., Landázuri, M.O. and Aragonés, J., (2012) HIF2α acts as an mTORC1 activator through the amino acid carrier SLC7A5. *Molecular cell*, [online] 485, pp.681–91. Available at: http://dx.doi.org/10.1016/j.molcel.2012.09.017 [Accessed 18 Apr. 2018].

Fernandez-Leiro, R. and Scheres, S.H.W.W., (2016) Unravelling biological macromolecules with cryo-electron microscopy. *Nature*, [online] 5377620, pp.339–346. Available at: http://www.nature.com/doifinder/10.1038/nature19948 [Accessed 3 Feb. 2019].

Fort, J., de la Ballina, L.R., Burghardt, H.E., Ferrer-Costa, C., Turnay, J., Ferrer-Orta, C., Usón, I., Zorzano, A., Fernández-Recio, J., Orozco, M., Lizarbe, M.A., Fita, I. and Palacín, M., (2007) The structure of human 4F2hc ectodomain provides a model for homodimerization and electrostatic interaction with plasma membrane. *The*

Journal of biological chemistry, [online] 28243, pp.31444–52. Available at: http://www.ncbi.nlm.nih.gov/pubmed/17724034.

Fotiadis, D., Kanai, Y. and Palacín, M., (2013) The SLC3 and SLC7 families of amino acid transporters. *Molecular aspects of medicine*, [online] 342–3, pp.139–58. Available at: http://www.ncbi.nlm.nih.gov/pubmed/23506863 [Accessed 12 Oct. 2014].

Frank, J., (2006) *Three-Dimensional Electron Microscopy of Macromolecular Assemblies*. [online] *Three-Dimensional Electron Microscopy of Macromolecular Assemblies: Visualization of Biological Molecules in Their Native State*. Oxford University Press. Available at: http://www.oxfordscholarship.com/view/10.1093/acprof:oso/9780195182187.001.0001/acprof-9780195182187 [Accessed 9 Jan. 2019].

Frumento, G., Rotondo, R., Tonetti, M., Damonte, G., Benatti, U. and Ferrara, G.B., (2002) Tryptophan-derived catabolites are responsible for inhibition of T and natural killer cell proliferation induced by indoleamine 2,3-dioxygenase. *The Journal of experimental medicine*, [online] 1964, pp.459–68. Available at: http://www.ncbi.nlm.nih.gov/pubmed/12186838 [Accessed 18 Apr. 2018].

Fukumoto, S., Hanazono, K., Fu, D.-R., Endo, Y., Kadosawa, T., Iwano, H. and Uchide, T., (2013) A new treatment for human malignant melanoma targeting L-type amino acid transporter 1 (LAT1): a pilot study in a canine model. *Biochemical and biophysical research communications*, [online] 4391, pp.103–8. Available at: http://www.ncbi.nlm.nih.gov/pubmed/23954667 [Accessed 13 Nov. 2014].

Galluccio, M., Pingitore, P., Scalise, M. and Indiveri, C., (2013) Cloning, Large Scale Over-Expression in E. coli and Purification of the Components of the Human LAT 1

(SLC7A5) Amino Acid Transporter. *The Protein Journal*, [online] 326, pp.442–448. Available at: http://link.springer.com/10.1007/s10930-013-9503-4.

Gao, X., Zhou, L., Jiao, X., Lu, F., Yan, C., Zeng, X., Wang, J. and Shi, Y., (2010) Mechanism of substrate recognition and transport by an amino acid antiporter. *Nature*, [online] 4637282, pp.828–832. Available at: http://eutils.ncbi.nlm.nih.gov/entrez/eutils/elink.fcgi?dbfrom=pubmed&id=20090677&retmode=ref&cmd=prlinks%5Cnpapers2://publication/doi/10.1038/nature08741.

Geier, E.G., Schlessinger, A., Fan, H., Gable, J.E., Irwin, J.J., Sali, A. and Giacomini, K.M., (2013) Structure-based ligand discovery for the Large-neutral Amino Acid Transporter 1, LAT-1. *Proceedings of the National Academy of Sciences of the United States of America*, [online] 11014, pp.5480–5. Available at: http://www.pubmedcentral.nih.gov/articlerender.fcgi?artid=3619328&tool=pmcentrez&rendertype=abstract [Accessed 7 Oct. 2014].

Gill, S.C. and von Hippel, P.H., (1989) Calculation of protein extinction coefficients from amino acid sequence data. *Analytical Biochemistry*, [online] 1822, pp.319–326. Available at: http://linkinghub.elsevier.com/retrieve/pii/0003269789906027 [Accessed 16 Sep. 2016].

Goehring, A., Lee, C.-H., Wang, K.H., Michel, J.C., Claxton, D.P., Baconguis, I., Althoff, T., Fischer, S., Garcia, K.C. and Gouaux, E., (2014) Screening and large-scale expression of membrane proteins in mammalian cells for structural studies. *Nature Protocols*, [online] 911, pp.2574–2585. Available at: http://www.nature.com/doifinder/10.1038/nprot.2014.173.

Griffeth, L.K., (2005) Use of PET/CT scanning in cancer patients: technical and

practical considerations. *Proceedings (Baylor University. Medical Center)*, [online] 184, pp.321–30. Available at: http://www.ncbi.nlm.nih.gov/pubmed/16252023 [Accessed 19 Apr. 2018].

Guan, L., Smirnova, I.N., Verner, G., Nagamori, S. and Kaback, H.R., (2006) Manipulating phospholipids for crystallization of a membrane transport protein. *Proceedings of the National Academy of Sciences of the United States of America*, 1036, pp.1723–1726.

Hanahan, D. and Weinberg, R.A., (2011) Hallmarks of Cancer: The Next Generation. *Cell*, [online] 1445, pp.646–674. Available at: http://www.cell.com/cell/pdf/S0092-8674(11)00127-9.pdf [Accessed 5 Apr. 2018].

Haselbach, D., Komarov, I., Agafonov, D.E., Hartmuth, K., Graf, B., Dybkov, O., Urlaub, H., Kastner, B., Lührmann, R. and Stark, H., (2018) Structure and Conformational Dynamics of the Human Spliceosomal Bact Complex. *Cell*, [online] 1723, p.454–464.e11. Available at: https://doi.org/10.1016/j.cell.2018.01.010 [Accessed 23 Dec. 2018].

Hattori, M., Hibbs, R.E. and Gouaux, E., (2012) A fluorescence-detection size-exclusion chromatography-based thermostability assay for membrane protein precrystallization screening. *Structure*, [online] 208, pp.1293–1299. Available at: http://linkinghub.elsevier.com/retrieve/pii/S0039606006007173.

Hayashi, K., Jutabha, P., Endou, H. and Anzai, N., (2012) c-Myc is crucial for the expression of LAT1 in MIA Paca-2 human pancreatic cancer cells. *Oncology reports*, [online] 283, pp.862–6. Available at: http://www.ncbi.nlm.nih.gov/pubmed/22736142 [Accessed 17 Nov. 2014].

Henderson, R., (1995) The potential and limitations of neutrons, electrons and X-

rays for atomic resolution microscopy of unstained biological molecules. *Quarterly reviews of biophysics*, [online] 282, pp.171–93. Available at: https://www-cambridge-org.liverpool.idm.oclc.org/core/services/aop-cambridge-core/content/view/D4FD094A3CA68FF6D8BE4878314DC72E/S003358350000305Xa.pdf/div-class-title-the-potential-and-limitations-of-neutrons-electrons-and-x-rays-for-atomic-resolution-mic [Accessed 2 Mar. 2017].

Henderson, R., (2013) Avoiding the pitfalls of single particle cryo-electron microscopy: Einstein from noise. *Proceedings of the National Academy of Sciences of the United States of America*, 11045.

Henderson, R., Sali, A., Baker, M.L., Carragher, B., Devkota, B., Downing, K.H., Egelman, E.H., Feng, Z., Frank, J., Grigorieff, N., Jiang, W., Ludtke, S.J., Medalia, O., Penczek, P.A., Rosenthal, P.B., Rossmann, M.G., Schmid, M.F., Schröder, G.F., Steven, A.C., Stokes, D.L., Westbrook, J.D., Wriggers, W., Yang, H., Young, J., Berman, H.M., Chiu, W., Kleywegt, G.J. and Lawson, C.L., (2012) Outcome of the first electron microscopy validation task force meeting. In: *Structure*. [online] Elsevier, pp.205–214. Available at: http://www.ncbi.nlm.nih.gov/pubmed/22325770 [Accessed 26 Dec. 2017].

Henderson, R. and Unwin, P.N.T., (1975) Three-dimensional model of purple membrane obtained by electron microscopy. *Nature*, [online] 2575521, pp.28–32. Available at: http://www.nature.com/articles/257028a0 [Accessed 5 Jan. 2019].

Herzik, M.A., Wu, M. and Lander, G.C., (2018a) Achieving better-than-3-Å resolution by single-particle cryo-EM at 200 keV. *Nature Methods*.

Herzik, M.A., Wu, M. and Lander, G.C., (2018b) How Low Can You Go? Size and Resolution Limits using Conventional Cryo-EM at 200 keV. *Biophysical Journal*,

[online] 1143, p.11a. Available at: https://linkinghub.elsevier.com/retrieve/pii/S0006349517313346 [Accessed 10 Jan. 2019].

Hinz, K.M., Meyer, K., Kinne, A., Schülein, R., Köhrle, J. and Krause, G., (2015) Structural Insights Into Thyroid Hormone Transport Mechanisms of the L-Type Amino Acid Transporter 2. *Molecular Endocrinology*, [online] 296, pp.933–942. Available at: http://press.endocrine.org/doi/10.1210/me.2015-1044.

Huttunen, K.M., Gynther, M., Huttunen, J., Puris, E., Spicer, J.A. and Denny, W.A., (2016) A Selective and Slowly Reversible Inhibitor of l -Type Amino Acid Transporter 1 (LAT1) Potentiates Antiproliferative Drug Efficacy in Cancer Cells. *Journal of Medicinal Chemistry*, 5912, pp.5740–5751.

Isoda, A., Kaira, K., Iwashina, M., Oriuchi, N., Tominaga, H., Nagamori, S., Kanai, Y., Oyama, T., Asao, T., Matsumoto, M. and Sawamura, M., (2014) Expression of L-type amino acid transporter 1 (LAT1) as a prognostic and therapeutic indicator in multiple myeloma. *Cancer Science*, [online] 10511, pp.1496–1502. Available at: http://doi.wiley.com/10.1111/cas.12529 [Accessed 13 Apr. 2018].

Jager, P.L., Vaalburg, W., Pruim, J., de Vries, E.G., Langen, K.J. and Piers, D.A., (2001) Radiolabeled amino acids: basic aspects and clinical applications in oncology. *Journal of nuclear medicine : official publication, Society of Nuclear Medicine*, [online] 423, pp.432–45. Available at: http://www.ncbi.nlm.nih.gov/pubmed/11337520 [Accessed 16 Apr. 2018].

Jardetzky, O., (1966) Simple allosteric model for membrane pumps. *Nature*, [online] 2115052, pp.969–70. Available at: http://www.ncbi.nlm.nih.gov/pubmed/5968307 [Accessed 17 Jan. 2019].

Jones, R.G. and Thompson, C.B., (2007) Revving the Engine: Signal Transduction Fuels T Cell Activation. *Immunity*, [online] 272, pp.173–178. Available at: https://www.sciencedirect.com/science/article/pii/S1074761307003676?via%3Dihub [Accessed 3 Apr. 2019].

Joubert, O., Nehmé, R., Bidet, M. and Mus-Veteau, I., (2010) Heterologous Expression of Human Membrane Receptors in the Yeast Saccharomyces cerevisiae. In: *Methods in molecular biology (Clifton, N.J.)*. [online] Humana Press, pp.87–103. Available at: http://link.springer.com/10.1007/978-1-60761-344-2_6 [Accessed 22 Oct. 2018].

Jungnickel, K.E.J., Parker, J.L. and Newstead, S., (2018) Structural basis for amino acid transport by the CAT family of SLC7 transporters. *Nature Communications*, [online] 91, p.550. Available at: http://www.nature.com/articles/s41467-018-03066-6.

Kageyama, T., Nakamura, M., Matsuo, A., Yamasaki, Y., Takakura, Y., Hashida, M., Kanai, Y., Naito, M., Tsuruo, T., Minato, N. and Shimohama, S., (2000) The 4F2hc/LAT1 complex transports L-DOPA across the blood-brain barrier. *Brain Research*, 879, pp.115–121.

Kanai, Y., Segawa, H., Miyamoto, K. -i., Uchino, H., Takeda, E. and Endou, H., (1998) Expression Cloning and Characterization of a Transporter for Large Neutral Amino Acids Activated by the Heavy Chain of 4F2 Antigen (CD98). *Journal of Biological Chemistry*, [online] 27337, pp.23629–23632. Available at: http://www.jbc.org/cgi/doi/10.1074/jbc.273.37.23629.

Kang, H.J., Lee, C. and Drew, D., (2013) Breaking the barriers in membrane protein crystallography. *The international journal of biochemistry & cell biology*, [online]

453, pp.636–44. Available at: http://www.ncbi.nlm.nih.gov/pubmed/23291355 [Accessed 11 Sep. 2016].

Kao, Y.H., Hewitt, D.P., Trexler-Schmidt, M. and Laird, M.W., (2010) Mechanism of antibody reduction in cell culture production processes. *Biotechnology and Bioengineering*, 1074, pp.622–632.

Kaper, T., Looger, L.L., Takanaga, H., Platten, M., Steinman, L. and Frommer, W.B., (2007) Nanosensor detection of an immunoregulatory tryptophan influx/kynurenine efflux cycle. *PLoS Biology*, [online] 510, pp.2201–2210. Available at: http://dx.plos.org/10.1371/journal.pbio.0050257 [Accessed 21 Jun. 2017].

Kazmier, K., Claxton, D.P. and Mchaourab, H.S., (2017) Alternating access mechanisms of LeuT-fold transporters: trailblazing towards the promised energy landscapes. *Current Opinion in Structural Biology*, [online] 45, pp.100–108. Available at: http://dx.doi.org/10.1016/j.sbi.2016.12.006 [Accessed 9 Jan. 2017].

Khoshouei, M., Radjainia, M., Baumeister, W. and Danev, R., (2017) Cryo-EM structure of haemoglobin at 3.2 Å determined with the Volta phase plate. *Nature Communications*, [online] 8, p.16099. Available at: http://www.nature.com/doifinder/10.1038/ncomms16099 [Accessed 9 Jan. 2019].

Khoshouei, M., Radjainia, M., Phillips, A.J., Gerrard, J.A., Mitra, A.K., Plitzko, J.M., Baumeister, W. and Danev, R., (2016) Volta phase plate cryo-EM of the small protein complex Prx3. *Nature communications*, [online] 7, p.10534. Available at: https://www.nature.com/articles/ncomms10534.pdf [Accessed 27 Sep. 2017].

Khunweeraphong, N., Nagamori, S., Wiriyasermkul, P., Nishinaka, Y., Wongthai, P., Ohgaki, R., Tanaka, H., Tominaga, H., Sakurai, H. and Kanai, Y., (2012) Establishment of Stable Cell Lines With High Expression of Heterodimers of Human 4F2hc and

Human Amino Acid Transporter LAT1 or LAT2 and Delineation of Their Differential Interaction With ^|^alpha;-Alkyl Moieties. *Journal of Pharmacological Sciences*, [online] 1194, pp.368–380. Available at: http://jlc.jst.go.jp/DN/JST.JSTAGE/jphs/12124FP?lang=en&from=CrossRef&type=abstract [Accessed 22 Oct. 2014].

Killian, D.M., Hermeling, S. and Chikhale, P.J., (2007) Targeting the cerebrovascular large neutral amino acid transporter (LAT1) isoform using a novel disulfide-based brain drug delivery system. *Drug delivery*, 141, pp.25–31.

Klug, A. and Berger, J.E., (1964) An optical method for the analysis of periodicities in electron micrographs, and some observations on the mechanism of negative staining. *Journal of Molecular Biology*, [online] 103, pp.565-IN15. Available at: https://ac-els-cdn-com.liverpool.idm.oclc.org/S0022283664800814/1-s2.0-S0022283664800814-main.pdf?_tid=de5db2ef-a361-4b9a-a0c1-1c6ef3a2f8ff&acdnat=1546946014_20a878b77b22f6d72974d6d1ca9aa3b2 [Accessed 8 Jan. 2019].

Klug, A. and De Rosier, D.J., (1966) Optical filtering of electron micrographs: reconstruction of one-sided images. *Nature*, [online] 2125057, pp.29–32. Available at: http://www.ncbi.nlm.nih.gov/pubmed/4164921 [Accessed 8 Jan. 2019].

Kobayashi, K., Ohnishi, A., Promsuk, J., Shimizu, S., Kanai, Y., Shiokawa, Y. and Nagane, M., (2008) Enhanced tumor growth elicited by L-type amino acid transporter 1 in human malignant glioma cells. *Neurosurgery*, [online] 622, pp.493-503; discussion 503–4. Available at: https://academic.oup.com/neurosurgery/article-lookup/doi/10.1227/01.neu.0000316018.51292.19 [Accessed 29 Jun. 2017].

Kolesnikova, T. V, Mannion, B.A., Berditchevski, F. and Hemler, M.E., (2001) β1 integrins show specific association with CD98 protein in low density membranes. *BMC Biochemistry*, [online] 21, pp.1–9. Available at: http://www.biomedcentral.com/1471-2091/2/10 [Accessed 3 Apr. 2019].

Kongpracha, P., Nagamori, S., Wiriyasermkul, P., Tanaka, Y., Kaneda, K., Okuda, S., Ohgaki, R. and Kanai, Y., (2017) Structure-activity relationship of a novel series of inhibitors for cancer type transporter L-type amino acid transporter 1 (LAT1). *Journal of Pharmacological Sciences*, [online] 1332, pp.96–102. Available at: http://ac.els-cdn.com/S1347861317300142/1-s2.0-S1347861317300142-main.pdf?_tid=fba1da00-2b5f-11e7-9892-00000aab0f27&acdnat=1493307870_afe0691ba8de420ff79175a4ee77e037 [Accessed 27 Apr. 2017].

Koterba, K.L., Borgschulte, T. and Laird, M.W., (2012) Thioredoxin 1 is responsible for antibody disulfide reduction in CHO cell culture. *Journal of Biotechnology*, 1571, pp.261–267.

Kowalczyk, L., Ratera, M., Paladino, A., Bartoccioni, P., Errasti-Murugarren, E., Valencia, E., Portella, G., Bial, S., Zorzano, A., Fita, I., Orozco, M., Carpena, X., Vázquez-Ibar, J.L. and Palacín, M., (2011) Molecular basis of substrate-induced permeation by an amino acid antiporter. *Proceedings of the National Academy of Sciences of the United States of America*, [online] 10810, pp.3935–3940. Available at: http://www.pnas.org/cgi/content/long/108/10/3935 [Accessed 27 Oct. 2015].

Kozakov, D., Hall, D.R., Xia, B., Porter, K.A., Padhorny, D., Yueh, C., Beglov, D. and Vajda, S., (2017) The ClusPro web server for protein-protein docking. *Nature protocols*, [online] 122, pp.255–278. Available at: https://cluspro.org [Accessed 8

Nov. 2018].

Kühlbrandt, W., (2014) The resolution revolution. *Science (New York, N.Y.)*, [online] 3436178, pp.1443–4. Available at: http://www.sciencemag.org/content/343/6178/1443.short.

de la Rosa-Trevín, J.M., Otón, J., Marabini, R., Zaldívar, A., Vargas, J., Carazo, J.M. and Sorzano, C.O.S., (2013) Xmipp 3.0: An improved software suite for image processing in electron microscopy. *Journal of Structural Biology*, [online] 1842, pp.321–328. Available at: http://linkinghub.elsevier.com/retrieve/pii/S1047847713002566 [Accessed 2 Mar. 2017].

Laganowsky, A., Reading, E., Allison, T.M., Ulmschneider, M.B., Degiacomi, M.T., Baldwin, A.J. and Robinson, C. V, (2014) Membrane proteins bind lipids selectively to modulate their structure and function. *Nature*, [online] 5107503, pp.172–5. Available at: http://www.ncbi.nlm.nih.gov/pubmed/24899312.

Lander, G.C., Saibil, H.R. and Nogales, E., (2012) Go hybrid: EM, crystallography, and beyond. *Current Opinion in Structural Biology*, [online] 225, pp.627–635. Available at: http://dx.doi.org/10.1016/j.sbi.2012.07.006.

Li, X., Mooney, P., Zheng, S., Booth, C.R., Braunfeld, M.B., Gubbens, S., Agard, D.A. and Cheng, Y., (2013) Electron counting and beam-induced motion correction enable near-atomic-resolution single-particle cryo-EM. *Nature methods*, [online] 106, pp.584–90. Available at: http://www.ncbi.nlm.nih.gov/pubmed/23644547 [Accessed 5 Jun. 2017].

Lin, C.-Y., Huang, Z., Wen, W., Wu, A., Wang, C. and Niu, L., (2015) Enhancing Protein Expression in HEK-293 Cells by Lowering Culture Temperature. *Plos One*,

[online] 104, p.e0123562. Available at: http://dx.plos.org/10.1371/journal.pone.0123562.

Lin, S.-H. and Guidotti, G., (2009) Chapter 35 Purification of Membrane Proteins. In: *Methods in enzymology*, 1st ed. [online] Elsevier Inc., pp.619–629. Available at: http://dx.doi.org/10.1016/S0076-6879(09)63035-4.

Lin, Y.-C., Boone, M., Meuris, L., Lemmens, I., Van Roy, N., Soete, A., Reumers, J., Moisse, M., Plaisance, S., Drmanac, R., Chen, J., Speleman, F., Lambrechts, D., Van de Peer, Y., Tavernier, J. and Callewaert, N., (2014) Genome dynamics of the human embryonic kidney 293 lineage in response to cell biology manipulations. *Nature Communications*, [online] 511, p.4767. Available at: http://www.nature.com/doifinder/10.1038/ncomms5767.

Linke, D., (2009) Detergents: an overview. *Methods in enzymology*, [online] 463C, pp.603–17. Available at: http://dx.doi.org/10.1016/S0076-6879(09)63034-2.

Lipfert, J., Columbus, L., Chu, V.B., Lesley, S.A. and Doniach, S., (2007) Size and Shape of Detergent Micelles Determined by Small-Angle X-ray Scattering. *The Journal of Physical Chemistry B*, [online] 11143, pp.12427–12438. Available at: http://pubs.acs.org/doi/abs/10.1021/jp073016l [Accessed 19 Dec. 2016].

Listowski, M.A., Leluk, J., Kraszewski, S. and Sikorski, A.F., (2015) Cholesterol Interaction with the MAGUK Protein Family Member, MPP1, via CRAC and CRAC-Like Motifs: An In Silico Docking Analysis. *Plos One*, [online] 107, p.e0133141. Available at: http://dx.plos.org/10.1371/journal.pone.0133141.

Lo, R. and Matthews, J., (2012) High-resolution genome-wide mapping of AHR and ARNT binding sites by ChIP-Seq. *Toxicological sciences : an official journal of the Society of Toxicology*, [online] 1302, pp.349–61. Available at:

https://watermark.silverchair.com/kfs253.pdf?token=AQECAHi208BE49Ooan9kkhW_Ercy7Dm3ZL_9Cf3qfKAc485ysgAAAagwggGkBgkqhkiG9w0BBwagggGVMIIBkQIBADCCAYoGCSqGSIb3DQEHATAeBglghkgBZQMEAS4wEQQMSEghYbO6RG5RS7SaAgEQgIIBWwMUO2kSPUrkw19rP1Y6SR6wNlGxZGuaoWPlf0S0stbFVoCh [Accessed 18 Apr. 2018].

Lomize, M.A., Pogozheva, I.D., Joo, H., Mosberg, H.I. and Lomize, A.L., (2012) OPM database and PPM web server: resources for positioning of proteins in membranes. *Nucleic acids research*, [online] 40Database issue, pp.D370-6. Available at: http://www.ncbi.nlm.nih.gov/pubmed/21890895 [Accessed 4 Dec. 2018].

Lovell, S.C., Davis, I.W., Arendall, W.B., de Bakker, P.I.W., Word, J.M., Prisant, M.G., Richardson, J.S. and Richardson, D.C., (2003) Structure validation by Cα geometry: φ,ψ and Cβ deviation. *Proteins: Structure, Function, and Bioinformatics*, [online] 503, pp.437–450. Available at: http://doi.wiley.com/10.1002/prot.10286 [Accessed 10 Oct. 2018].

Ludtke, S.J., (2016) *Single-Particle Refinement and Variability Analysis in EMAN2.1*. 1st ed. [online] *The Resolution Revolution: Recent Advances In cryoEM*, Elsevier Inc. Available at: http://linkinghub.elsevier.com/retrieve/pii/S0076687916300362.

Le Maire, M., Champeil, P. and Møller, J. V., (2000) Interaction of membrane proteins and lipids with solubilizing detergents. *Biochimica et Biophysica Acta - Biomembranes*, 15081–2, pp.86–111.

Mastroberardino, L., Spindler, B., Pfeiffer, R., Skelly, P.J., Loffing, J., Shoemaker, C.B. and Verrey, F., (1998) Amino-acid transport by heterodimers of 4F2hc/CD98 and members of a permease family. *Nature*, [online] 3956699, pp.288–91. Available at: http://www.nature.com/nature/journal/v395/n6699/abs/395288a0.html [Accessed

22 Oct. 2014].

McMullan, G., Faruqi, A.R. and Henderson, R., (2016) Direct Electron Detectors. In: *The Resolution Revolution: Recent Advances In cryoEM*, 1st ed. [online] Elsevier Inc., pp.1–17. Available at: http://dx.doi.org/10.1016/bs.mie.2016.05.056.

Meier, C., Ristic, Z., Klauser, S. and Verrey, F., (2002) Activation of system L heterodimeric amino acid exchangers by intracellular substrates. *The EMBO journal*, [online] 214, pp.580–9. Available at: http://emboj.embopress.org/cgi/doi/10.1093/emboj/21.4.580.

Meury, M., Costa, M., Harder, D., Stauffer, M., Jeckelmann, J.-M., Brühlmann, B., Rosell, A., Ilgü, H., Kovar, K., Palacín, M. and Fotiadis, D., (2014) Detergent-Induced Stabilization and Improved 3D Map of the Human Heteromeric Amino Acid Transporter 4F2hc-LAT2. *PLoS ONE*, [online] 910, p.e109882. Available at: http://www.ncbi.nlm.nih.gov/pubmed/25299125 [Accessed 10 Oct. 2014].

Mouritsen, O.G. and Zuckermann, M.J., (2004) What's so special about cholesterol? *Lipids*, [online] 3911, pp.1101–1113. Available at: http://link.springer.com/10.1007/s11745-004-1336-x.

Nagamori, S., Wiriyasermkul, P., Okuda, S., Kojima, N., Hari, Y., Kiyonaka, S., Mori, Y., Tominaga, H., Ohgaki, R. and Kanai, Y., (2016) Structure-activity relations of leucine derivatives reveal critical moieties for cellular uptake and activation of mTORC1-mediated signaling. *Amino Acids*, [online] 484, pp.1045–1058. Available at: http://download.springer.com/static/pdf/428/art%253A10.1007%252Fs00726-015-2158-z.pdf?originUrl=https%3A%2F%2Flink.springer.com%2Farticle%2F10.1007%2Fs00726-015-2158-

z&token2=exp=1498059311~acl=%2Fstatic%2Fpdf%2F428%2Fart%25253A10.1007%25252Fs00726-015-21 [Accessed 21 Jun. 2017].

Nakamura, E., Sato, M., Yang, H., Miyagawa, F., Harasaki, M., Tomita, K., Matsuoka, S., Noma, A., Iwai, K. and Minato, N., (1999) 4F2 (CD98) heavy chain is associated covalently with an amino acid transporter and controls intracellular trafficking and membrane topology of 4F2 heterodimer. *Journal of Biological Chemistry*, [online] 2745, pp.3009–3016. Available at: http://www.ncbi.nlm.nih.gov/pubmed/9915839 [Accessed 30 Oct. 2018].

Nakane, T., Kimanius, D., Lindahl, E. and Scheres, S.H., (2018) Characterisation of molecular motions in cryo-EM single-particle data by multi-body refinement in RELION. *eLife*, [online] 7, p.e36861. Available at: https://elifesciences.org/articles/36861 [Accessed 4 Jun. 2018].

Napolitano, L., Galluccio, M., Scalise, M., Parravicini, C., Palazzolo, L., Eberini, I. and Indiveri, C., (2017a) Novel insights into the transport mechanism of the human amino acid transporter LAT1 (SLC7A5). Probing critical residues for substrate translocation. *Biochimica et biophysica acta. General subjects*, [online] 18614, pp.727–736. Available at: https://www.sciencedirect.com/science/article/pii/S0304416517300132?via%3Dihub [Accessed 19 Jan. 2019].

Napolitano, L., Scalise, M., Galluccio, M., Pochini, L., Albanese, L.M. and Indiveri, C., (2015) LAT1 is the transport competent unit of the LAT1/CD98 heterodimeric amino acid transporter. *The international journal of biochemistry & cell biology*, [online] 67, pp.25–33. Available at: http://linkinghub.elsevier.com/retrieve/pii/S1357272515002058%5Cnhttp://www.

ncbi.nlm.nih.gov/pubmed/26256001.

Napolitano, L., Scalise, M., Koyioni, M., Koutentis, P., Catto, M., Eberini, I., Parravicini, C., Palazzolo, L., Pisani, L., Galluccio, M., Console, L., Carotti, A. and Indiveri, C., (2017b) Potent inhibitors of human LAT1 (SLC7A5) transporter based on dithiazole and dithiazine compounds for development of anticancer drugs. *Biochemical Pharmacology*, [online] 143, pp.39–52. Available at: http://linkinghub.elsevier.com/retrieve/pii/S0006295217304835.

Nawashiro, H., Otani, N., Uozumi, Y., Ooigawa, H., Toyooka, T., Suzuki, T., Katoh, H., Tsuzuki, N., Ohnuki, A., Shima, K., Shinomiya, N., Matsuo, H. and Kanai, Y., (2005) High expression of L-type amino acid transporter 1 in infiltrating glioma cells. *Brain Tumor Pathology*, [online] 222, pp.89–91. Available at: http://link.springer.com/10.1007/s10014-005-0188-z [Accessed 29 Jun. 2017].

Nettleship, J., (2012) Structural Biology of Glycoproteins. In: *Glycosylation*. [online] InTech, pp.41–62. Available at: http://cdn.intechopen.com/pdfs/39447/InTech-Structural_biology_of_glycoproteins.pdf.

Nettleship, J.E., Assenberg, R., Diprose, J.M., Rahman-Huq, N. and Owens, R.J., (2010) Recent advances in the production of proteins in insect and mammalian cells for structural biology. *Journal of Structural Biology*, [online] 1721, pp.55–65. Available at: https://www.sciencedirect.com/science/article/pii/S1047847710000535?via%3Dihub [Accessed 23 Oct. 2018].

Newby, Z.E.R., O'Connell, J.D., Gruswitz, F., Hays, F.A., Harries, W.E.C., Harwood, I.M., Ho, J.D., Lee, J.K., Savage, D.F., Miercke, L.J.W. and Stroud, R.M., (2009) A general protocol for the crystallization of membrane proteins for X-ray structural

investigation. *Nature Protocols*, [online] 45, pp.619–637. Available at: http://www.nature.com/doifinder/10.1038/nprot.2009.27.

Nicklin, P., Bergman, P., Zhang, B., Triantafellow, E., Wang, H., Nyfeler, B., Yang, H., Hild, M., Kung, C., Wilson, C., Myer, V.E., MacKeigan, J.P., Porter, J.A., Wang, Y.K., Cantley, L.C., Finan, P.M. and Murphy, L.O., (2009) Bidirectional transport of amino acids regulates mTOR and autophagy. *Cell*, [online] 1363, pp.521–34. Available at: http://dx.doi.org/10.1016/j.cell.2008.11.044 [Accessed 13 Jan. 2015].

Nodwell, M.B., Yang, H., Čolović, M., Yuan, Z., Merkens, H., Martin, R.E., Bénard, F., Schaffer, P. and Britton, R., (2017) 18 F-Fluorination of Unactivated C–H Bonds in Branched Aliphatic Amino Acids: Direct Synthesis of Oncological Positron Emission Tomography Imaging Agents. *Journal of the American Chemical Society*, [online] 13910, pp.3595–3598. Available at: http://pubs.acs.org/doi/abs/10.1021/jacs.6b11533 [Accessed 29 Jun. 2017].

O'Malley, M.A., Helgeson, M.E., Wagner, N.J. and Robinson, A.S., (2011) The morphology and composition of cholesterol-rich micellar nanostructures determine transmembrane protein (GPCR) activity. *Biophysical journal*, [online] 1002, pp.L11–L13. Available at: http://www.sciencedirect.com/science/article/B94RW-5200HBH-3/2/0edb4706ab9c05aab2993294491e05d1%5Cnhttp://www.pubmedcentral.nih.gov/articlerender.fcgi?artid=3021673&tool=pmcentrez&rendertype=abstract.

Oda, K., Hosoda, N., Endo, H., Saito, K., Tsujihara, K., Yamamura, M., Sakata, T., Anzai, N., Wempe, M.F., Kanai, Y. and Endou, H., (2010) L-Type amino acid transporter 1 inhibitors inhibit tumor cell growth. *Cancer Science*, 1011, pp.173–179.

Ohi, M., Li, Y., Cheng, Y. and Walz, T., (2004) Negative Staining and Image

Classification - Powerful Tools in Modern Electron Microscopy. *Biological procedures online*, [online] 61, pp.23–34. Available at: http://www.pubmedcentral.nih.gov/articlerender.fcgi?artid=389902&tool=pmcentrez&rendertype=abstract [Accessed 8 Sep. 2016].

Opitz, C.A., Litzenburger, U.M., Sahm, F., Ott, M., Tritschler, I., Trump, S., Schumacher, T., Jestaedt, L., Schrenk, D., Weller, M., Jugold, M., Guillemin, G.J., Miller, C.L., Lutz, C., Radlwimmer, B., Lehmann, I., von Deimling, A., Wick, W. and Platten, M., (2011) An endogenous tumour-promoting ligand of the human aryl hydrocarbon receptor. *Nature*, [online] 4787368, pp.197–203. Available at: http://www.ncbi.nlm.nih.gov/pubmed/21976023%5Cnhttp://www.nature.com/nature/journal/v478/n7368/pdf/nature10491.pdf.

Ostermeier, C. and Michel, H., (1997) Crystallization of membrane proteins. *Current opinion in structural biology*, [online] 75, pp.697–701. Available at: http://www.ncbi.nlm.nih.gov/pubmed/9345629 [Accessed 11 Sep. 2016].

Palazzolo, L., Parravicini, C., Laurenzi, T., Guerrini, U., Indiveri, C., Gianazza, E. and Eberini, I., (2018) In silico Description of LAT1 Transport Mechanism at an Atomistic Level. *Frontiers in Chemistry*, [online] 6, p.350. Available at: www.frontiersin.org.

Pardridge, W.M., (2005) The blood-brain barrier: bottleneck in brain drug development. *NeuroRx : the journal of the American Society for Experimental NeuroTherapeutics*, [online] 2January, pp.3–14. Available at: http://www.ncbi.nlm.nih.gov/pubmed/15717053%5Cnhttp://www.pubmedcentral.nih.gov/articlerender.fcgi?artid=PMC539316.

Passmore, L.A. and Russo, C.J., (2016) *Specimen Preparation for High-Resolution Cryo-EM*. 1st ed. [online] *The Resolution Revolution: Recent Advances In cryoEM*,

Elsevier Inc. Available at:
http://linkinghub.elsevier.com/retrieve/pii/S0076687916300295.

Pei, J., Kim, B.-H. and Grishin, N. V., (2008) PROMALS3D: a tool for multiple protein sequence and structure alignments. *Nucleic Acids Research*, [online] 367, pp.2295–2300. Available at: http://nar.oxfordjournals.org/lookup/doi/10.1093/nar/gkn072.

Penmatsa, A., Wang, K.H. and Gouaux, E., (2013) X-ray structure of dopamine transporter elucidates antidepressant mechanism. *Nature*, [online] 5037474, pp.85–90. Available at:
http://www.pubmedcentral.nih.gov/articlerender.fcgi?artid=3904663&tool=pmcentrez&rendertype=abstract [Accessed 16 Jul. 2014].

Penmatsa, A., Wang, K.H. and Gouaux, E., (2015) X-ray structures of Drosophila dopamine transporter in complex with nisoxetine and reboxetine. *Nature Structural & Molecular Biology*, [online] 226, pp.506–508. Available at:
http://www.nature.com/doifinder/10.1038/nsmb.3029.

Pettersen, E.F., Goddard, T.D., Huang, C.C., Couch, G.S., Greenblatt, D.M., Meng, E.C. and Ferrin, T.E., (2004) UCSF Chimera - A visualization system for exploratory research and analysis. *Journal of Computational Chemistry*, [online] 2513, pp.1605–1612. Available at: http://www.ncbi.nlm.nih.gov/pubmed/15264254 [Accessed 5 Jun. 2017].

Peura, L., Malmioja, K., Laine, K., Leppänen, J., Gynther, M., Isotalo, A. and Rautio, J., (2011) Large amino acid transporter 1 (LAT1) prodrugs of valproic acid: New prodrug design ideas for central nervous system delivery. *Molecular Pharmaceutics*, 85, pp.1857–1866.

Pfeiffer, R., Spindler, B., Loffing, J., Skelly, P.J., Shoemaker, C.B. and Verrey, F.,

(1998) Functional heterodimeric amino acid transporters lacking cysteine residues involved in disulfide bond. *FEBS Letters*, 439, pp.157–162.

Phillips, R., Ursell, T., Wiggins, P. and Sens, P., (2009) Emerging roles for lipids in shaping membrane-protein function. *Nature*, 4597245, pp.379–385.

Pineda, M., Fernández, E., Torrents, D., Estévez, R., López, C., Camps, M., Lloberas, J., Zorzano, A. and Palacín, M., (1999) Identification of a Membrane Protein, LAT-2, That Co-expresses with 4F2 Heavy Chain, an L-type Amino Acid Transport Activity with Broad Specificity for Small and Large Zwitterionic Amino Acids. *Journal of Biological Chemistry*, [online] 27428, pp.19738–19744. Available at: http://www.ncbi.nlm.nih.gov/pubmed/10391915 [Accessed 29 Dec. 2018].

Pintilie, G.D., Zhang, J., Goddard, T.D., Chiu, W. and Gossard, D.C., (2010) Quantitative analysis of cryo-EM density map segmentation by watershed and scale-space filtering, and fitting of structures by alignment to regions. *Journal of structural biology*, [online] 1703, pp.427–38. Available at: https://ac.els-cdn.com/S1047847710000845/1-s2.0-S1047847710000845-main.pdf?_tid=7089bd42-e663-11e7-9e3f-00000aab0f26&acdnat=1513870222_b3502f6e0170906be83d92ec9ec592da [Accessed 21 Dec. 2017].

Powlesland, A.S., Hitchen, P.G., Parry, S., Graham, S. a., Barrio, M.M., Elola, M.T., Mordoh, J., Dell, A., Drickamer, K. and Taylor, M.E., (2009) Targeted glycoproteomic identification of cancer cell glycosylation. *Glycobiology*, 198, pp.899–909.

Privé, G.G., (2007) Detergents for the stabilization and crystallization of membrane proteins. *Methods*, [online] 414, pp.388–397. Available at: http://linkinghub.elsevier.com/retrieve/pii/S1046202307000102.

Punjani, A., Rubinstein, J.L., Fleet, D.J. and Brubaker, M.A., (2017) cryoSPARC: algorithms for rapid unsupervised cryo-EM structure determination. *Nature methods*, [online] 143, pp.290–296. Available at: http://www.nature.com/doifinder/10.1038/nmeth.4169.

Puris, E., Gynther, M., Huttunen, J., Petsalo, A. and Huttunen, K.M., (2017) L-type amino acid transporter 1 utilizing prodrugs: How to achieve effective brain delivery and low systemic exposure of drugs. *Journal of Controlled Release*, [online] 261June, pp.93–104. Available at: http://dx.doi.org/10.1016/j.jconrel.2017.06.023 [Accessed 4 Jul. 2017].

Rautio, J., Gynther, M. and Laine, K., (2013) LAT1-mediated prodrug uptake: a way to breach the blood–brain barrier? *Therapeutic Delivery*, [online] 43, pp.281–284. Available at: http://www.ncbi.nlm.nih.gov/pubmed/23442072%0Ahttp://www.future-science.com/doi/10.4155/tde.12.165.

Reeves, P.J., Callewaert, N., Contreras, R. and Khorana, H.G., (2002) Structure and function in rhodopsin: High-level expression of rhodopsin with restricted and homogeneous N-glycosylation by a tetracycline-inducible N-acetylglucosaminyltransferase I-negative HEK293S stable mammalian cell line. *Proceedings of the National Academy of Sciences*, [online] 9921, pp.13419–13424. Available at: http://www.pnas.org/cgi/doi/10.1073/pnas.212519299.

Rice, P., Longden, L. and Bleasby, A., (2000) EMBOSS: The European Molecular Biology Open Software Suite. *Trends in Genetics*, [online] 166, pp.276–277. Available at: http://www.ncbi.nlm.nih.gov/pubmed/10827456 [Accessed 4 Dec. 2018].

Ripstein, Z.A. and Rubinstein, J.L., (2016) *Processing of Cryo-EM Movie Data*. 1st ed. [online] *The Resolution Revolution: Recent Advances In cryoEM*, Elsevier Inc. Available at: http://linkinghub.elsevier.com/retrieve/pii/S0076687916300271.

Ritchie, J.W. and Taylor, P.M., (2001) Role of the System L permease LAT1 in amino acid and iodothyronine transport in placenta. *The Biochemical journal*, [online] 356Pt 3, pp.719–725. Available at: https://www.ncbi.nlm.nih.gov/pmc/articles/PMC1221898/pdf/11389679.pdf [Accessed 29 Dec. 2018].

Rohou, A. and Grigorieff, N., (2015) CTFFIND4: Fast and accurate defocus estimation from electron micrographs. *Journal of Structural Biology*, [online] 1922, pp.216–221. Available at: http://www.ncbi.nlm.nih.gov/pubmed/26278980 [Accessed 11 Jan. 2019].

Rosell, A., Meury, M., Álvarez-Marimon, E., Costa, M., Pérez-Cano, L., Zorzano, A., Fernández-Recio, J., Palacín, M. and Fotiadis, D., (2014) Structural bases for the interaction and stabilization of the human amino acid transporter LAT2 with its ancillary protein 4F2hc. *Proceedings of the National Academy of Sciences of the United States of America*, [online] 1118, pp.2966–71. Available at: http://www.pubmedcentral.nih.gov/articlerender.fcgi?artid=3939895&tool=pmcentrez&rendertype=abstract [Accessed 22 Oct. 2014].

Rosenthal, P.B., (2016) *Testing the Validity of Single-Particle Maps at Low and High Resolution*. 1st ed. [online] *The Resolution Revolution: Recent Advances In cryoEM*, Elsevier Inc. Available at: http://linkinghub.elsevier.com/retrieve/pii/S0076687916301537.

Rosenthal, P.B. and Henderson, R., (2003) Optimal determination of particle

orientation, absolute hand, and contrast loss in single-particle electron cryomicroscopy. *Journal of Molecular Biology*, [online] 3334, pp.721–45. Available at: http://www.ncbi.nlm.nih.gov/pubmed/14568533 [Accessed 5 Jun. 2017].

De Rosier, D.J. and Klug, A., (1968) Reconstruction of three dimensional structures from electron micrographs. *Nature*, [online] 2175124, pp.130–4. Available at: http://www.nature.com/articles/217130a0 [Accessed 8 Jan. 2019].

Russo, C.J. and Passmore, L.A., (2016) Progress towards an optimal specimen support for electron cryomicroscopy. *Current opinion in structural biology*, [online] 37, p.8189. Available at: http://dx.doi.org/10.1016/j.sbi.2015.12.007.

Safe, S., Cheng, Y. and Jin, U.-H., (2017) The aryl hydrocarbon receptor (AhR) as a drug target for cancer chemotherapy. *Current Opinion in Toxicology*, [online] 2, pp.24–29. Available at: http://dx.doi.org/10.1016/j.cotox.2017.01.012 [Accessed 6 Apr. 2018].

Sakata, T., Ferdous, G., Tsuruta, T., Satoh, T., Baba, S., Muto, T., Ueno, A., Kanai, Y., Endou, H. and Okayasu, I., (2009) L-type amino-acid transporter 1 as a novel biomarker for high-grade malignancy in prostate cancer. *Pathology International*, 59, pp.7–18.

Saxton, R.A., Knockenhauer, K.E., Wolfson, R.L., Chantranupong, L., Pacold, M.E., Wang, T., Schwartz, T.U. and Sabatini, D.M., (2016) Structural basis for leucine sensing by the Sestrin2-mTORC1 pathway. *Science*, [online] 3516268, pp.53–58. Available at: http://www.ncbi.nlm.nih.gov/pubmed/26586190 [Accessed 7 Sep. 2016].

Scheres, S.H.W., (2012a) A Bayesian view on cryo-EM structure determination. *Journal of molecular biology*, [online] 4152, pp.406–18. Available at:

http://www.ncbi.nlm.nih.gov/pubmed/22100448 [Accessed 5 Jun. 2017].

Scheres, S.H.W., (2012b) RELION: implementation of a Bayesian approach to cryo-EM structure determination. *Journal of structural biology*, [online] 1803, pp.519–30. Available at: http://www.ncbi.nlm.nih.gov/pubmed/23000701 [Accessed 5 Jun. 2017].

Scheres, S.H.W., (2016) *Processing of Structurally Heterogeneous Cryo-EM Data in RELION*. 1st ed. [online] *The Resolution Revolution: Recent Advances In cryoEM*, Elsevier Inc. Available at: http://linkinghub.elsevier.com/retrieve/pii/S0076687916300301.

Schlessinger, A., Matsson, P., Shima, J.E., Pieper, U., Yee, S.W., Kelly, L., Apeltsin, L., Stroud, R.M., Ferrin, T.E., Giacomini, K.M. and Sali, A., (2010) Comparison of human solute carriers. *Protein science : a publication of the Protein Society*, [online] 193, pp.412–28. Available at: http://www.ncbi.nlm.nih.gov/pubmed/20052679 [Accessed 29 Dec. 2018].

Shen, M. and Sali, A., (2006) Statistical potential for assessment and prediction of protein structures. *Protein Science*, [online] 1511, pp.2507–2524. Available at: http://doi.wiley.com/10.1110/ps.062416606 [Accessed 27 Nov. 2018].

Sigworth, F.J., (2016) Principles of cryo-EM single-particle image processing. *Microscopy*, [online] 651, pp.57–67. Available at: http://jmicro.oxfordjournals.org/lookup/doi/10.1093/jmicro/dfv370.

Sinclair, L. V., Neyens, D., Ramsay, G., Taylor, P.M. and Cantrell, D.A., (2018) Single cell analysis of kynurenine and System L amino acid transport in T cells. *Nature Communications*, [online] 91, p.1981. Available at: http://www.nature.com/articles/s41467-018-04366-7 [Accessed 22 May 2018].

Sinclair, L. V, Rolf, J., Emslie, E., Shi, Y.-B., Taylor, P.M. and Cantrell, D. a, (2013) Control of amino-acid transport by antigen receptors coordinates the metabolic reprogramming essential for T cell differentiation. *Nature immunology*, [online] 145, pp.500–8. Available at: http://www.pubmedcentral.nih.gov/articlerender.fcgi?artid=3672957&tool=pmcentrez&rendertype=abstract [Accessed 22 Oct. 2014].

Singh, N. and Ecker, G., (2018) Insights into the Structure, Function, and Ligand Discovery of the Large Neutral Amino Acid Transporter 1, LAT1. *International Journal of Molecular Sciences*, [online] 195, p.1278. Available at: http://www.mdpi.com/1422-0067/19/5/1278.

Soding, J., Biegert, A. and Lupas, A.N., (2005) The HHpred interactive server for protein homology detection and structure prediction. *Nucleic Acids Research*, [online] 33Web Server, pp.W244–W248. Available at: https://academic.oup.com/nar/article-lookup/doi/10.1093/nar/gki408 [Accessed 8 Oct. 2018].

Stroud, Z., Hall, S.C.L. and Dafforn, T.R., (2018) Purification of membrane proteins free from conventional detergents: SMA, new polymers, new opportunities and new insights. *Methods (San Diego, Calif.)*. [online] Available at: https://www.sciencedirect.com/science/article/pii/S1046202317304887?via%3Dihub [Accessed 10 May 2018].

Tafuri, A., Alferink, J., Möller, P., Hämmerling, G.J. and Arnold, B., (1995) T cell awareness of paternal alloantigens during pregnancy. *Science (New York, N.Y.)*, [online] 2705236, pp.630–3. Available at: http://science.sciencemag.org/content/281/5380/1191.long [Accessed 3 Apr.

2019].

Terpe, K., (2006) Overview of bacterial expression systems for heterologous protein production: from molecular and biochemical fundamentals to commercial systems. *Applied microbiology and biotechnology*, [online] 722, pp.211–22. Available at: http://link.springer.com/10.1007/s00253-006-0465-8 [Accessed 22 Oct. 2018].

Thal, D.M., Vuckovic, Z., Draper-Joyce, C.J., Liang, Y.L., Glukhova, A., Christopoulos, A. and Sexton, P.M., (2018) *Recent advances in the determination of G protein-coupled receptor structures*. *Current Opinion in Structural Biology*, Available at: https://doi.org/10.1016/j.sbi.2018.03.002 [Accessed 20 Mar. 2018].

Thompson, R.F., Iadanza, M.G., Hesketh, E.L., Rawson, S. and Ranson, N.A., (2019) Collection, pre-processing and on-the-fly analysis of data for high-resolution, single-particle cryo-electron microscopy. *Nature Protocols*, [online] 141, pp.100–118. Available at: http://www.nature.com/articles/s41596-018-0084-8 [Accessed 9 Jan. 2019].

Thompson, R.F., Walker, M., Siebert, C.A., Muench, S.P. and Ranson, N.A., (2016) An introduction to sample preparation and imaging by cryo-electron microscopy for structural biology. *Methods (San Diego, Calif.)*, [online] 100, pp.3–15. Available at: http://www.sciencedirect.com/science/article/pii/S1046202316300330.

Tomblin, J.K., Arthur, S., Primerano, D.A., Chaudhry, A.R., Fan, J., Denvir, J. and Salisbury, T.B., (2016) Aryl hydrocarbon receptor (AHR) regulation of L-Type Amino Acid Transporter 1 (LAT-1) expression in MCF-7 and MDA-MB-231 breast cancer cells. *Biochemical Pharmacology*, [online] 106, pp.94–103. Available at: http://dx.doi.org/10.1016/j.bcp.2016.02.020.

Trexler-Schmidt, M., Sargis, S., Chiu, J., Sze-Khoo, S., Mun, M., Kao, Y.H. and Laird,

M.W., (2010) Identification and prevention of antibody disulfide bond reduction during cell culture manufacturing. *Biotechnology and Bioengineering*, 1063, pp.452–461.

Trott, O. and Olson, A.J., (2010) AutoDock Vina: improving the speed and accuracy of docking with a new scoring function, efficient optimization, and multithreading. *Journal of computational chemistry*, [online] 312, pp.455–61. Available at: http://onlinelibrary.wiley.com.liverpool.idm.oclc.org/store/10.1002/jcc.21334/asset/21334_ftp.pdf;jsessionid=CFD0B8BCFD6A646833CD63AD68F7215C.f03t01?v=1&t=j3edmurc&s=c7e2775351b914920bf203012983405d12b53377 [Accessed 1 Jun. 2017].

Uchino, H., Kanai, Y., Kim, D.K., Wempe, M.F., Chairoungdua, A., Morimoto, E., Anders, M.W. and Endou, H., (2002) Transport of amino acid-related compounds mediated by L-type amino acid transporter 1 (LAT1): insights into the mechanisms of substrate recognition. *Molecular pharmacology*, [online] 614, pp.729–737. Available at: http://molpharm.aspetjournals.org/content/61/4/729.short [Accessed 22 Oct. 2014].

Unwin, P.N.T. and Henderson, R., (1975) Molecular structure determination by electron microscopy of unstained crystalline specimens. *Journal of molecular biology*, [online] 943, pp.425–40. Available at: https://ac-els-cdn-com.liverpool.idm.oclc.org/0022283675902120/1-s2.0-0022283675902120-main.pdf?_tid=4905d4d8-8435-4daa-b771-bce7edb8625a&acdnat=1546946873_0bdbd531cee3f8e1429a78d30be096dc [Accessed 8 Jan. 2019].

Vargas, J., Abrishami, V., Marabini, R., de la Rosa-Trevín, J.M., Zaldivar, A., Carazo,

J.M. and Sorzano, C.O.S., (2013) Particle quality assessment and sorting for automatic and semiautomatic particle-picking techniques. *Journal of Structural Biology*, [online] 1833, pp.342–353. Available at: http://linkinghub.elsevier.com/retrieve/pii/S1047847713001950 [Accessed 2 Mar. 2017].

Vinothkumar, K.R., (2015) Membrane protein structures without crystals, by single particle electron cryomicroscopy. *Current Opinion in Structural Biology*, [online] 33, pp.103–114. Available at: https://www.sciencedirect.com/science/article/pii/S0959440X15001074 [Accessed 11 Sep. 2016].

Vinothkumar, K.R. and Henderson, R., (2010) *Structures of membrane proteins.* [online] *Quarterly reviews of biophysics*, Available at: http://journals.cambridge.org/action/displayFulltext?type=6&fid=7854115&jid=QRB&volumeId=43&issueId=01&aid=7854114&bodyId=&membershipNumber=&societyETOCSession=&fulltextType=RV&fileId=S0033583510000041#cjofig_fig001.

Walls, J., Sinclair, L. and Finlay, D., (2016) Nutrient sensing, signal transduction and immune responses. *Seminars in Immunology*, [online] pp.152–160. Available at: http://dx.doi.org/10.1016/j.smim.2016.09.001.

Wang, K.H., Penmatsa, A. and Gouaux, E., (2015) Neurotransmitter and psychostimulant recognition by the dopamine transporter. *Nature*, [online] 5217552, pp.322–327. Available at: http://www.nature.com/doifinder/10.1038/nature14431.

Waterhouse, A.M., Procter, J.B., Martin, D.M.A., Clamp, M. and Barton, G.J., (2009) Jalview Version 2--a multiple sequence alignment editor and analysis workbench.

Bioinformatics, [online] 259, pp.1189–1191. Available at: http://www.ncbi.nlm.nih.gov/pubmed/19151095 [Accessed 18 Sep. 2016].

Webb, B. and Sali, A., (2016) Comparative Protein Structure Modeling Using MODELLER. *Current protocols in bioinformatics*, [online] 541, p.5.6.1-5.6.37. Available at: http://doi.wiley.com/10.1002/cpbi.3 [Accessed 10 Oct. 2018].

Wei, L., Tominaga, H., Ohgaki, R., Wiriyasermkul, P., Hagiwara, K., Okuda, S., Kaira, K., Oriuchi, N., Nagamori, S. and Kanai, Y., (2016) Specific transport of 3-fluoro-L-α-methyl-tyrosine by LAT1 explains its specificity to malignant tumors in imaging. *Cancer Science*, [online] 1073, pp.347–352. Available at: http://doi.wiley.com/10.1111/cas.12878.

Wiriyasermkul, P., Nagamori, S., Tominaga, H., Oriuchi, N., Kaira, K., Nakao, H., Kitashoji, T., Ohgaki, R., Tanaka, H., Endou, H., Endo, K., Sakurai, H. and Kanai, Y., (2012) Transport of 3-Fluoro-L- -Methyl-Tyrosine by Tumor-Upregulated L-Type Amino Acid Transporter 1: A Cause of the Tumor Uptake in PET. *Journal of Nuclear Medicine*, [online] 538, pp.1253–1261. Available at: http://jnm.snmjournals.org/cgi/doi/10.2967/jnumed.112.103069.

Xu, D. and Zhang, Y., (2011) Improving the physical realism and structural accuracy of protein models by a two-step atomic-level energy minimization. *Biophysical Journal*, [online] 10110, pp.2525–2534. Available at: http://www.ncbi.nlm.nih.gov/pubmed/22098752 [Accessed 18 Sep. 2016].

Yanagida, O., Kanai, Y., Chairoungdua, A., Kim, D.K., Segawa, H., Nii, T., Cha, S.H., Matsuo, H., Fukushima, J., Fukasawa, Y., Tani, Y., Taketani, Y., Uchino, H., Kim, J.Y., Inatomi, J., Okayasu, I., Miyamoto, K., Takeda, E., Goya, T. and Endou, H., (2001) Human L-type amino acid transporter 1 (LAT1): characterization of function and

expression in tumor cell lines. *Biochimica et biophysica acta*, [online] 15142, pp.291–302. Available at: http://www.sciencedirect.com/science/article/pii/S0005273601003844%5Cnhttp://www.ncbi.nlm.nih.gov/pubmed/11557028.

Ylikangas, H., Malmioja, K., Peura, L., Gynther, M., Nwachukwu, E.O., Lepp??nen, J., Laine, K., Rautio, J., Lahtela-Kakkonen, M., Huttunen, K.M., Poso, A., Leppänen, J., Laine, K., Rautio, J., Lahtela-Kakkonen, M., Huttunen, K.M. and Poso, A., (2014) Quantitative insight into the design of compounds recognized by the L-type amino acid transporter 1 (LAT1). *ChemMedChem*, [online] 912, pp.2699–2707. Available at: http://doi.wiley.com/10.1002/cmdc.201402281 [Accessed 18 Dec. 2018].

Ylikangas, H., Peura, L., Malmioja, K., Leppänen, J., Laine, K., Poso, A., Lahtela-Kakkonen, M. and Rautio, J., (2013) Structure-activity relationship study of compounds binding to large amino acid transporter 1 (LAT1) based on pharmacophore modeling and in situ rat brain perfusion. *European Journal of Pharmaceutical Sciences*, [online] 483, pp.523–531. Available at: http://dx.doi.org/10.1016/j.ejps.2012.11.014 [Accessed 18 Dec. 2018].

Yoshimoto, M., Kurihara, H., Honda, N., Kawai, K., Ohe, K., Fujii, H., Itami, J. and Arai, Y., (2013) Predominant contribution of L-type amino acid transporter to 4-borono-2-18F-fluoro-phenylalanine uptake in human glioblastoma cells. *Nuclear Medicine and Biology*, [online] 405, pp.625–629. Available at: http://ac.els-cdn.com/S0969805113000450/1-s2.0-S0969805113000450-main.pdf?_tid=88d56120-5cd0-11e7-a674-00000aab0f6b&acdnat=1498743819_50610abaf86e2326c7790526e81bf373 [Accessed 29 Jun. 2017].

Yue, M., Jiang, J., Gao, P., Liu, H. and Qing, G., (2017) Oncogenic MYC Activates a Feedforward Regulatory Loop Promoting Essential Amino Acid Metabolism and Tumorigenesis. *Cell Reports*, [online] 2113, pp.3819–3832. Available at: http://www.cell.com/cell-reports/pdf/S2211-1247(17)31798-9.pdf [Accessed 18 Apr. 2018].

Yun, D.-W., Lee, S.A., Park, M.-G., Kim, J.-S., Yu, S.-K., Park, M.-R., Kim, S.-G., Oh, J.-S., Kim, C.S., Kim, H.-J., Kim, J.-S., Chun, H.S., Kanai, Y., Endou, H., Wempe, M.F. and Kim, D.K., (2014) JPH203, an L-Type Amino Acid Transporter 1–Selective Compound, Induces Apoptosis of YD-38 Human Oral Cancer Cells. *Journal of Pharmacological Sciences*, [online] 1242, pp.208–217. Available at: http://jlc.jst.go.jp/DN/JST.JSTAGE/jphs/13154FP?lang=en&from=CrossRef&type=abstract.

Zhang, K., (2016) Gctf: Real-time CTF determination and correction. [online] 1931, pp.1–12. Available at: http://ac.els-cdn.com/S1047847715301003/1-s2.0-S1047847715301003-main.pdf?_tid=af8e4cfa-8336-11e7-9c84-00000aab0f01&acdnat=1502965835_90ed4f91a3844c0bbf0c6f06b6209b96 [Accessed 18 May 2017].

Zhao, Y., Wang, L. and Pan, J., (2015) The role of L-type amino acid transporter 1 in human tumors. *Intractable & Rare Diseases Research*, [online] 44, pp.165–169. Available at: www.irdrjournal.com [Accessed 5 Sep. 2016].

Zheng, S.Q., Palovcak, E., Armache, J.-P., Verba, K.A., Cheng, Y. and Agard, D.A., (2017) MotionCor2: anisotropic correction of beam-induced motion for improved cryo-electron microscopy. *Nature Methods*, [online] 144, pp.331–332. Available at: http://www.nature.com/articles/nmeth.4193 [Accessed 29 Dec. 2018].

Zhu, J., Penczek, P.A., Schröder, R. and Frank, J., (1997) Three-dimensional reconstruction with contrast transfer function correction from energy-filtered cryoelectron micrographs: procedure and application to the 70S Escherichia coli ribosome. *Journal of structural biology*, [online] 1183, pp.197–219. Available at: https://www.sciencedirect.com/science/article/pii/S1047847797938454?via%3Dihub [Accessed 14 Jan. 2019].

Zhu, Y., Carragher, B., Glaeser, R.M., Fellmann, D., Bajaj, C., Bern, M., Mouche, F., De Haas, F., Hall, R.J., Kriegman, D.J., Ludtke, S.J., Mallick, S.P., Penczek, P.A., Roseman, A.M., Sigworth, F.J., Volkmann, N. and Potter, C.S., (2004) Automatic particle selection: Results of a comparative study. In: *Journal of Structural Biology*. [online] pp.3–14. Available at: http://ac.els-cdn.com.liverpool.idm.oclc.org/S1047847703002004/1-s2.0-S1047847703002004-main.pdf?_tid=d9c6ebf4-0725-11e7-b2b2-00000aacb35d&acdnat=1489324660_11ba02c368c87cb1a9f3b54f7f7c230d [Accessed 12 Mar. 2017].

Zivanov, J., Nakane, T., Forsberg, B.O., Kimanius, D., Hagen, W.J.H., Lindahl, E. and Scheres, S.H.W., (2018) New tools for automated high-resolution cryo-EM structure determination in RELION-3. *eLife*, [online] 7, p.421123. Available at: http://dx.doi.org/10.1101/421123 [Accessed 1 Dec. 2018].

Zur, A.A., Chien, H.-C., Augustyn, E., Flint, A., Heeren, N., Finke, K., Hernandez, C., Hansen, L., Miller, S., Lin, L., Giacomini, K.M., Colas, C., Schlessinger, A. and Thomas, A.A., (2016) LAT1 activity of carboxylic acid bioisosteres: Evaluation of hydroxamic acids as substrates. *Bioorganic & Medicinal Chemistry Letters*, [online] 2620, pp.5000–5006. Available at:

http://linkinghub.elsevier.com/retrieve/pii/S0960894X16309313.